Spring 5-2012

Surface, Bulk, and Rheological Properties of Polyhedral Oligomeric Silsesquioxane/High Density Polyethylene Nanocomposites

Robert Douglas Cook Jr.
University of Southern Mississippi

The University of Southern Mississippi

SURFACE, BULK, AND RHEOLOGICAL PROPERTIES OF POLYHEDRAL OLIGOMERIC SILSESQUIOXANE/HIGH DENSITY POLYETHYLENE NANOCOMPOSITES

by

Robert Douglas Cook, Jr.

Abstract of a Dissertation
Submitted to the Graduate School
of The University of Southern Mississippi
in Partial Fulfillment of the Requirements
for the Degree of Doctor of Philosophy

May 2012

ABSTRACT

SURFACE, BULK AND RHEOLOGICAL PROPERTIES OF POLYHEDRAL OLIGOMERIC SILSESQUIOXANE/HIGH DENSITY POLYETHYLENE NANOCOMPOSITES

by Robert Douglas Cook, Jr.

May 2012

In the formulation of high performance nanocomposites, control of miscibility and dispersion of filler material through a polymer matrix is of utmost importance. Due to their inorganic nature most nanofillers are insoluble in polymers, leading to costly/complicated surface modification as a primary means of increasing miscibility and interaction with organic matrices. Polyhedral oligomeric silsesquioxane (POSS) nanostructured chemicals offer an attractive alternative to conventional nanofillers. Due to their hybrid organic-inorganic nature, POSS has the potential to be tailored for miscibility in a wide range of organic matrices not by chemical surface modification but through modification of the molecular structure of the filler itself. The overall goal of this research is to investigate how changes to POSS molecular structure affect miscibility and dispersion in physically blended high density polyethylene (HDPE)/POSS blends. The primary objective of the first section is to understand the effect of POSS cage structure, physical state and R-group alkyl chain length on miscibility and blend performance through a wide range of characterization techniques. Special attention will be paid to rheological, bulk and surface performance of the blends as compared to the neat HDPE matrix. The primary objective of the second section is to determine the utility of theoretical solubility parameter calculations as a means of predicting POSS miscibility

in the HDPE matrix. This section will focus on solubility parameters calculated using both group contribution and molecular dynamics simulation methods, determining their proximity to each other, and qualifying their applicability in predicting POSS miscibility and blend performance.

This dissertation is comprised of six chapters. Chapter I provides an introduction to nanocomposites, as well as background information on HDPE, POSS, pertinent POSS blends and solubility parameter theory. Chapter II gives an overview of the research goals and specific objectives of this research. Chapter III probes the influence of POSS functionality, cage structure and physical state on the bulk properties (thermal, rheological, mechanical) of the melt-processed HDPE/POSS blends. Chapter IV explores HDPE surface modification as a function of POSS incorporation, as well as aggregation and migrational behavior of the POSS molecules. Chapter V surveys POSS theoretical solubility parameter calculations via both group contribution theory and molecular dynamics simulations and correlates these values with observed blend behavior due to incorporation of POSS. Finally, Chapter VI provides recommendations for future work in an attempt to further refine our understanding of the complex behaviors and trends observed in our HDPE/POSS systems.

The University of Southern Mississippi

SURFACE, BULK, AND RHEOLOGICAL PROPERTIES OF POLYHEDRAL OLIGOMERIC SILSESQUIOXANE/HIGH DENSITY POLYETHYLENE NANOCOMPOSITES

by

Robert Douglas Cook, Jr.

A Dissertation
Submitted to the Graduate School
of The University of Southern Mississippi
in Partial Fulfillment of the Requirements
for the Degree of Doctor of Philosophy

Approved:

_Sarah E. Morgan_____
Director

_Scott G. Piland_____

_James W. Rawlins_____

_Robson F. Storey_____

_Jeffrey S. Wiggins_____

_Susan A. Siltanen_____
Dean of the Graduate School

May 2012

DEDICATION

This dissertation is dedicated to my loving mother, Sherri Cook, whose selfless sacrifices have allowed me to become the man I am today.

ACKNOWLEDGMENTS

First and foremost I would like to express my sincere appreciation and gratitude to Dr. Sarah E. Morgan, whose leadership and guidance has allowed me to achieve success in my research. From the beginning of my graduate career, Dr. Morgan has been a constant source of encouragement and support, allowing me to develop as both a research professional and a human being. Her generosity and encouragement of industry interaction is a source of inspiration for our department and the primary contribution to my success in obtaining a wide network of both research professionals and job opportunities. Additionally, I would like to thank those who have served on my graduate committee, including Dr. Scott Piland, Dr. James Rawlins, Dr. Robson Storey and Dr. Jeffrey Wiggins.

I would also like to thank the current and past members of the Morgan research group for their friendship and support through the duration of my career, in particular, Dr. Rahul Misra, Dr. Alp Alidedeoglu, Dr. Paul Jones, Dr. Mithun Bhattacharya, Chris Sahagun, Lea Paslay, Yuhong Wei, Xiaonan Kou, Sarah Exley, Elana Lewis, Yan Zong, Qi Qu, Chris Harris, Chris Jackson, Kelly McLeod, Chelsea Wahl and Tyler Brown. I would also like to specially thank Matthew Williams, whose consistent support over the last few years has resulted in a significant contribution to my research and success. I would also like to thank those within the department who have had a direct impact on my research, in particular Dr. Andreas Plagge and Mrs. Kim Wingo.

I have had the opportunity to work with multiple great companies, I am especially grateful to Hybrid Plastics for their support of my research and use of their laboratory facilities, in particular, I would like to thank Dr. Joe Lichtenhan, Dr. Joe Schwab and Dr.

Paul Wheeler. I would like to acknowledge General Electric for presenting me with a wonderful internship opportunity, in particular, Dr. Wendy Lin, Dr. Peter Davis and Dr. Michael O'Brien. I would also like to thank Dr. Dwight Waddell, director of the Cognitive Neurophysiology Laboratory at The University of Mississippi, for hosting me as a summer research intern. I would like to thank Chevron-Phillips Chemical for their support of my research. Finally, I would like to thank the National Science Foundation's GK-12 program for giving me the opportunity for an amazing fellowship, as well as Hattiesburg High School, in particular Mr. James Brownlow, for partnering with me in the program.

TABLE OF CONTENTS

LIST OF TABLES

Table

LIST OF ILLUSTRATIONS

Figure

CHAPTER I

INTRODUCTION

Polymer Nanocomposites

Polymeric nanocomposites, defined as blends consisting of filler material with at least one dimension less than 100 nm, have been the focus of intense research and development efforts over the last 25 years.[1-3] This has inherently been catalyzed by technological advancements in microscopic characterization, allowing researchers to probe the effects of nanofillers on polymer morphology and structure at a molecular level.[1,2,4,5] Additionally, advancements in computer molecular dynamics simulations have presented researchers with a powerful new tool to model and screen composite performance without the high costs of material processing.[6,7] Utilization of nanocomposites is appealing for a variety of applications due to the unique property sets attainable through the use of a wide range of nano-scale filler materials, as well as ready availability of required processing equipment. In general, nanocomposites display characteristics of both the polymer matrix and the filler, as well as synergistic effects on overall composite morphology.[1,2,5,8]

The first instance of commercial application of a nanocomposite was in the early 1990s by Toyota Research Laboratories, which reported significant improvements in both mechanical and thermal performance of Nylon-6 through incorporation of small amounts of nanoscale clay.[9] Enhancements in performance through the use of nanofillers are attributed to their small size, which result in very large surface area, and therefore the potential of high levels of physical interaction between the matrix and the filler surfaces. As filler size is decreased from micro to nanoscale, a significant increase in surface area

relative to volume is realized. Nanofillers span a range of layered materials, fibers and particles, examples of which are nanotubes[10-13], nanofibers[14-17], nanowires[18-21], fullerenes[22-25], nanoclays[26-30], and inorganic nanoparticles.[31-34] Properties generally associated with these nanofillers are high stiffness/modulus, high thermal stability, and good electrical conductivity, attributes generally not associated with organic polymers.[8] In addition to surface to volume ratios, level of dispersion is also a dominant factor affecting nanocomposite performance. A more homogenous dispersion of filler generally results in greater levels of performance enhancement, while poor dispersion can lead to properties inferior to that of the neat matrix.[35] Optimizing mixing and dispersion of filler into a polymer matrix is commonly accomplished through modification of the filler surfaces, which can lead to increased solubility and interaction between the matrix and filler material allowing for tuning of nanocomposite properties.[8,35,36]

Of the three major categories of nanofillers, layered silicates have received a relatively large level of research effort.[26-30,37,38] Catalyzed by the research reported by Toyota relative to Nylon-6/clay nanocomposites, successful processing of layered silicate-based nanocomposites has resulted in materials with enhanced thermal, mechanical and barrier properties, leading to use in a variety of high performance applications.[37] Level of enhancement is shown to be completely dependent on level of exfoliation and dispersion of the high aspect ratio silicates through the bulk of the matrix, which due to their inorganic nature, can be a significant challenge. In general, surface modification of the clay filler is necessary to increase solubility and interaction with organic polymer matrices, leading to increased processing time and the use of solvents which may be detrimental to overall composite performance.[26,29,30]

Similar to layered silicates, both single-wall and multi-wall carbon nanotubes have also been shown to impart significant thermal, mechanical and electrical property enhancements to a wide variety of polymer matrices.[10-13,39] Again, level of enhancement has been shown to depend almost entirely on level of dispersion, as well as level of interaction between the matrix and filler. Like layered silicates, the propensity of carbon nanotubes to self-segregate when dispersed into polymer matrices is a significant concern, especially due to their high cost. Multiple methods of surface treatments have been explored to increase the miscibility of nanotubes in organic matrices, though the high costs associated with nanotube utilization generally outweighs potential benefits.[39]

Composites consisting of inorganic nanoparticles are of particular interest due to the wide range of filler properties available, as well as a wide range of processing techniques. Melt-compounding, solution blending, in-situ polymerization and high shear mixing have all been used to process inorganic particle nanocomposites, with processing technique highly related to desired property enhancements and filler characteristics.[31-34] Examples of inorganic nanofillers that have been researched span the range of metals (Al, Fe, Ag Au, etc.), metal oxides (TiO_2, Al_2O_3, ZnO, etc) and nonmetals (fullerenes, layered silicates, SiO_2, etc).[31-34] In general, particle-based nanocomposites prepared via chemical interaction between the filler and matrix provide enhanced properties over composites prepared via mechanical mixing, in which interactions are primarily hydrogen bonding and van der Waals forces, though both can result in substantial improvements to thermal, mechanical, gas barrier and electrical performance.[31]

High Density Polyethylene

Molecularly, high density polyethylene (HDPE) can be regarded as the "purest" form of polyethylene in that its characteristic limited branching and limited defects result in a product that is almost entirely linear.[40] This linearity results in a material with a high level of crystallinity (67-72%), as well as a relatively high density (0.94-0.98 g/cm^3) compared to many other polyolefins.[41] The elevated levels of crystallinity result in a material with high mechanical modulus/stiffness and low permeability compared to other polyolefins. High abrasion resistance, crack resistance, corrosion resistance, low T_g and low coefficient of friction are also properties inherent to HDPE.[42] By the late 1990s, annual consumption of polyethylene in the United States surpassed 26 billion pounds, with HDPE accounting for almost half of that estimate.[40] The primary products are mass-produced consumer items such as bottles, food packaging films, bags, pipes and tanks, due almost entirely to the low cost of acquiring and processing HDPE.

Low cost, high linearity and limited molecular defects recommend HDPE as an ideal composite matrix, though limited research has been reported due to the difficulty of processing and dispersion of inorganic filler materials into the highly-crystalline, organic matrix.[43-45] Blends of HDPE and SiO_2 have been reported to display enhanced tensile modulus and thermal stability compared to the neat matrix, though only at very low loading levels.[46,47] HDPE/nano-clay blends have also been reported to display enhanced tensile modulus, though tensile strength was said to decrease due to poor miscibility and the formation of large clay aggregates.[48-50] To promote exfoliation and dispersion, surface treatment has been shown to be effective in increasing miscibility and dispersion of clay into HDPE, with the resulting blends displaying enhanced mechanical

performance compared to the neat matrix.[49,50] There have also been reports of improved mechanical, thermal and electrical performance through the processing of HDPE/carbon nanotube systemss.[51,52] In a recent study, Chrissafis et al. compared HDPE nanocomposites consisting of SiO_2, clay or multi-wall carbon nanotube (MWCNT) nanofillers, and reported that the SiO_2 blends displayed the largest enhancements in mechanical performance and thermal stability.[53] This was attributed to their small size, enhanced miscibility, and good dispersion in the HDPE matrix. Though SiO_2 nanoparticles were reported to cause a slight decrease in bulk crystallinity of the HDPE matrix, N_2, O_2 and CO_2 permeability were all reduced for the nanocomposites, attributed to well dispersed SiO_2 particles (as verified by TEM-EDAX) creating a tortuous path for gas transmission. The SiO_2 particles used in this study were on the order of 12 nm in diameter, and in one case, were not surface treated. Analyzing the above articles, a common theme observed is that reducing the size of the nanofiller, and therefore increasing surface volume interaction with the polymer matrix, generally results in increased interaction with polymer chains and enhanced reinforcement compared to larger fillers. [46,47,53] Additionally, tailoring the solubility of the nanofillers through surface modification appears to result in the ability to tune miscibility in a wide range of organic matrices.[8,35,36] Fortunately, small size and cost-effective tunable miscibility are offered by an exciting class of silicate nanofiller called Polyhedral Oligomeric Silsesquioxane (POSS).[54]

Polyhedral Oligomeric Silsesquioxane (POSS) Nanochemicals

Silsesquioxanes are a unique class of inorganic nanoparticles. Relative to the conditions under which these materials are synthesized, they can have structures ranging

from ladders and cages (both closed and partial), to random networks.[54] The first occurrence of oligomeric silsesquioxanes in literature was reported by Scott et al., who in 1946 isolated the material through the thermolysis of products formed through the cohydrolysis of methyltricholorsilane and dimethylchlorosilane.[55] Recent research efforts have focused on the cubic polysilsesquioxanes, or polyhedral oligomeric silsesquioxanxes, which have the general molecular formula $(RSiO_{1.5})n$.[56-58] In this case, R can be a wide variety of organic functional groups and n is usually 8, 10 or 12.[54] The Si-O-Si cage structure, which comprises the stiff core of the POSS molecule, is surrounded by a corona of interchangeable organic R-groups, giving rise to a material that is both organic and inorganic in nature. Figure 1 shows a schematic of the general closed-cage POSS molecular structure.

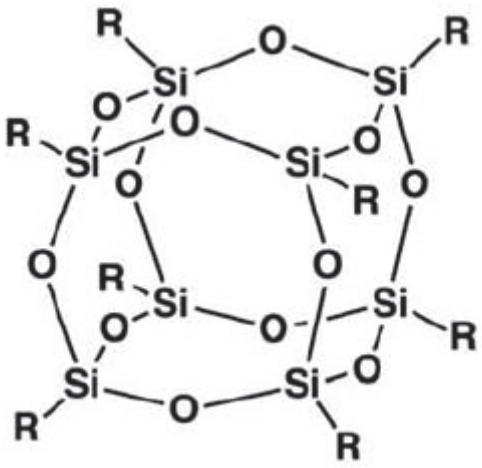

Figure 1. Schematic of the general closed-cage POSS molecular structure.

Tuning of the organic groups, which are attached to the corner Si atoms of the cage, can lead to increased solubility and miscibility in a wide range of polymer matrices without the use of solvents and/or surface modification techniques generally required for successful incorporation of inorganic fillers into a polymer matrix.[54,56-59] In addition to

R-group tuning for miscibility purposes, one of the R-groups can be replaced with a reactive X-group in some applications, leading to utility of POSS not just as a mechanically-blended nanofiller, but as a co-monomer or cross-linking point.[54,59]

In terms of general structure, the inorganic Si-O-Si cage of the POSS molecule leads to a material with incredibly high stiffness/modulus, as well as good thermal, oxidative, and electrical performance.[54] Physically, POSS exists as a crystalline solid or viscous liquid, with physical state dependent on type of R-group functionality. As long as good POSS dispersion in an organic matrix is obtained, commonly verified through a combination of TEM elemental mapping and surface/bulk AFM, high surface to volume ratios due to the small (1-3 nm in diameter) size of the POSS molecules can lead to desirable property enhancement without affecting the optical performance of the resulting blends.[58] Additionally, the nanoscale size of the POSS molecule is comparable in size to most polymer coils, leading to the potential of filler-matrix interactions at a molecular level.[54] Inherently, POSS can be thought of as the smallest possible form of silica. Compared to layered silicates (which generally only have 1 dimension less than 100 nm) and carbon nanotubes/nanowires (which generally only have 2 dimensions less than 100 nm), the three-dimensional nano-scale nature of POSS can lead to the formation of nanocomposites with properties superior to that of conventional nanofillers.[11,12,26,27,30,59]

In addition to the completely condensed cage structure of the most common POSS molecule, it is also possible to create POSS cores that have an open-cage structure. In 1965, Brown and Vogt et al. synthesized an incompletely-condensed POSS triol through the hydrolytic condensation of trichlorosilane, though 60-70% yields were said to come only after three-years of reaction.[60] Figure 2 shows a schematic diagram of the trisilanol

POSS structure. Feher et al. expanded upon this research to enhance the rate of triol formation through controlled acid cleavage of the fully-condensed POSS molecules, as well as the substitution of different R-group functionality to the molecule.[61] The Si–OH functionality within the cage structure of these incompletely-condensed "trisilanol" POSS types gave rise to a new level of POSS utilization through cross-linking and grafting reactions, as well as slightly different property sets compared to their closed-cage analogues.[59,62]

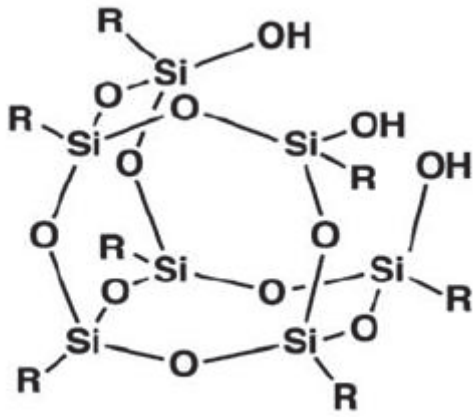

Figure 2. Schematic of the general open-cage "trisilanol" POSS structure.

Over the last 15 years, POSS has been utilized to create a wide range of hybrid organic-inorganic nanocomposites.[58,59] In general, incorporation into a polymer matrix takes place through grafting, copolymerization or mechanical blending.[57-59] To this point, the majority of POSS research has surrounded systems in which POSS is covalently bonded to the polymer backbone, or grafted as a pendent group.[58,59,63-76] Blends formulated by this method generally show enhanced mechanical performance, as well as decreased gas permeability and enhanced thermal properties. Additionally, T_g is generally increased through covalent bonding of POSS. Organic matrices which have been modified through covalent bonding of POSS include, but are not limited to,

epoxies[64,66], polysiloxanes[63,68], polyurethanes[65,67], polyolefins[69-72] and poly(methyl methacrylates).[73-76] A trending theme is that covalent bonding of POSS to polymer backbones is not always desirable in that it generally requires the use of solvents and complicated synthesis schemes which may limit the applicability of the resulting product. Additionally, covalent bonding of POSS has been found to decrease processing efficiency attributed to an anchoring effect caused by the pendent POSS groups, leading to increased melt viscosity and decreased rheological performance.[77-79] Bizet et al. evaluated the mobility of POSS using mean square displacement simulations, and reported that poly(methyl methacrylate) (PMMA) modified with 10 mol % octaisobutyl (OiB) POSS had three times less chain mobility than neat PMMA, attributed to POSS anchoring.[80] For these reasons, it is desirable to look at melt blending as a potential low cost and effective method by which to create HDPE/POSS nanocomposites.

Applicability of POSS in the Melt Blending

Due to the complexities in achieving good dispersion of filler into organic polymer matrices, processing of small-molecule-reinforced polymer composites is not a trivial matter.[8,35] Extrusion processing, a common type of melt-blending, is generally considered a low cost, fast, environmentally friendly, and highly efficient way to compound and process organic polymers.[81] Additionally, the compounding of composites and nanocomposites usually requires only slight equipment modifications to basic extrusion set-ups.[82] Unlike other processing methods, which generally require the use of complex polymerization protocols or solvents which could be detrimental to composite performance, nanocomposite processing via melt blending is an attractive alternative for both industry and academia alike.[8,35] Consequently, methods to process conventional

nanofillers such as carbon nanotubes[45,83-86], carbon black[87-90], and layered silicates[91-95] in polyolefin matrices have all be thoroughly researched and developed via melt blending.

As described, realization of the complete potential of including nanofillers into an organic matrix usually requires thorough, homogeneous dispersion of the filler through the bulk of a composite matrix.[96] In some rare cases surface segregation of the nanofiller may be desirable in terms of enhanced surface properties, which will be discussed later, but the majority of desirable thermal and physical property enhancements expected through utilization of a nanofiller require good dispersion and strong matrix interactions.[97] Though melt-blending is a fast and effective way to process organic polymers, it should be noted that both the processing conditions under which melt-blending is conducted, as well as the physical/chemical interaction between the filler material and polymer matrix, are proven to be crucial to the overall dispersion and performance of the nanocomposite.[81,82,96] In terms of processing conditions, items such as extruder zone temperatures, residence time, screw design, zone pressures (level of shear), and method by which the extruded molten polymer is cooled all have an effect on the level of filler dispersion and over-all physical properties of the resulting material.[81,82,96] In terms of the physical/chemical interaction between the filler material and organic matrix, it has already been stated that the organic corona of POSS molecules can be tailored for different applications, leading to nanofillers that are custom-synthesized to have good theoretical interaction/solubility in the organic matrix with which they are to be mixed. In principal, this should give researchers the ability to finely tune the dispersion of POSS molecules into any organic matrix, though it should be noted that POSS molecules have the propensity to self associate, leading to the formation of aggregates even in

theoretically miscible conditions.[98] This is especially true for POSS molecules with shorter corona R-groups.[99]

Properties of POSS/Polyolefin Melt Blends

Relatively limited research has been conducted on the melt-blending of POSS into polymer matrices, compared to POSS copolymerization and grafting studies.[57-59,100-102] Research into melt-blends spans a range of organic polymers, including but not limited to polyolefines[59,97,101,103-115], polyesters[116-119], polyamides[120-123], polycarbonate[124-126], and vinyl-polymer matricies.[74,76,127-129] In general, the creation of POSS blends through melt-processing has been shown to impart a wide range of rheological, thermal, physical and surface enhancements compared to the neat matrix. In terms of polyolefin research, many of these studies show mixed results as to the effect of POSS on blend bulk behavior. Chronologically the first attempt at melt-blending POSS into a polyolefin matrix was that of Fu et al., who blended octamethyl (OM) POSS into polypropylene.[107] Though no indication of level of POSS dispersion was revealed, insight into the effect of POSS on polypropylene crystallization was addressed. Isothermal DSC analysis revealed that incorporation of POSS resulted in decreased time to reach exothermic maximum by 52%, attributed to POSS nanocrystals serving as nucleation sites for the molten polymer. The greatest levels of nucleation were found to occur at 15 wt. % POSS loading, attributed to fine miscibility of POSS. Once POSS loading was increased to 30 wt. %, decreased crystallization rate was observed, attributed to the formation of POSS aggregates large enough to hinder the mobility of the polypropylene chains during blend cooling. In a similar paper, Chen et al. studied the effect of blending smaller loading levels of OM POSS (compared to the large amounts used in the previous study) on the

crystallization rate of polypropylene.[104] The authors reported that as POSS concentration was incrementally increased from 0 to 10 wt. %, a decrease in the time needed to reach the exothermic maximum, as well as a slight increase in peak crystallization temperature (9-17°C for 1-10 wt % blends), was observed. Again, this was attributed to POSS nanocrystals serving as nucleation points in the polymer matrix.

Different crystallization behavior relative to incorporation of POSS into a polyolefin matrix was reported by Joshi et al., who monitored both the isothermal and non-isothermal crystallization of HDPE/OM POSS blends.[109,110] In the non-isothermal study OM POSS was reported to have no effect on HDPE crystallization behavior until a loading level of 10 wt. % POSS was reached, after which bulk crystallinity was reported to decrease by 3% (verified by both DSC and WAXD) attributed to POSS aggregates hindering chain mobility during crystallization. In the isothermal study OM POSS was reported to have a minimal effect on crystallization rate at low concentration, followed by decreasing crystallization rate as POSS concentration was increased to higher concentration.

Though most of the initial studies of melt-blended POSS systems involved the use of POSS with methyl substituents, the major appeal of POSS is the wide variety of functionalities available for melt-blend performance tuning. Scapini et al. examined the melt-blending of OiB POSS with a HDPE, ethylene-vinyl acetate (EVA), and an HDPE/EVA copolymer, and its effect on blend thermal and morphological properties compared to the neat materials.[113] TEM microscopy verified good distribution of POSS through the bulk of the neat HDPE, EVA and copolymer at low POSS concentration (1 wt. %), while at higher concentration the formation of large POSS aggregates was

reported. This was attributed to surpassing the solubility limit of OiB POSS in the matrices, leading to phase separation and POSS self-association. Unlike the previous studies, it was also reported that at no concentration did POSS have an effect on the crystallization of the blends compared to the neat materials, attributed to POSS having limited effect on chain mobility.

The first study into the effect of melt–blending POSS with various side groups into a polyolefin matrix was by that of Fina et al., who blended multiple POSS types (OM, OiB and octaisooctyl (OiO) into a polypropylene matrix.[99] The authors reported vastly different morphologies for the different nanocomposites relative to organic functionality. Via TEM, they reported that all POSS molecules had good dispersion at low concentration, but at 3 wt. % loading the OM POSS was found to cause micron-sized aggregates in the matrix. They argued that the methyl POSS, due to its decreased organic corona size, had a higher propensity for self-association due the forces of attraction between the relatively unprotected Si-O-Si cages. The OiB and OiO POSS types, due to their larger organic substituents and resulting shielding of the POSS cage (reduced cohesive forces between the POSS molecules), were said to have decreased propensity for self association, resulting in superior miscibility and dispersion.

In a complimentary study, Pracella et al. monitored the effect of POSS with different functionalities on both the isothermal and non-isothermal crystallization and melting behavior of polypropylene melt-blends.[112] This study was conducted under the premise that POSS types with different organic functionalities would have different dispersion characteristics in the polymer matrix, possibly resulting in different crystallization behavior. At all concentrations examined (0-10 wt. %) OM POSS was

shown to have a nucleating effect on the polypropylene (2% increase in bulk crystallinity at all concentrations), while OiO POSS was shown reduced blend crystallinity by up to 4%. They attributed the reduction in crystallinity associated with OiO POSS to its higher level of theoretical miscibility in the polypropylene matrix, with the assumption that a high level of dispersion hindered the macromolecular dynamics of the polypropylene chains. Relative to the OiB POSS, at lower concentrations (6 wt. %) the well-dispersed POSS was reported to hinder chain dynamics similar to the OiO POSS, resulting in a 6% decrease in bulk crystallinity. At higher concentration, the formation of larger POSS aggregates was reported to slightly increase bulk crystallinity by 1% compared to the neat polypropylene attributed to POSS nanocrystals having a nucleating effect on the polypropylene chains.

Effects of POSS on Polyolefin Physical and Rheological Properties

In addition to crystallization effects, incorporation of POSS has also been shown to result in mixed mechanical performance when melt blended with polyolefin matrices. Baldi et al. studied the effect of incorporation of POSS molecules with different organic functionalities on the mechanical performance of polypropylene.[103] The authors reported a 3-8% increase Young's modulus and decreased ultimate yield strength with increasing concentration of OM POSS (3-10 wt. %) compared to the neat polypropylene samples. Alternatively, OiB and OiO POSS were both reported to decrease Young's modulus (as much as 26%) and yield stress, the effects increasing with increasing POSS content. The authors attributed this behavior to the dynamics of the organic POSS corona, and its soft nature as compared to the stiff siliceous core of the POSS molecule. They argued that increasing the length of the POSS substituents resulted in decreased stress transfer from

the matrix to the hard POSS core, resulting in inferior properties compared to the methyl POSS.

Lim et al. examined the effect of POSS on the thermal and mechanical properties of a polyethylene matrix, and reported very different results than the previous study.[111] OM, OiB and octaphenyl (OP) POSS were melt blended with a relatively low molecular weight polyethylene at concentrations of 0.5, 1 and 2 wt. % POSS. Mechanically, they reported that at all concentrations the tensile strength of the POSS blends was higher than that of the neat polyethylene, with OiB showing the highest level of enhancement (92% increase) at 0.5 wt. %. As concentration was increased tensile strength was found to decrease, but even at the highest loading levels was still superior to the neat polyethylene. The authors argued that the superior reinforcing potential of the OiB POSS compared to the OM and OP molecules was due to the high level of theoretical solubility of the OiB POSS into the polyethylene matrix, leading to superior stress transfer from the matrix to the stiff POSS cage.[130]

As far as rheology is concerned, Joshi et al. probed the relationship between OM POSS loading level and viscoelastic performance of HDPE.[110] The authors reported that at low concentrations (<0.5 wt%) the introduction of OM POSS resulted in an 8% decrease in melt viscosity, attributed to well-dispersed POSS nanocrystals serving to decrease chain entanglement and consequently increase free volume in the melt. At higher concentrations (> 0.5 wt%) OM POSS was shown to increase melt viscosity compared to the neat HDPE, attributed to larger POSS aggregates hindering chain mobility. These findings are similar to those of Xie et al., who reported a 40% decrease in complex viscosity for nanocomposites of PVC and 2 wt. % nano-$CaCO_3$ filler (40-65

nm in diameter via TEM). The authors argued that spherical nano-$CaCO_3$ particles could serve as nano "ball bearings" thereby increasing inter-chain spacing and decreasing blend complex viscosity at low filler concentration, while at higher concentration clustering of nanoparticles reduced these effects.[11]

A similar study was conducted by Zhou et al., who compared the effects of melt blending compared to reactive blending of octavinyl (OV) POSS with an isotactic polypropylene matrix.[115] The authors reported an 18% decrease in complex viscosity for the blends compared to the neat polypropylene at low POSS concentration (0.5 wt. %), followed by an increase in viscosity with increasing POSS concentration (45% increase compared to neat polypropylene at 10 wt. % POSS). These findings are in agreement with the previous study, though different results relative to the effects of POSS on storage and loss modulus were reported. For the reactively blended systems, it was reported that blend viscosity increased with increasing POSS loading, displaying solid-like behavior at POSS loading levels of 1 wt. % and higher. It was argued that the increased viscosity of the reactively-blended samples was due to the strong interactions between the POSS and matrix, resulting in sample gelatin that is not present in the melt-blended systems.

Looking at a slightly more complex system, Fu et al. examined the rheological behavior of melt-blended POSS/ethylene-propylene copolymers.[106] Both OM and OiB POSS samples were processed and examined. In opposition to the above studies, the authors reported increased viscosity compared to the neat matrix at all POSS concentrations, with a transition from melt-like rheological behavior for the neat sample to solid-like behavior for all POSS blends. They argue that the thorough dispersion of POSS nanocrystals forms a 3D network which imparts solid-like rheological behavior in

the blends. Additionally, decreased chain mobility due to the formation of POSS crystallites (verified by WAXD) is also mentioned as a potential explanation for the solid-like behavior.

Effects of POSS on Surface and Dispersion Properties

At this time, little has been reported in the literature relative to the surface properties of POSS melt-blends.[97,120,127] Surface studies that are reported have primarily focus on either fluorinated POSS derivatives, or systems in which POSS is chemically bonded to the polymer matrix. Miyamoto et al. and Paul et al. reported enhanced dewetting of thin films of polystyrene and poly(tert-butyl acrylate), respectively, attributed to surface blooming of chemically incorporated POSS cages.[131,132] In the poly(tert-butyl acrylate study, it was reported that increasing annealing temperature from 75°C to 95°C resulted in enhanced POSS phase separation and surface segregation, as verified by AFM and X-ray photoelectron spectroscopy.[132] Mammeri et al. chemically reacted dimethylsiloxy isobutyl POSS with both cyclohexylmethacrylate and tetra-ethoxylatedbisphenol-A, and goniometry reported a 30° water contact angle increase for the POSS blends, attributed to effects of the highly-polar POSS cages residing on the sample surfaces.[133] Tujeta et al. and Iacono et al. have reported highly hydrophobic and oleophobic surfaces for blends of fluorinated POSS with PMMA and perfluorocyclobutyl aryl ether polymers, respectively, attributed to increased surface roughness and enhanced reentrant surface effects.[134,135] Koh et al. have also reported surface enrichment for fluorinated POSS/PMMA nanocomposites, where XPS analysis revealed a 50% increase in POSS surface enrichment for annealed samples (180°C for five days) compared to non-annealed samples, as well as a depth-dependent POSS concentration gradient (15 wt.

% POSS decrease over the first 8 nm of penetration).[136] Enhanced surface enrichment was attributed to the low surface free energy of the POSS molecules, whereby annealing led to increased surface segregation.[136]

In melt-blended systems, results from our lab show preferential surface segregation of crystalline POSS in a variety of organic matrices.[97,120,127] AFM revealed that incorporation of 10 wt. % OiB POSS into polypropylene resulted in a 90% increase in RMS surface roughness and an 80% decrease in nano-scale coefficient of friction, while nanoindentation revealed a 100% increase in surface modulus. Increased surface roughness and modulus were attributed to migration of the robust POSS nanocrystals to the sample surface, thus affecting overall surface energy and mechanical performance. Variable-angle ATR-FTIR analysis of the same nanocomposites revealed higher concentrations of POSS near the sample surface as compared to the bulk, attributed to decreased miscibility and competing enthalpic/entropic interactions between the highly-polar POSS molecules and the non-polymer matrices driving segregation.[97] Additional findings reported from our lab are decreased surface energy for Nylon-6 upon incorporation of 10 wt. % OiB and trisilanol phenyl (TSP) POSS (48% and 45%, respectively), as well as changes in observed POSS miscibility (verified by TEM-EDAX) based on molecular structure.[120,127] At the present time, no reports have been found in the literature which relate POSS substituent chain length, cage structure, or physical state to observed surface behaviors of POSS/polymer blends. Additionally, no surface-specific studies have been found relative to incorporation of POSS into a highly-crystalline matrix. Degree of crystallinity has been shown to be a dominant factor in polyethylene surface properties.[40] Though depth profiling has shown the propensity of POSS to

surface segregate in melt-blended POSS/polypropylene systems, there are no reports as to the effects of POSS on surface degree of crystallinity.

Solubility Parameters

As has been reviewed, realization of the full potential of nanofiller utilization is only accomplished when there is good interaction between the filler and matrix. Miscibility between the different components of a blend is governed by the Gibb's free energy of mixing (ΔG_m) equation:

$$\Delta G_m = \Delta S_m - T\Delta S_m \tag{1}$$

where ΔH_m is the enthalpy of mixing, T is the absolute temperature of the system, and ΔS_m is the resultant entropy of mixing. A negative ΔG_m generally indicates good mixing between components, while a positive ΔG_m is indicative of phase separation due to poor miscibility. For polymer composites consisting of only two components, calculations of ΔG_m, ΔH_m and ΔS_m can be completed using the Flory-Huggins equations:

$$\frac{\Delta G_m}{V} = B\Phi_A\Phi_B + RT\left(\frac{\rho_A\Phi_A \ln\Phi_A}{M_A} + \frac{\rho_B\Phi_B \ln\Phi_B}{M_B}\right) \tag{2}$$

$$\frac{\Delta H_m}{V} = B\Phi_A\Phi_B \tag{3}$$

$$\frac{\Delta S_m}{V} = R\left(\frac{\rho_A\Phi_A \ln\Phi_A}{M_A} + \frac{\rho_B\Phi_B \ln\Phi_B}{M_B}\right) \tag{4}$$

where V is the total volume of the composite, B is an interaction parameter, R is the ideal gas constant, M is the molecular weight of components A and B, Φ is the volume fraction of components A and B, and ρ is the density of components A and B. Hildebrand expanded upon these equations to take into account experimental solubility parameter (δ), resulting in the equation:

$$\frac{\Delta G_m}{V} = \left(\delta_A - \delta_B\right)^2 \Phi_A \Phi_B + RT\left(\frac{\rho_A \Phi_A \ln \Phi_A}{M_A} + \frac{\rho_B \Phi_B \ln \Phi_B}{M_B}\right) \quad (5)$$

and leading to the derivation of:

$$\Delta H_m = V\left(\delta_1 - \delta_2\right)^2 \Phi_1 \Phi_2 \quad (6)$$

Equation 6 states that for good mixing (minimization of ΔH_m), the solubility parameters of components 1 and 2 of a composite should be as similar as possible.

For most polymers and solvents, solubility parameters are estimated based on experimental data from either light scattering or heat of vaporization studies. These data allow estimations of cohesive energy density (E_{coh}), which can be related to solubility parameter by the equation:

$$\delta = {E_{coh}}^2 \quad (7)$$

Unfortunately, many nanofillers (such as POSS) have limited solvent solubility and do not readily vaporize, leading to theoretical estimations as the only means of solubility parameter calculations. The Hoy and van Krevelen group contribution methods are the two most widely accepted methods for theoretical solubility parameter estimation. Both rely heavily on the molecular architecture of the material in question, as well as the structural groups present, and utilize the formula:

$$\delta = \left(\frac{\rho \sum G_i}{M_o}\right) \quad (8)$$

where δ is the calculated solubility parameter, ρ is the material density, G_i is a molar attraction constant representing a structural groups present in the molecule, and M_o is the molecular weight of the material. Molar attraction constants for the two methods are estimated via a library of experimentally determined values. As such, the greater the

number of a particular type of structural group present in the library, the more accurate the molar attraction constant for that particular group will become.[137] A fundamental problem with POSS relative to solubility parameter calculations is that the molecule is comprised of a siloxane core, a chemical structure that is not well represented in group contribution libraries. There have been studies reported in literature where authors utilized molar attraction constants associated with polydimethylsiloxane (PDMS) as a substitute for that of the S-O siloxane cage structure, though PDMS is of a different chemical structure and does not accurately differentiate between open and close-cage types of POSS.[138-140] Another method reported is to assume that the siloxane part of the POSS molecule does not interact with the organic matrix material, and thus the functional groups on the outer part of the POSS molecule dominate the solubility parameter.[141,142] Though these methods give a rather crude estimation of the solubility parameter of the various types of POSS, all of the studies have found correlation between the values calculated and experimental data returned (i.e., POSS types with similar theoretically-calculated solubility parameters to the polymer matrix exhibit better homogeneity and physical properties). Theoretical solubility parameter estimations present an interesting venue for modeling dispersion of different POSS types into a range of organic matrices.

Motivation and Contribution of Research

It has been shown that incorporation of small amounts of POSS can have dramatic effects on melt-blend properties. Although multiple polyolefin matrices have been examined relative to POSS incorporation, the literature shows mixed results relative to crystallization, mechanical and rheological effects due to incorporation of POSS into melt-blended polyolefin matrices. Additionally, very few studies have examined the

effect of POSS on a highly-crystalline polymer matrix. In regards to POSS cage structure, there is limited research directly comparing the physical properties of POSS blends prepared using both closed and open-cage derivatives, or the effect of potential trisilanol cage condensation reactions on blend properties. In terms of blend viscoelastic properties, relatively few studies have been completed which gauge the utilization of POSS as a potential rheological processing aid, or the difference in observed properties relative to the use of solid compared to liquid POSS derivatives. This study seeks to further refine how POSS structure and physical state relate to observed bulk and surface behaviors in HDPE. Of primary interest is to refine how POSS molecular structure and physical state correspond to miscibility in a highly-crystalline HDPE matrix, as well as to determine if compatibility and property enhancement can be predicted based on said structure. Effects of POSS on processing and melt-state behavior will be monitored through analysis of extruder output during melt-blending, as well as parallel-plate rheological analysis. Bulk thermal and mechanical analysis will be conducted relative to a series of standardized testing methods. Surface effects will be probed using both scanning probe techniques, as well as by IR spectroscopy. Ultimately, behavioral trends will be related to observed POSS miscibility for the various POSS molecules, as well as their dependence on physical state and cage structure.

This dissertation is comprised of six chapters. Chapter II gives an overview of the research goals and specific objectives of this research. Chapter III probes the influence of POSS functionality, cage structure and physical state on the bulk properties (thermal, rheological, mechanical) of the melt-blended HDPE/POSS blends. Chapter IV explores surface modification as a function of POSS incorporation, as well as aggregation and

migrational behavior of the POSS molecules. Chapter V surveys POSS theoretical solubility parameter estimations via both group contribution theory and molecular dynamics simulations, and correlates these values with observed effects of POSS on blend morphology. Finally, Chapter VI provides recommendations for future work in an attempt to further refine the complex behaviors and trends observed in our HDPE/POSS systems.

REFERENCES

1. Hall, L. M.; Jayaraman, A.; Schweizer, K. S. Curr. Opin. Solid State Mater. Sci. **2010**, 14, 38-48.

2. Jancar, J.; Douglas, J.; Starr, F. W.; Kumar, S.; Cassagnau, P.; Lesser, A.; Sternstein, S. S.; Buehler, M. Polymer **2010**, 51, 3321-3343.

3. Vaia, R. A.; Giannelis, E. P. MRS Bull. **2001**, 26, 394-401.

4. Binnig, G.; Quate, C. F.; Gerber, C. Phys. Rev. Lett. **1986**, 56, 930-933.

5. Tjong, S. Mater. Sci. Eng., R **2006**, 53, 73-197.

6. Haile, J. M. Introduction. In *Molecular dynamics simulation: elementary methods*; John Wiley & Sons, Inc.: New York, 1992; Chapter 1, pp 4-11.

7. Starr, F. W.; Schroder, T. B.; Glotzer, S. C. Macromolecules **2002**, 35, 4481-4492.

8. Hussain, F.; Hojjati, M.; Okamoto, M.; Gorga, R. E. J. Compos. Mater. **2006**, 40, 1511-1575.

9. Usuki, A.; Kojima, Y.; Kawasumi, M.; Okada, A.; Fukushima, Y.; Kurauchi, T.; Kamigaito, O. J. Mater. Res. **1993**, 8, 1179-1184.

10. Ajayan, P.; Zhou, O. Carbon Nanotubes **2001**, 391-425.

11. Ebbesen, T.; Ajayan, P. Nature **1992**, 358, 220-222.

12. Saito, R.; Dresselhaus, G.; Dresselhaus, M. S. Elastic properties of carbon nanotubes. In *Physical properties of carbon nanotubes*; Imperial College Press: London, 1998; Chapter 11, pp 207-221.

13. Harris, P. J. F.; Hernandez, E.; Yakobson, B. I. Am. J. Phys. **2004**, 72, 415.

14. Rodriguez, N. J. Mater. Res. **1993**, 8, 3233-3250.

15. Huang, Z. M.; Zhang, Y. Z.; Kotaki, M.; Ramakrishna, S. Compos. Sci. Technol. **2003**, 63, 2223-2253.

16. Frenot, A.; Chronakis, I. S. Curr. Opin. Colloid Interface Sci. **2003**, 8, 64-75.

17. De Jong, K. P.; Geus, J. W. Catal. Rev.: Sci. Eng. **2000**, 42, 481-510.

18. Huang, M. H.; Wu, Y.; Feick, H.; Tran, N.; Weber, E.; Yang, P. Advan. Mater. **2001**, 13, 113-116.

19. Wu, Y.; Cui, Y.; Huynh, L.; Barrelet, C. J.; Bell, D. C.; Lieber, C. M. Nano Letters **2004**, 4, 433-436.

20. Murphy, C. J.; Jana, N. R. Adv. Mater. **2002**, 14, 80.

21. Hu, J.; Odom, T. W.; Lieber, C. M. Acc. Chem. Res. **1999**, 32, 435-445.

22. Dresselhaus, M. S.; Dresselhaus, G.; Eklund, P. Carbon materials. In *Science of fullerenes and carbon nanotubes*; Elsevier: San Diego, 1996; Chapter 2, pp. 15-20.

23. Jensen, A. W.; Wilson, S. R.; Schuster, D. I. Bioorg. Med. Chem. **1996**, 4, 767-779.

24. Haddon, R. Science **1993**, 261, 1545.

25. Hirsch, A. The parent fullerenes. In *The chemistry of the fullerenes*; Thieme Medical Publishers: New York, **1994**; Chapter 1, pp 25-29.

26. LeBaron, P. C.; Wang, Z.; Pinnavaia, T. J. Appl. Clay Sci. **1999**, 15, 11-29.

27. Galgali, G.; Agarwal, S.; Lele, A. Polymer **2004**, 45, 6059-6069.

28. Batra, M.; Gotam, S.; Dadarwal, P.; Nainwani, R.; Sharma, M.

29. Manias, E.; Touny, A.; Wu, L.; Strawhecker, K.; Lu, B.; Chung, T. Chem. Mater. **2001**, 13, 3516-3523.

30. Lau, K.; Gu, C.; Hui, D. Composites, Part B **2006**, 37, 425-436.

31. Fendler, J. H. Synthesis of silicon nanoclusters. In *Nanoparticles and nanostructured films: preparation, characterization and applications*; Wiley: New York, 1998; Chapter 5, pp 111-116.

32. Schmidt, G.; Malwitz, M. M. Curr. Opin. Colloid Interface Sci. **2003**, 8, 103-108.

33. Yu, L.; Andriola, A. Talanta **2010**, 82, 869-875.

34. Balazs, A. C.; Emrick, T.; Russell, T. P. Science **2006**, 314, 1107.

35. Jordan, J.; Jacob, K. I.; Tannenbaum, R.; Sharaf, M. A.; Jasiuk, I. Mater. Sci. Eng., A **2005**, 393, 1-11.

36. Gacitua, W.; Ballerini, A.; Zhang, J. Maderas. Cienc. Tecnol. (Washington, D. C.) **2005**, 7, 159-178.

37. Pavlidou, S.; Papaspyrides, C. Prog. Polym. Sci. **2008**, 33, 1119-1198.

38. Sinha Ray, S.; Okamoto, M. Prog. Polym. Sci. **2003**, 28, 1539-1641.

39. Coleman, J. N.; Khan, U.; Blau, W. J.; Gun'ko, Y. K. Carbon **2006**, 44, 1624-1652.

40. Peacock, A. J. Use and fabrication of polyethylene products. In *Handbook of polyethylene: structures, properties, and applications*; CRC Press: New York, 2000, Chapter 9, pp 502-204.

41. Tincer, T.; Corükun, M. Polym. Eng. Sci. **1993**, 33, 1243-1250.

42. Yu, T.; Wilkes, G. L. Polymer **1996**, 37, 4675-4687.

43. Li, Y.; Hu, C.; Yu, Y. Composites, Part A **2008**, 39, 570-578.

44. Zou, Y.; Feng, Y.; Wang, L.; Liu, X. Carbon **2004**, 42, 271-277.

45. Tang, W.; Santare, M. H.; Advani, S. G. Carbon **2003**, 41, 2779-2785.

46. Bula, K.; Jesionowski, T. Compos. Interfaces **2010**, 5, 603-614.

47. Gao, J. L.; Liu, Y. H.; Wei, S. D. Adv. Mater. Res. **2011**, 279, 115-119.

48. Xu, W.; Zhai, H.; Guo, H.; Zhou, Z.; Whitely, N.; Pan, W. P.J. Therm. Anal. Calorim. **2004**, 78, 101-112.

49. Liang, G.; Xu, J.; Bao, S.; Xu, W. J. Appl. Polym. Sci. **2004**, 91, 3974-3980.

50. Min, K. D.; Kim, M. Y.; Choi, K. Y.; Lee, J. H.; Lee, S. G. Polym. Bull. **2006**, 57, 101-108.

51. Kanagaraj, S.; Varanda, F. R.; Zhil'tsova, T. V.; Oliveira, M. S. A.; Simules, J. A. O. Compos. Sci. Technol. **2007**, 67, 3071-3077.

52. Haggenmueller, R.; Fischer, J. E.; Winey, K. I. Macromolecules **2006**, 39, 2964-2971.

53. Chrissafis, K.; Paraskevopoulos, K.; Tsiaoussis, I.; Bikiaris, D. J. Appl. Polym. Sci. **2009**, 114, 1606-1618.

54. Lichtenhan, J. D. Comments on Inorg. Chem. **1995**, 17, 115-130.

55. Scott, D. W. J. Am. Chem. Soc. **1946**, 68, 356.

56. Kannan, R. Y.; Salacinski, H. J.; Butler, P. E.; Seifalian, A. M. Acc. Chem. Res. **2005**, 38, 879-884.

57. Phillips, S. H.; Haddad, T. S.; Tomczak, S. J. Curr. Opin. Solid State Mater. Sci. **2004**, 8, 21-29.

58. Gnanasekaran, D.; Madhavan, K.; Reddy, B. J. Sci. Ind. Res. **2009**, 68, 437-464.

59. Fina, A.; Monticelli, O.; Camino, G. J. Mater. Chem. **2010**, 20, 9297-9305.

60. Brown, J. F., Vogt, L.H. J. Am. Chem. Soc. **1965**, 87, 4313.

61. Feher, F. J., Soulivong, D. Lewis, G.T. J. Am. Chem. Soc. **1997**, 119, 11323.

62. Hu, J. K.; Zhang, Q. C.; Gong, S. L. Chin. Chem. Lett. **2011**, 23, 181-184.

63. Baumann, T. F.; Jones, T. V.; Wilson, T.; Saab, A. P.; Maxwell, R. S. J. Polym. Sci., Part A: Polym. Chem. **2009**, 47, 2589-2596.

64. Huang, J. M.; Huang, H. J.; Wang, Y. X.; Chen, W. Y.; Chang, F. C. J. Polym. Sci., Part B: Polym. Phys. **2009**, 47, 1927-1934.

65. Lach, R.; Michler, G. H.; Grellmann, W. Macromol. Mater. Eng. **2010**, 295, 484-491.

66. Liang, K.; Toghiani, H.; Pittman, C. U. J. Inorg. Organomet. Polym. Mater. **2011**, 1-15.

67. Madbouly, S. A.; Otaigbe, J. U. Progress in polymer science **2009**, 34, 1283-1332.

68. Paul, D. R.; Mark, J. E. Prog. Polym Sci. **2010**, 35, 893-901.

69. Zheng, L. Diss. Abstr. Int., B **2002,** 63, 4708-4806.

70. Qin, Y. W.; Dong, J. Y. Chin. Sci. Bull. **2009**, 54, 38-45.

71. Zhang, H.; Shin, Y.; Yoon, K.; Lee, D. Eur. Polym. J. **2009**, 45, 40-46.

72. Zhou, Z.; Cui, L.; Zhang, Y.; Yin, N. Eur. Polym. J. **2008**, 44, 3057-3066.

73. Xu, H.; Yang, B.; Wang, J.; Guang, S.; Li, C. J. Polym. Sci., Part A: Polym. Chem. **2007**, 45, 5308-5317.

74. Kopesky, E. T.; Haddad, T. S.; McKinley, G. H.; Cohen, R. E. Polymer **2005**, 46, 4743-4752.

75. Zhang, W.; Fu, B. X.; Seo, Y.; Schrag, E.; Hsiao, B.; Mather, P. T.; Yang, N. L.; Xu, D.; Ade, H.; Rafailovich, M. Macromolecules **2002**, 35, 8029-8038.

76. Kopesky, E. T.; Haddad, T. S.; Cohen, R. E.; McKinley, G. H. Macromolecules **2004**, 37, 8992-9004.

77. Lee, A.; Xiao, J.; Feher, F. J. Macromolecules **2005**, 38, 438-444.

78. Wu, J.; Haddad, T. S.; Kim, G. M.; Mather, P. T. Macromolecules **2007**, 40, 544-554.

79. Romo-Uribe, A.; Mather, P.; Haddad, T.; Lichtenhan, J. J. Polym. Sci., Part B: Polym. Phys. **1998**, 36, 1857-1872.

80. Bizet, S.; Galy, J.; Grachard, J. F. Polymer **2006**, 47, 8219-8227.

81. Tadmor, Z.; Gogos, C. G. Mixing. In *Principles of polymer processing*; Wiley: New York, 2006, Chapter 7, pp 322-357.

82. Mackay, M. E.; Tuteja, A.; Duxbury, P. M.; Hawker, C. J.; Van Horn, B.; Guan, Z.; Chen, G.; Krishnan, R. Science **2006**, 311, 1740.

83. McNally, T.; P√∂tschke, P.; Halley, P.; Murphy, M.; Martin, D.; Bell, S. E. J.; Brennan, G. P.; Bein, D.; Lemoine, P.; Quinn, J. P. Polymer **2005**, 46, 8222-8232.

84. Bhattacharyya, A. R.; Sreekumar, T.; Liu, T.; Kumar, S.; Ericson, L. M.; Hauge, R. H.; Smalley, R. E. Polymer **2003**, 44, 2373-2377.

85. Kashiwagi, T.; Grulke, E.; Hilding, J.; Harris, R.; Awad, W.; Douglas, J. Macromol. Rapid Commun. **2002**, 23, 761-765.

86. Zhang, Q.; Rastogi, S.; Chen, D.; Lippits, D.; Lemstra, P. J. Carbon **2006**, 44, 778-785.

87. Narkis, M.; Ram, A.; Stein, Z. J. Appl. Polym. Sci. **1980**, 25, 1515-1518.

88. Thongruang, W.; Balik, C. M.; Spontak, R. J. J. Polym. Sci., Part B: Polym. Phys. **2002**, 40, 1013-1025.

89. Zhang, Q. H.; Chen, D. J. J. Mater. Sci. **2004**, 39, 1751-1757.

90. Huang, J. C. Adv. Polym. Technol. **2002**, 21, 299-313.

91. Faruk, O.; Matuana, L. M. Compos. Sci. Technol. **2008**, 68, 2073-2077.

92. Kawasumi, M.; Hasegawa, N.; Kato, M.; Usuki, A.; Okada, A. Macromolecules **1997**, 30, 6333-6338.

93. Lei, Y.; Wu, Q.; Clemons, C. M.; Yao, F.; Xu, Y. J. Appl. Polym. Sci. **2007**, 106, 3958-3966.

94. Baniasadi, H.; Ramazani SA, A.; Javan Nikkhah, S. Mater. Des. **2010**, 31, 76-84.

95. Lertwimolnun, W.; Vergnes, B. Polymer **2005**, 46, 3462-3471.

96. Andersen, P. Appl. Rheol. **2006,** 16, 198-205.

97. Misra, R.; Fu, B. X.; Morgan, S. E. J. Polym. Sci., Part B: Polym. Phys. **2007**, 45, 2441-2455.

98. Fu, B.; Hsiao,B.; Pagola, S.; Stephens, H.; White, H.; Rafilovich, J.; Sokolov, J.; Mather, P.; Jeon, H.; Phillips, S.; Lichtenhan, J.; Schwab, J. Polymer **2001**, 42, 599-611.

99. Fina, A.; Tabuani, D.; Frache, A.; Camino, G. Polymer **2005**, 46, 7855-7866.

100. Li, G.; Wang, L.; Ni, H.; Pittman, C. U. Journal of Inorganic and Organometallic Polymers **2001**, 11, 123-154.

101. Waddon, A.; Zheng, L.; Farris, R.; Coughlin, E. B. Nano Lett. **2002**, 2, 1149-1155.

102. Zheng, L.; Farris, R. J.; Coughlin, E. B. Journal of Polymer Science Part A: Polymer Chemistry **2001**, 39, 2920-2928.

103. Baldi, F.; Bignotti, F.; Fina, A.; Tabuani, D.; Ricco, T. J. Appl. Polym. Sci. **2007**, 105, 935-943.

104. Chen, J. H.; Yao, B. X.; Su, W. B.; Yang, Y. B. Polymer **2007**, 48, 1756-1769.

105. Fina, A.; Tabuani, D.; Carniato, F.; Frache, A.; Boccaleri, E.; Camino, G. Thermochim. Acta **2006**, 440, 36-42.

106. Fu, B. X.; Gelfer, M. Y.; Hsiao, B. S.; Phillips, S.; Viers, B.; Blanski, R.; Ruth, P. Polymer **2003**, 44, 1499-1506.

107. Fu, B. X.; Yang, L.; Somani, R. H.; Zong, S. X.; Hsiao, B. S.; Phillips, S.; Blanski, R.; Ruth, P. J Polym. Sci., Part B: Polym. Phys. **2001**, 39, 2727-2739.

108. Joshi, M.; Butola, B. Polymer **2004**, 45, 4953-4968.

109. Joshi, M.; Butola, B. J. Appl. Polym. Sci. **2007**, 105, 978-985.

110. Joshi, M.; Butola, B.; Simon, G.; Kukaleva, N. Macromolecules **2006**, 39, 1839-1849.

111. Lim, S. K.; Hong, E. P.; Choi, H. J.; Chin, I. J. J. Ind. Eng. Chem. (Washington, D. C.) **2010**, 16, 189-192.

112. Pracella, M.; Chionna, D.; Fina, A.; Tabuani, D.; Frache, A.; Camino, G. Macromol. Symp. **2006**, 234, 59-67.

113. Scapini, P.; Figueroa, C. A.; Amorim, C. L. G.; Machado, G.; Mauler, R. S.; Crespo, J. S.; Oliveira, R. V. B. Polym. Int. **2010**, 59, 175-180.

114. Wheeler, P. A.; Misra, R.; Cook, R. D.; Morgan, S. E. J. Appl. Polym. Sci. **2008**, 108, 2503-2508.

115. Zhou, Z.; Cui, L.; Zhang, Y.; Yin, N. J. Polym. Sci., Part B: Polym. Phys. **2008**, 46, 1762-1772.

116. Lee, S.; Hahm, W.; Kikutani, T.; Kim, B. Polym. Eng. Sci. **2009**, 49, 317-323.

117. Vannier, A.; Duquesne, S.; Bourbigot, S.; Castrovinci, A.; Camino, G.; Delobel, R. Polym. Degrad. Stab. **2008**, 93, 818-826.

118. Zeng, J.; Kumar, S.; Iyer, S.; Schiraldi, D. A.; Gonzalez, R. High Perf. Polym. **2005**, 17, 403-424.

119. Zeng, J.; Bennett, C.; Jarrett, W. L.; Iyer, S.; Kumar, S.; Mathias, L. J.; Schiraldi, D. A. Compos. Interfaces, **2005**, 8, 673-685.

120. Misra, R.; Fu, B. X.; Plagge, A.; Morgan, S. E. J. Polym. Sci., Part B: Polym. Phys. **2009**, 47, 1088-1102.

121. Zhao, F.; Bao, X.; McLauchlin, A. R.; Gu, J.; Wan, C.; Kandasubramanian, B. Appl. Clay Sci. **2010**, 47, 249-256.

122. Dasari, A.; Yu, Z. Z.; Mai, Y. W.; Cai, G.; Song, H. Polymer **2009**, 50, 1577-1587.

123. Li, B.; Zhang, Y.; Wang, S.; Ji, J. Eur. Polym. J. **2009**, 45, 2202-2210.

124. Zhao, Y.; Schiraldi, D. A. Polymer **2005**, 46, 11640-11647.

125. Sanchez-Soto, M.; Schiraldi, D. A.; Illescas, S. Eur. Polym. J. **2009**, 45, 341-352.

126. Song, L.; He, Q.; Hu, Y.; Chen, H.; Liu, L. Polym. Degrad. Stab. **2008**, 93, 627-639.

127. Misra, R.; Alidedeoglu, A. H.; Jarrett, W. L.; Morgan, S. E. Polymer **2009**, 50, 2906-2918.

128. Kopesky, E. T.; Boyes, S. G.; Treat, N.; Cohen, R. E.; McKinley, G. H. Rheol. Acta **2006**, 45, 971-981.

129. Liu, L.; Hu, Y.; Song, L.; Nazare, S.; He, S.; Hull, R. J. Mater. Sci. **2007**, 42, 4325-4333.

130. Krevelen, D. W. Cohesive properties and solubility. In *Properties of polymers*; Elsevier: New York, **2009**, Chapter 7, pp 201-221.

131. Miyamoto, K.; Hosaka, N.; Kobayashi, M.; Otsuka, H.; Yamada, N.; Torikai, N.; Takahara, A. Polym. J. **2007**, 39, 1247-1252.

132. Paul, R.; Karabiyik, U.; Swift, M. C.; Esker, A. R. Langmuir **2008**, 24, 5079-5090.

133. Mammeri, F.; Bonhomme, C.; Ribot, F.; Babonneau, F.; Direa, S. Chem. Mater. **2009**, 21, 4163-4171.

134. Tuteja, A.; Choi, W.; Ma, M.; Mabry, J. M.; Mazzella, S. A.; Rutledge, G. C.; McKinley, G. H.; Cohen, R. E. Science **2007**, 318, 1618-1621.

135. Iacono, S. T.; Budy, S. M.; Smith, D. W.; Mabry, J. M. J. Mater. Chem. **2010**, 20, 2979-2984.

136. Koh, K.; Sugiyama, S.; Morinaga, T.; Ohno, K.; Tsujii, Y.; Fukuda, T.; Yamahiro, M.; Iijima, T.; Oikawa, H.; Watanabe, K. Macromolecules **2005**, 38, 1264-1270.

137. Hansen, C. M. Statistical thermodynamic calculations of the hydrogen bonding, dipolar, and dispersion solubility parameters. In *Hansen solubility parameters: a user's handbook*; CRC Press: New York, **2007**, Chapter 3, pp 33-43.

138. Liu, L.; Ming, T.; Liang, G.; Chen, W.; Zhang, L.; Mark, J. E. J. Macromol. Sci., Part A Pure Appl. Chem. **2007**, 44, 659-664.

139. Misra, R.; Fu, B. X.; Plagge, A.; Morgan, S. E. J. Polym. Sci., Part B: Polym. Phys. **2009**, 47, 1088-1102.

140. Gadodia, G. A.; Yang, L.; Cardoen, G.; Russell, T. P.; Coughlin, E. B. PMSE Prepr. **2007**, 96, 41-42.

141. Lim, S.-K.; Hong, E.-P.; Choi, H. J.; Chin, I.-J. J. Ind. Eng. Chem. (Amsterdam, Neth.) **2010**, 16, 189-192.

142. Fu, B. X.; Namani, M.; Lee, A. Polymer **2003**, 7739-7747.

CHAPTER II

OBJECTIVES OF RESEARCH

The use of nano-scale filler material in the creation of polymer composites has the potential to provide property enhancements that are not easily attainable through the use of conventional micro-scale fillers. Examples of this are improved mechanical and thermal performance, with limited to no effect on processing behavior. This is inherently due to the large surface to volume ratios that typically define nano-filler geometry, as well as the relatively small concentrations of filler necessary to realize desirable property enhancements. As with all filler material, level of property enhancement is strongly related to level of interaction with the polymer matrix: if there is poor miscibility between the matrix and nanofiller, aggregation and phase separation may lead to blend characteristics similar to those of microcomposites, negating the potential benefits associated with the use of nanofillers.

Understanding the factors that control the molecular dispersion of a particular nanofiller through a composite matrix is essential to obtain optimum property enhancements. Polymer nanocomposites processed with nanofillers such as clays, nanotubes, nanowires, fullerenes and nanosilicas have all been shown to provide increased mechanical and thermal performance, with level of enhancement coinciding with level of dispersion and miscibility. Many methods have been attempted to control the miscibility and dispersion of nanofillers within polymer matrices, but almost all require the use of costly surface treatments that can be detrimental to matrix performance. Polyhedral oligomeric silsesquioxane (POSS) nanochemicals provide a unique approach to controlling miscibility not through surface treatment, but through altering the

molecular structure of the molecule itself. Physically, POSS molecules consist of a Si-O-Si framework inorganic core that is surrounded by a corona of organic substituents. These R-group substituents, which are attached to the corner silicon atoms, can be interchanged to a wide variety of organic functionalities, thereby allowing chemical tailoring of the molecular structure of the filler itself. Currently there are over 150 commercially available derivatives of POSS, encompassing a wide range of inorganic cage structures and organic functionalities.

When blended with organic matrices, POSS has been shown to provide a wide variety of mechanical, thermal, electrical and rheological performance enhancements. Level of property enhancement varies between systems, but it is suggested that degree of miscibility and dispersion of POSS through a matrix is a crucial factor affecting blend performance. In this work, we postulate that a fundamental understanding of the factors that affect POSS miscibility through a high density polyolefin matrix can be realized through monitoring blend performance relative to changes in the molecular structures and physical state of the various POSS derivatives analyzed.

This research document consists of two major sections, both concentrating on the miscibility of different POSS derivatives blended into a highly-crystalline HDPE matrix. The primary objective of the first section is to understand the effect of POSS cage structure, physical state and R-group alkyl chain length on miscibility and blend performance through a wide range of characterization techniques. Special attention will be paid to rheological, bulk and surface performance of the blends as compared to the neat matrix. The primary objective of the second section is to determine the utility of theoretical solubility parameter estimations as a means of predicting POSS miscibility in

the HDPE matrix. This section will focus on solubility parameters calculated using both group contribution and molecular dynamics simulation methods, determining their proximity to each other, and qualifying their applicability in predicting POSS miscibility/blend performance.

The specific goals of this research are to:

(1) Select appropriate POSS derivatives that are theoretically miscible in the polyethylene matrix, while also having slightly different individual solubility parameters and molecular structures.

(2) Successfully melt-blend HDPE/POSS systems over a range of applicable filler loading levels (0, 0.25, 0.5, 1, 2 and 5 wt. % POSS)

(3) Demonstrate the processing and rheological effects of POSS as a function of POSS molecular structure, physical state and loading level.

(4) Determine blend thermal property effects under both inert and thermooxidative conditions due to the incorporation of POSS.

(5) Analyze the effect of POSS on surface and bulk crystallinity via thermal, X-ray and variable-angle IR analysis.

(6) Assess the effect of POSS on blend mechanical performance (tensile, impact) relative to POSS molecular structure, physical state and loading level.

(7) Evaluate the miscibility and dispersion of POSS through the HDPE bulk and surface as a function of POSS molecular structure, physical state and loading level.

(8) Determine if there is correlation and/or applicability of theoretical solubility parameter estimates in terms of POSS/HDPE blend performance relative to POSS molecular structure.

(9) Develop an understanding of the relationship between POSS molecular structure (cage structure, R-group alkyl chain length) and interaction/dispersion within the highly-crystalline HDPE matrix.

Completion of the above goals has resulted in a thorough fundamental understanding of the effect of POSS molecular structure on miscibility and interaction with the highly-crystalline HDPE matrix. Additionally, the effects of POSS physical state and cage structure are also assessed in terms of theoretical and experimentally-determined miscibility. By understanding the dynamics that govern the dispersion of POSS molecules comprised of various physical states/cage structures, a more concrete screening process can be created relative to selection of POSS type relative to desired blend properties.

CHAPTER III

BULK AND RHEOLOGICAL PROPERTIES OF HIGH DENSITY POLYETHYLENE (HDPE)/POLYHEDRAL OLIGOMERIC SILSESQUIOXANE (POSS) BLENDS

Abstract

Hybrid organic/inorganic blends based on polyhedral oligomeric silsesquioxane (POSS) nanostructured chemicals and high density polyethylene (HDPE) were prepared via melt blending. Five POSS molecules were identified as suitable for evaluation due to their predicted compatibility with the HDPE matrix, as well as their thermal stability under the necessary HDPE processing conditions. POSS derivatives chosen were octamethyl (OM), octaisobutyl (OiB), octaisooctyl (OiO), trisilanol isobutyl (TSiB) and trisilanol isooctyl (TSiO). Bulk characterization of processed blends revealed that system behavior is dependent not only on POSS R-group functionality, but also on POSS physical state and cage structure. Rheological and mechanical property modification was shown to be governed primarily by the physical state of the POSS molecules, while POSS miscibility was shown to dominate thermal behavior. Within POSS molecules of similar physical state, miscibility was shown to be governed by alkyl chain length. Additionally, the effects of trisilanol POSS cage condensation on miscibility and bulk properties are addressed.

Introduction

Polymeric nanocomposites have been the focus of intense research and development efforts over the last 25 years.[1-3] Research into the field was catalyzed in 1990 by Toyota Research Laboratories, who reported significant improvement in both mechanical and thermal performance of Nylon-6 through incorporation of small amounts

of nanoscale clay.[4] Compared to micro-scale fillers, enhanced composite performance through the use of nanofillers can be attributed to their small size, which results in very large surface area and therefore the potential of higher levels of physical interaction between the matrix and the filler surfaces.[2] Nanofillers span a wide range of layered materials, fibers and particles, examples of which are nanotubes,[5] nanofibers,[6] nanowires,[7] fullerenes,[8] nanoclays[9] and inorganic nanoparticles.[10,11] Properties generally associated with nanofillers are high stiffness/modulus, high thermal stability and good electrical conductivity, attributes generally not associated with organic polymers.[12] In terms of property enhancement, level of filler dispersion has been shown to be a dominant factor affecting nanocomposite performance.[13] In general, a more homogenous filler dispersion results in greater levels of performance enhancement, while poor dispersion can lead to properties below that of the neat matrix.[14] Unfortunately, surface modification of the filler is usually necessary to increase solubility and interaction with organic polymer matrices, leading to the use of solvents which may be detrimental to overall composite performance.[9,15,16]

Among the various types of nanofillers, an exciting class of material exists which has the potential to be tailored for miscibility in a wide range of polymer matrices not by chemical surface modification, but through modification of the molecular structure of the filler itself. Polyhedral oligomeric silsesquioxane (POSS) molecules are hybrid organic-inorganic nanostructures consisting of an inorganic Si-O-Si cage surrounded by a corona of organic substituents, described by the molecular formula $(RSiO)_{1.5}$.[17] The inorganic cage may be a fully condensed “closed” or “open” structure (Figure 3).

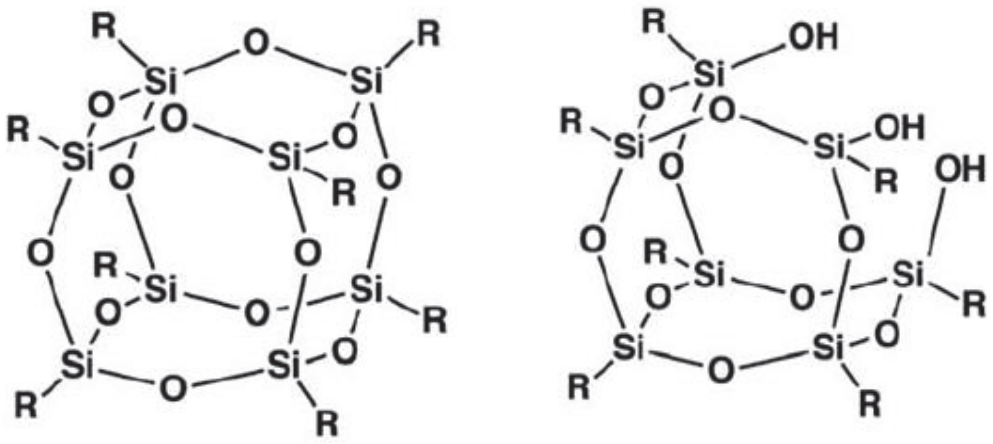

Figure 3. Molecular structure of the closed-cage (left) and open-cage (right) POSS molecules.

The organic groups (R) are attached to the cage at the corner silicon atoms, and can be modified to tailor the performance and solubility characteristics of the POSS molecule. To this point, the majority of POSS research has been directed to systems in which POSS is covalently bonded to a polymer backbone, or grafted as a pendent group.[18-36] Blends formulated by this method generally show enhanced thermal and mechanical performance due to the robust POSS cage, as well as decreased gas permeability.[24-26] Additionally, T_g is usually increased through covalent bonding of POSS due to reduced polymer chain mobility.[32,33] A common theme is that covalent bonding of POSS is not always desirable in that it usually requires the use of solvents and complicated/time consuming synthesis schemes which may limit the applicability of the resulting blends. Additionally, covalent bonding of POSS has been found to decrease processing efficiency due to an anchoring effect caused by the pendent POSS molecules, leading to increased melt viscosity and decreased rheological performance.[34-36] For these reasons, it is desirable to look at physical mixing through melt blending as a potential low cost and effective method by which to create POSS nanocomposites.

In our lab as well as others, POSS has been shown to produce a wide range of remarkable surface and bulk property enhancements when dispersed in melt-blended polyolefin matrices.[37-51] Unfortunately, many of these studies show mixed results as to the effect of POSS on blend performance. Chen et al. reported up to an 8% increase in bulk percent crystallinity of polypropylene with increasing concentration of octamethyl (OM) POSS (0-10 wt. %), attributed to POSS nanocrystals serving as nucleation sites.[38] Fu et al. reported similar results for polypropylene/OM POSS nanocomposites, where isothermal differential scanning calorimetry (DSC) analysis revealed that incorporation of POSS resulted in decreased time to reach exothermic maximum by 50%. At higher concentration, (>30 wt.%) POSS was said to decrease bulk crystallinity, attributed to the formation of POSS crystallites (verified by polarized optical microscopy) which were said to hinder chain mobility during crystallization.[41] Analyzing HDPE/POSS blends, Joshi et al. reported no changes in crystallinity due to incorporation of OM POSS at low concentration, but reported a 3% decrease in bulk crystallinity at high POSS concentrations (> 5 wt. %) due to aggregate formation and chain hinderance.[42,43] Pracella et al. examined the effect of increasing POSS alkyl chain length (methyl<isobutyl<isooctyl) on crystallization of polypropylene/POSS blends, and reported that increased POSS miscibility resulted in a 2-4% decrease in bulk crystallinity attributed to well dispersed POSS serving to interfere with chain mobility, and that only after OM and octaisobutyl (OiB) POSS had formed large aggregates was nucleation promoted.[47]

There have also been mixed results reported relative to tensile properties of polyolefin/POSS blends. Lim et al. reported a 90% increase in tensile modulus for

OiB/polypropylene blends (0.5 wt. % POSS) in comparison to OM/polypropylene blends (62% increase at 0.5 wt. % POSS), attributed to the longer OiB substituents having better interaction and miscibility with the matrix.[45] Baldi et al. reported opposite behavior, observing that OM/polypropylene blends displayed up to three times better tensile modulus than OiB/polypropylene blends, attributed to the longer isobutyl chains causing decreased transfer of stresses from the matrix to the hard POSS core.[37] In both cases, once the solubility limit for POSS in the matrix had been reached, POSS was reported to form large aggregates, causing decreased performance.

Joshi et al. and Zhou et al. reported that incorporation of small amounts (0.5 wt. %) of crystalline POSS resulted in decreased complex viscosity for HDPE (8% reduction) and polypropylene (18% reduction) matrices, respectively, followed by an increase in viscosity at higher POSS concentrations.[44,50] This behavior was attributed to increased free volume in the polymer melt due to POSS cages reducing chain entanglement, followed by restriction in chain mobility at high concentration due to POSS aggregation. Though both authors reported a decrease in complex viscosity due to POSS at low concentration, mixed results relative to the effects of POSS on storage and loss modulus were reported.

The above studies show mixed results relative to the effects of incorporation of POSS into melt-blended polyolefin matrices. Though processing of POSS via melt-blending is an attractive and potentially low cost method by which to prepare nanocomposites, relatively few studies have been conducted into the characterization of melt-blended POSS/polyolefin systems as a function of loading and dispersion level of POSS molecules with different functionalities.[37,39,40,45,47] Even fewer studies have been

conducted involving the melt blending of POSS with highly-crystalline polyolefin matrices.[42-44,48] Additionally, no studies have been found in the literature that relate POSS physical state or cage structure to observed properties in melt-blended polyolefin systems. For these reasons, there is still much to be learned about the mechanisms that govern the melt-blending of POSS molecules with polyolefins, and how the properties of said blends reflect the influence of POSS molecular structure and concentration on the system.

This study was an attempt to understand the effect of POSS physical state, cage structure and R-group functionality on miscibility and bulk properties of HDPE/POSS blends prepared via melt-processing. Five types of POSS were identified as suitable for evaluation due to their predicted compatibility with the HDPE matrix, as well as their thermal stability under the necessary HDPE processing conditions. Effects of POSS incorporation on HDPE processing was monitored by analyzing extruder torque during melt-blending as well as melt-state rheological investigations. Thermal behavior of the HDPE/POSS blends was examined using both thermal gravimetric analysis (TGA) and DSC. Effects of POSS on bulk crystallinity were quantified using wide-angle X-ray diffraction (WAXD) and DSC. Finally, mechanical performance was evaluated by conducting standardized tensile and impact analysis.

Experimental

Materials

Marlex HXM-50100 high-density polyethylene (HDPE, M_w~203,000) was supplied by Chevron-Phillips (The Woodlands, TX). POSS nanostructured chemicals were supplied by Hybrid Plastics (Hattiesburg, MS). POSS types analyzed are

octamethyl (OM, crystalline powder), octaisobutyl (OiB, crystalline powder) octaisooctyl (OiO, viscous liquid), trisilanol isobutyl (TSiB, crystalline powder) and trisilanol isooctyl (TSiO, viscous liquid). Materials were used as received.

Sample Preparation

Melt blends of POSS and HDPE were prepared using a B&P Processing CT-25 co-rotating twin screw extruder (Saginaw, MI) with a screw diameter of 22mm and a L:D ratio of 44:1. Samples were extruded at 235°C and 300 RPM. Blends were prepared at 0, 0.25, 0.5, 1, 2 and 5 wt. % POSS. Extruder torque was recorded as a function of POSS concentration. Specimens for tensile and rheological analysis were injection molded using a Milacron 55-Ton Vista Sentry injection molder (Cincinnati, OH). During molding, the temperatures of the barrel, die and mold were held constant at 210°C, 205°C and 200°C, respectively. Mold pressure was varied between 800 and 2000 PSI for each concentration to produce test specimens of appropriate dimensions. Specimens for AFM, tribological and nanoindentation analyses were compression molded on clean silicon using a Carver hydraulic press (Wabash, IN). During molding, the temperature of the platens was held constant at 160°C. Mold pressure was held constant at 3000 PSI to produce repeatable test specimens, while specimen thickness was controlled using an aluminum picture-frame mold. For evaluation of the bulk morphology (1μm depth), a small section of the sample was prepared using a Leica EM FC6 cryomicrotome (Buffalo Grove, IL) at -120°C with a diamond knife.

Thermogravimetric Analysis (TGA)

TGA analysis was conducted on a TA Instruments Q500 (New Castle, DE). Samples of 12-14 mg were heated at a rate of 20°C per minute from 25°C to 600°C under

both air and nitrogen blankets flowing at 60mL per minute. Maximum-rate-of-degradation temperatures were recorded for each sample, as well as residual weight. Data analysis was conducted using the TA Universal Analysis software suite.

Capillary Melting Point

Capillary melting point analysis was conducted on a Thomas Hoover Uni-Melt (Philadelphia, PA). Capillary tubes were packed to a sample height of 3 mm, and heated at a rate of 5°C until a clear point was observed. Three samples were analyzed per POSS type, with average melting point (clear point) reported.

Differential Scanning Calorimetry (DSC)

DSC analysis was conducted on a TA Instruments Q100 (New Castle, DE). Samples of 10-12 mg were analyzed under a nitrogen blanket flowing at 40 mL/min. To erase sample thermal history, each sample was initially heated at 10°C per minute from 25°C to 150°C and held for three min, then cooled at a rate of 10°C/min to 25°C and held for three additional minutes. Samples were then reheated and cooled at the same rate and to the same temperatures for data analysis. Data analysis was conducted using the TA Universal Analysis software suite. Melting temperature and crystallization temperature were recorded by calculating the peak maxima of the exothermic and endothermic peaks of the thermograms, respectively. Specific heat was calculated as a function of heat flow into the sample relative to heating rate and initial sample mass. Percent crystallinity was calculated as the ratio of calculated sample specific heat to that of a theoretical polyethylene sample with 100% crystallinity (specific heat 290 J/g).

Wide Angle X-ray Diffraction (WAXD)

WAXD analysis was conducted on compression molded samples to determine the % crystallinity and crystal thickness. Diffraction patterns were obtained using a Rigaku D/MAX-ULTIM III diffractometer (The Woodlands, TX) operated in transmission mode at room temperature using Cu Ka (λ=0.154 nm) radiation at a tube current of 44 mA and an acceleration voltage of 40 kV. The scan range was 2°–30° at a step interval of 0.1° and a scanning rate of 0.5°/min. The percent crystallinity of the blends was determined by segregating the crystalline contribution of the $I\theta$ vs. θ diffraction scans obtained from WAXD spectra and using the following formula:

$$X_c = \frac{\int_0^a S^2 I_c(S)\,ds}{\int_0^a S^2 I_s(S)\,ds} \tag{9}$$

$$S = 2\sin\frac{\theta}{\lambda} \tag{10}$$

where X_c is the crystalline mass fraction, I_c is the crystalline diffraction intensity, I_s is the total diffraction intensity, λ = 1.54 Å, and θ is Bragg's angle. The Origin Pro 8.5 software suite was used to smooth, deconvolute and fit the WAXD spectra.

Rheology – Processing Enhancement

Processing enhancement was monitored relative to extruder torque output. During processing, extruder torque was recorded as a function of both POSS loading level and POSS type. For each POSS concentration, a torque recording was noted only after the extruder had reached a steady state.

Rheology – Parallel Plate

Parallel plate rheology was conducted on a TA Instruments ARES rheometer (New Castle, DE) operated in dynamic mode. Isothermal time sweeps conducted at 210°C for 2 h showed no heat-induced degradation of the HDPE. All analysis was performed at 210°C under a nitrogen blanket. Specimens of 25 mm diameter were die cut from injection-molded plates (2 mm in thickness) at each POSS concentration. Initial strain sweeps were completed to determine an appropriate strain value for analysis (λ=10%). The effect of POSS concentration on storage modulus (G'), loss modulus, (G'') and complex viscosity (η^*) was determined using strain-controlled frequency sweep experiments over the frequency range 0.1-100 rad/s, with data collected at five points per decade. Data analysis was conducted using the TA Orchestrator software suite.

Tensile Testing

Tensile testing was conducted on a MTS Insight material testing station (Eden Prairie, MN) in accordance with ASTM D638. Samples were injected molded according to ASTM D638 Type 2 specifications, and analyzed at a crosshead speed of 2 in/min. All testing took place in a temperature (22°C) and humidity (40-45%) controlled room. Sample modulus, ultimate tensile load, ultimate tensile stress, strain at yield and strain at break were recorded. Ten specimens were analyzed per POSS concentration, with the resulting data averaged and a standard deviation calculated.

Izod Impact Testing

Izod impact testing was conducted on a Tinius Olsen 892 Impact Tester (Horsham, PA) in accordance with ASTM D256-05. Samples were injection molded to dimensional tolerances in accordance with the named ASTM standard. Prior to testing,

each bar was notched and its width recorded. All testing took place in a temperature (22°C) and humidity (40-45%) controlled room. Impact energy was recorded as a function of specimen thickness. Ten specimens were analyzed per concentration, with the resulting data averaged and a standard deviation assigned.

Results and Discussion

Thermal Analysis

Table 1 shows the physical form of the POSS molecules at room temperature, as well as measured melting point and temperature of maximum rate of degradation, T_d, of the neat HDPE and neat POSS materials.

Table 1

Room temperature physical state, peak melting temperatures (T_m)and temperatures of maximum rate of degradation (T_d) of the neat HDPE and neat POSS materials

Material	Physical State at 20°C	T_m (cap.) (°C)	T_m (DSC) (°C)	T_d (air) (°C)	T_d (N_2) (°C)
HDPE	solid	-	131	393	479
OM	solid	400+	340	240	246
OiB	solid	280	280	253	254
OiO	liquid	-	-	311	364
TSiB	solid	190	200	336	342
TSiO	Liquid	-	-	333	367

T_d was determined via TGA by recording the peak maximum of differential thermal analysis (DTA) thermograms of the materials, and is reported under nitrogen and air atmospheres. Measured T_d of OM, OiB and OiO POSS are in agreement with those previously reported by Mantz et al. and Fina et al.[52,53] Under nitrogen, the primary

degradation mechanism of OM, OiB and OiO POSS is evaporation.[52] Under air, OM is found to sublime, while OiB and OiO are found to undergo the competing reactions of melting, evaporation and oxidation.[53] The mechanisms of degradation of the open-cage trisilanol POSS molecules are different than those of the closed-cage species. Trisilanol POSS molecules have been reported to condense at elevated temperature, leading to the formation of condensation products with molecular weights both above and below that of the starting material.[54,55] Though reports of the exact condensation or degradation temperatures of trisilanol POSS molecules with different organic substituents were not found in the literature, Feher et al. reported that condensation of the trisilanol cyclohexane POSS molecule occurs at temperatures above 200°C.[54] In a more recent work, Zeng et al. reported that trisilanol isooctyl POSS condenses at temperatures between 250°C and 280°C in a time and environment-dependent process.[55]

Melting points for OM and OiB POSS, both in literature reports and in our own measurements, appear to be higher than the measured temperatures of degradation.[39,52,53,56] Additionally, widely different melting points are observed in DSC and capillary melting point apparatus measurements for OM POSS. These apparent discrepancies are attributed to sublimation of the OM POSS upon degradation and differences in vapor pressures experienced under the different testing conditions. The higher melting point observed in the capillary melting point apparatus is attributed to increased vapor pressure in the sample vessel due to OM POSS sublimation, which results in the formation of a supercritical fluid that delays the observed melting point.[57] It has also been reported that heating rate in TGA analysis affects T_d, with an increase in

heating rate generally resulting in an increase in measured T_d.[39,52,53] Table 2 shows T_d for HDPE and the HDPE/POSS blends under nitrogen atmosphere.

Table 2

DTA temperatures of maximum rate of degradation (T_d) of neat HDPE and HDPE/POSS blends under nitrogen atmosphere

Material	T_d 0 wt. % (°C)	0.25 wt. % (°C)	0.5 wt. % (°C)	1 wt. % (°C)	2 wt. % (°C)	5 wt. % (°C)
HDPE	479	-	-	-	-	-
OM	-	476	477	477	478	482
OiB	-	475	477	476	477	474
OiO	-	476	480	479	477	477
TSiB	-	478	479	480	478	477
TSiO	-	478	477	475	476	477

Table 3

TGA percent residual char for neat HDPE and HDPE/POSS blends under nitrogen atmosphere

Material	Residue 0 wt. % (%)	0.25 wt. % (%)	0.5 wt. % (%)	1 wt. % (%)	2 wt. % (%)	5 wt. % (%)
HDPE	0.1	-	-	-	-	-
OM	-	0.2	0.2	0.2	0.2	0.3
OiB	-	0.3	0.3	0.3	0.4	0.4
OiO	-	0.3	0.3	0.2	0.4	0.4
TSiB	-	0.2	0.2	0.2	0.3	0.3
TSiO	-	0.2	0.2	0.2	0.3	0.4

No significant change in T_d is observed as a function of POSS type or concentration. The T_d of neat HDPE in nitrogen atmosphere is significantly higher than that of all of the neat POSS molecules. It was suggested by Fina et al. that at the degradation temperature of most polyolefins, the majority of POSS has already degraded/evaporated and thus has limited effect on the degradation of polyolefins.[39] Evidence of POSS evaporation is found in the data in Table 3, which show that there is negligible residual char for the HDPE/POSS blends after heating to 600°C under nitrogen.

T_d data for HDPE and the HDPE/POSS blends under air atmosphere are shown in Table 4. In air, POSS blends show generally increased T_d in comparison to that of the neat HDPE. Enhanced thermooxidative behavior of POSS blends has been attributed to formation of a protective char layer and/or dispersed silica degradation products that restrict oxygen diffusion in the organic matrix.[39,53]

Table 4

DTA temperatures of maximum rate of degradation (T_d) of neat HDPE and HDPE/POSS blends under air atmosphere

Material	T_d 0 wt. % (°C)	0.25 wt. % (°C)	0.5 wt. % (°C)	1 wt. % (°C)	2 wt. % (°C)	5 wt. % (°C)
HDPE	393	-	-	-	-	-
OM	-	403	404	401	401	387
OiB	-	395	403	409	400	398
OiO	-	406	413	408	406	402
TSiB	-	402	405	413	402	402
TSiO	-	407	404	396	398	389

Table 5

TGA percent residual char for neat HDPE and HDPE/POSS blends under air atmosphere

Material	Residue 0 wt. % (%)	0.25 wt. % (%)	0.5 wt. % (%)	1 wt. % (%)	2 wt. % (%)	5 wt. % (%)
HDPE	0.6	-	-	-	-	-
OM	-	0.6	0.6	0.6	0.6	0.6
OiB	-	0.6	0.8	1.1	1.6	3.1
OiO	-	0.6	0.6	1.0	1.3	2.9
TSiB	-	0.6	0.6	0.9	1.1	2.5
TSiO	-	0.5	0.6	0.8	0.9	2.5

This is evidenced by the increased residual char levels observed in POSS blends in air (Table 5). The degree of improvement in T_d depends on the type of POSS and the concentration of POSS in the HDPE matrix. Contrary to the findings of Fina et al. for OM and OiB POSS in polypropylene, who report increasing T_d with increasing POSS concentration (3-10 wt. %), we observe a maximum in T_d at POSS concentrations of 0.5 to 1.0 weight percent. The differences in T_d are attributed to differences in the dispersion level of POSS in the HDPE matrix. At low loading levels, it is expected that the POSS molecules are well dispersed in the polymer matrix, which results in formation of a homogeneous protective silica layer. At higher loading levels, greater POSS aggregation and phase separation is expected. This morphology may not provide as effective a barrier to oxygen diffusion as the more homogeneous system.

To determine if POSS condensation reactions were likely to occur during melt processing, the trisilanol POSS molecules were heated isothermally in open-air flasks

first to 200°C and then 280°C and held for 10 min, slightly longer than the approximate residence time of extrusion (7 min). Heating TSiB POSS to 200°C for 10 min, slightly above its crystalline melting temperature recorded by DSC to be 198°C, resulted in the formation of a liquid which upon cooling returned to a solid state. Heating TSiB POSS to 280°C for 10 min, well above the proposed temperature of trisilanol cage condensation, resulted in the formation of a viscous liquid which upon cooling did not return to its solid state, indicating that a chemical reaction had taken place. No effect was noticed relative to the physical state of the TSiO POSS at either heating temperature. This is in agreement with work conducted by Zeng et al. who did not see significant degradation of TSiO POSS when melt blended with PBT at 285°C with a residence time of 15 min.[58] These findings indicate that the organic substituent affects the condensation rate of the trisilanol POSS molecule. At the extrusion temperatures employed in this study, it is likely that TSiO POSS does not significantly condense or degrade, while TSiB POSS likely undergoes condensation and rearrangement reactions.

In addition to degradation studies of the HDPE/POSS blends, the effect of POSS on peak melting temperature, peak crystallization temperature and bulk crystallinity was analyzed via DSC (Table 6). No significant effect on peak melting or peak crystallization temperatures was observed for the POSS concentrations analyzed. This is in agreement with studies conducted by Joshi et al., who report no effect of OM POSS on the melting or crystallization temperatures of HDPE until loading levels greater than 5 wt. % POSS.[42,43] Bulk crystallinity decreases slightly with increasing POSS loadings.

Table 6

DSC bulk percent crystallinity of neat HDPE and HDPE/POSS blends, as well as peak melting temperatures (T_m) and peak crystallization temperatures (T_c) for the 5 wt. % blends

Material	% Cryst. 0 wt. % (%)	% Cryst. 0.25 wt. % (%)	% Cryst. 0.5 wt. % (%)	T_m 1 wt. % (°C)	T_c 2 wt. % (°C)
HDPE	70	-	-	131	115
OM	-	68	63	132	115
OiB	-	69	67	131	115
OiO	-	70	69	131	115
TSiB	-	68	65	131	115
TSiO	-	70	68	130	115

OM POSS, which has the shortest chain alkyl substituents, displays the greatest reduction in bulk crystallinity of the POSS molecules evaluated. This is attributed to decreased interaction with the polymer matrix, leading to formation of POSS aggregates large enough to hinder chain mobility and consequently alter crystallization kinetics.[42] As alkyl chain size is increased to isobutyl and then isooctyl, decreased effects on bulk crystallinity are noted. This is attributed to greater interaction of the longer alkyl substituents with the HDPE chains, resulting in a finer dispersion of POSS molecules and smaller effects on bulk crystallinity.

Wide Angle X-ray Diffraction (WAXD)

WAXD was conducted as a complementary technique to DSC to determine the effect of POSS type and concentration on the bulk crystallinity of the HDPE/POSS blends. Figure 4 shows WAXD spectra for the three neat, crystalline POSS molecules.

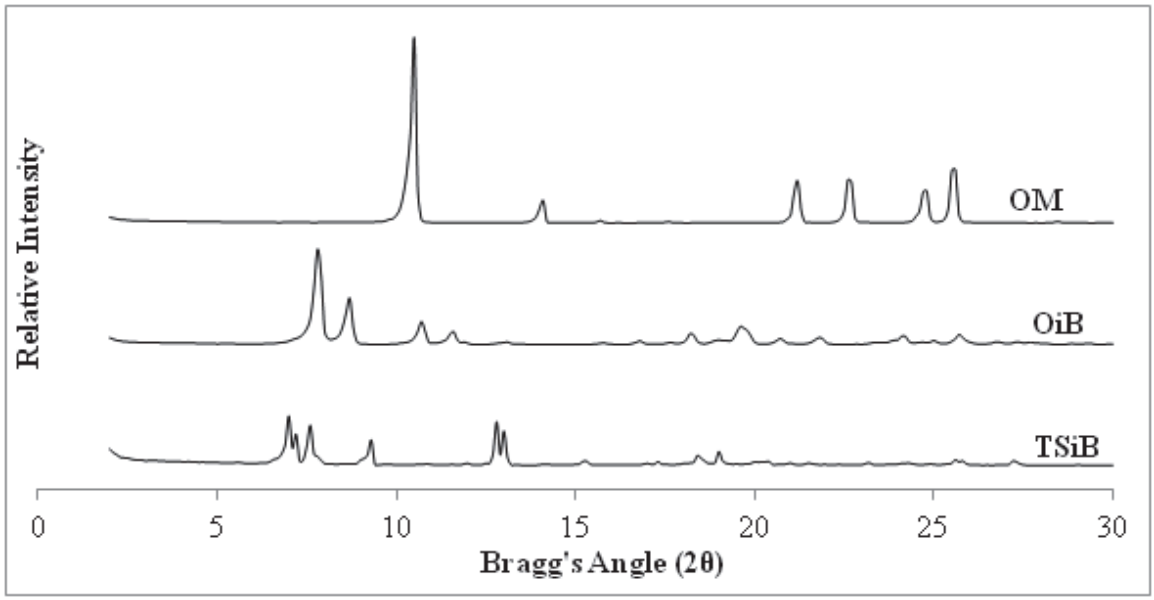

Figure 4. WAXD spectra of neat crystalline POSS materials.

OM POSS displays a characteristic crystalline peak at 10.5 2θ, while OiB POSS displays two characteristic peaks at 7.8 and 8.6 2θ.[39,44] TSiB POSS displays three characteristics peaks at 7.0, 7.3 and 9.3 2θ.

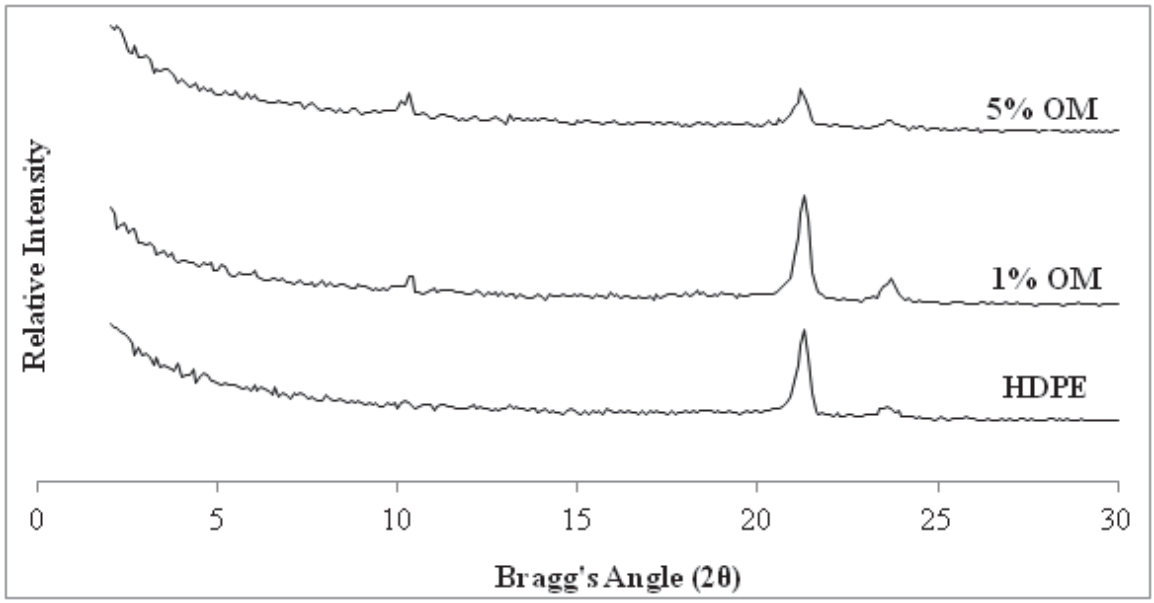

Figure 5. WAXD spectra of neat HDPE and HDPE/OM POSS blends.

Figure 5 shows WAXD spectra for the neat HDPE, as well as the 1 and 5 wt. % OM POSS blends. Neat HDPE shows characteristic crystalline peaks at 21.2 and 23.3 2θ, in agreement with literature.[44,59,60] The HDPE/OM POSS blends show characteristics of both the neat HDPE and OM POSS, indicating the presence of crystalline OM POSS aggregates in the HDPE matrix.[39,44] As concentration is increased, a decrease in the HDPE crystalline peak intensity is noted, as well as a slight increase in intensity of the crystalline POSS peak. Similar results have been reported by Joshi et al. and Fina et al. relative to the dispersion of OM POSS in HDPE and polypropylene respectively, and are attributed to limited compatibility between the matrix and filler leading to preferential POSS self-association and aggregation.[39,44]

Figure 6 shows WAXD spectra for the neat HDPE, as well as the 1 and 5 wt. % OiB POSS blends.

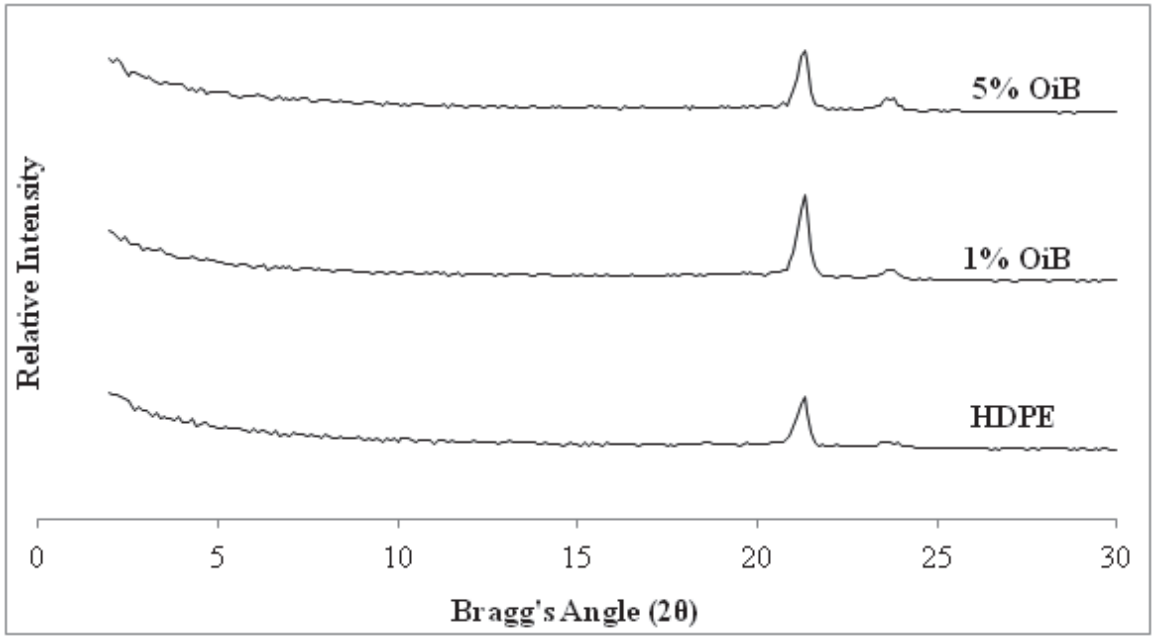

Figure 6. WAXD spectra of neat HDPE and HDPE/OiB POSS blends.

Unlike the OM POSS blends, which display a distinct peak due to the presence of POSS crystallites, no characteristic POSS peaks are noted for the OiB POSS blends. Though AFM analysis, which will be presented later, shows the appearance of small POSS aggregates on the surfaces of both the 1 and 5 wt. % OiB blends, the lack of appearance of crystalline POSS peaks indicates good miscibility of POSS in the HDPE, with a fine level of dispersion of POSS crystals that are not detected in WAXD analysis. Fina et al. reported similar results for three wt. % OiB/polypropylene composites, where no characteristic POSS peaks were observed via WAXD, though TEM clearly revealed the presence of POSS aggregates.[39]

Figure 7 shows WAXD spectra for neat HDPE, as well as the 1 and 5 wt. % TSiB POSS blends.

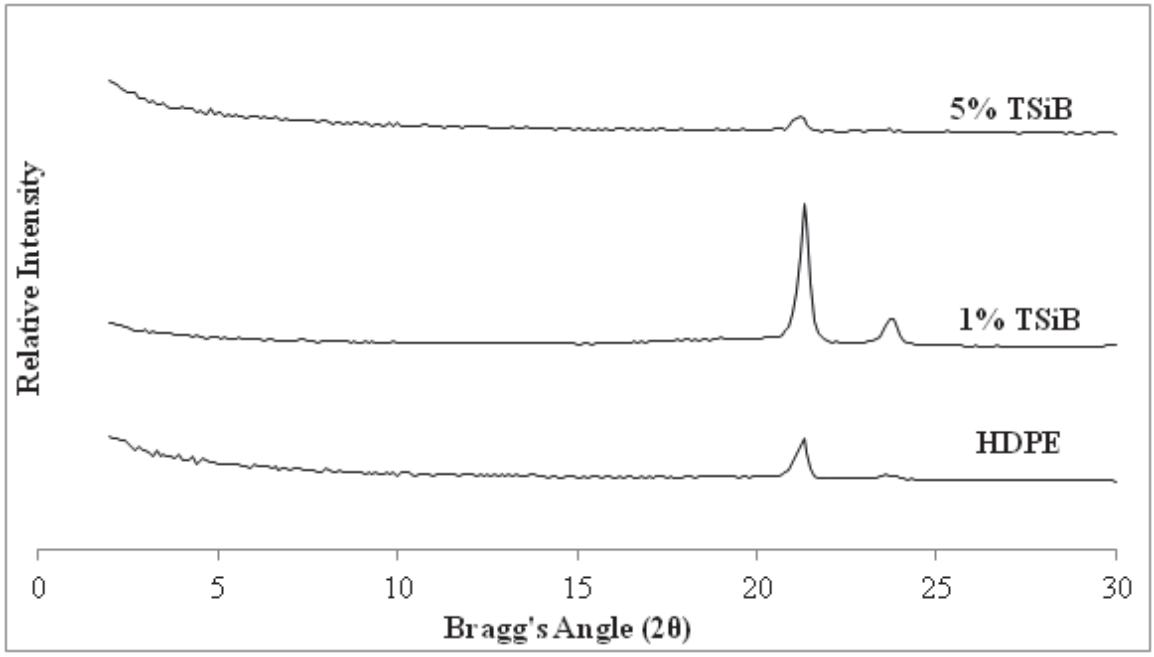

Figure 7. WAXD spectra of neat HDPE and HDPE/TSiB blends.

As observed for the OiB blends, no POSS crystalline peaks are detected. Two different mechanisms may be at play in this system. If the TSiB POSS remains a crystalline solid

after processing, then, as in the case of the OiB blends, the lack of crystalline POSS peaks is attributed to good miscibility and dispersion of the small POSS crystallites.[39] If the TSiB POSS undergoes condensation during extrusion, resulting in formation of a non-recoverable liquid, as is evidenced by rheological and mechanical analysis, peaks due to crystallinity would not be expected.[39] OiO and TSiO blends show similar spectra with no discernable POSS peaks, as is expected for the liquid POSS molecules.

Table 7 shows percent crystallinity determined by WAXD for the neat HDPE and HDPE/POSS blends as a function of increasing POSS concentration.

Table 7

WAXD bulk percent crystallinity of the neat HDPE and HDPE/POSS blends

Material	% Cryst. 0 wt. % (%)	% Cryst. 1 wt. % (%)	% Cryst 5 wt. % (%)
HDPE	70	-	-
OM	-	69	57
OiB	-	63	63
OiO	-	66	61
TSiB	-	62	42
TSiO	-	68	57

Due to the complexities in de-convoluting and curve fitting WAXD data, degree of crystallinity of the neat HDPE and HDPE/POSS blends is estimated within +/- 5% error, which is similar to error associated with DSC.[61-63] For all POSS molecules tested, an increase in POSS loading results in a decrease in bulk crystallinity. This is in agreement with the data collected by DSC, though the crystallinity values measured by WAXD for 5

wt. % POSS are more dramatically reduced. Trends observed at 5% loading are somewhat different than those observed in DSC analysis, though OM and TSiB POSS blends show the greatest decreases in crystallinity as determined by both methods. POSS substituent chain length and solubility appear to play a dominant role in blend crystallinity. OM POSS, predicted to be the least soluble of the POSS types due to its short alkyl substituents, displays large POSS crystallites that affect bulk crystallinity at higher concentration by hindering chain mobility during blend cooling.[64] OiB POSS, which is predicted to be the most soluble of the solid POSS types, does not display crystalline POSS peaks or a significant decrease in bulk crystallinity, attributed to superior miscibility in the HDPE matrix. Of the liquid POSS molecules, the open-cage trisilanols appear to reduce crystallinity levels to a greater degree than does the OiO POSS. This is attributed to decreased miscibility, as well as effects of trisilanol POSS condensation products on chain mobility.[54,55] TSiO POSS, with its longer chain alkyl substituents, is predicted to have better miscibility with HDPE than TSiB POSS, and shows a smaller effect on bulk crystallinity in the HDPE blend.

Processing Enhancement and Rheology

Initial rheological investigation of the HDPE/POSS systems was accomplished through monitoring torque during melt processing. Figure 8 shows the effect of increasing POSS concentration on percentage of maximum extruder torque. In comparison with the neat HDPE, for all POSS molecules, a reduction in torque is observed that increases with increasing POSS loading. The level of torque reduction increases with increasing chain length of the alkyl substituent (methyl < isobutyl < isooctyl), and the open-cage POSS structures provide slightly larger torque reductions

than their closed-cage analogues. In a previous study, we observed somewhat higher levels of torque reduction in melt blends of polyphenylsulfone with trisilanol phenyl (TSP) and dodecaphenyl POSS.[65]

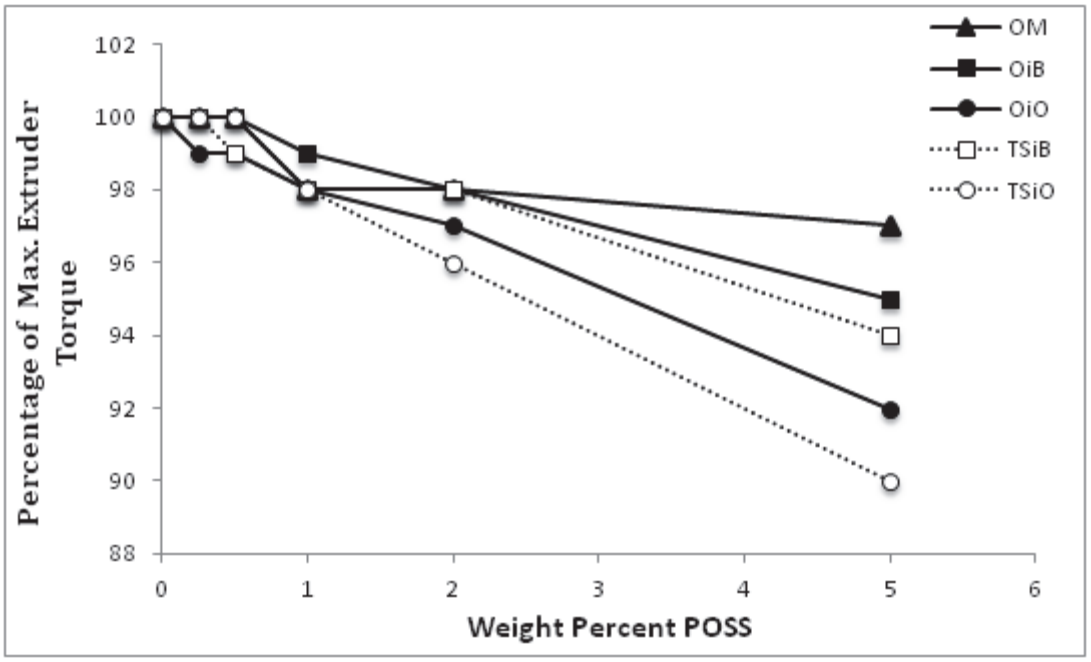

Figure 8. Percentage of maximum extruder torque as a function of increasing POSS concentration.

Parallel plate rheological studies were also performed. Figure 9 shows complex viscosity as a function of POSS concentration for closed-cage POSS molecules at a constant frequency of 10 rad/s. Joshi et al. reported concentration-dependent rheological behavior for HDPE/OM POSS blends, where an unusual viscosity reduction was observed at low concentration while viscosity increased at higher concentrations of POSS.[44] Similar low POSS concentration decreases in viscosity followed by increases in viscosity at higher concentration are observed in the current study for OM POSS and OiB POSS blends (Figure 9). A different type of behavior is observed, however, for the OiO-substituted closed-cage POSS and the open cage POSS molecules (Figure 10), where viscosity decreases as POSS concentration increases over the entire concentration range.

This behavior is consistent with the flow enhancement observed in the extruder torque studies for the same compositions.

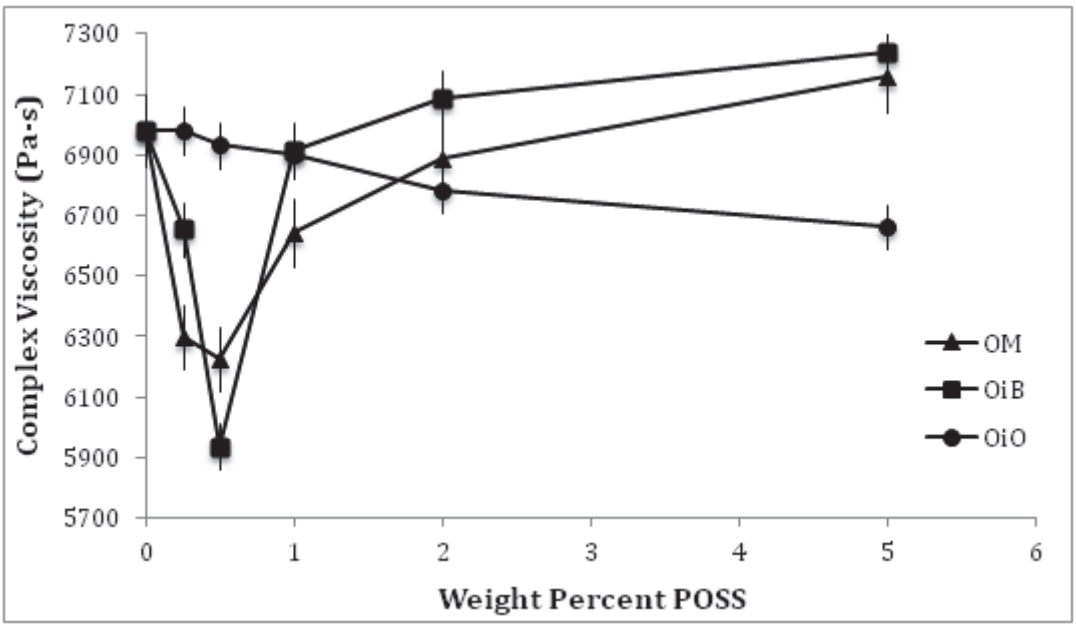

Figure 9. Complex viscosity of the closed-cage POSS blends as a function of increasing POSS concentration.

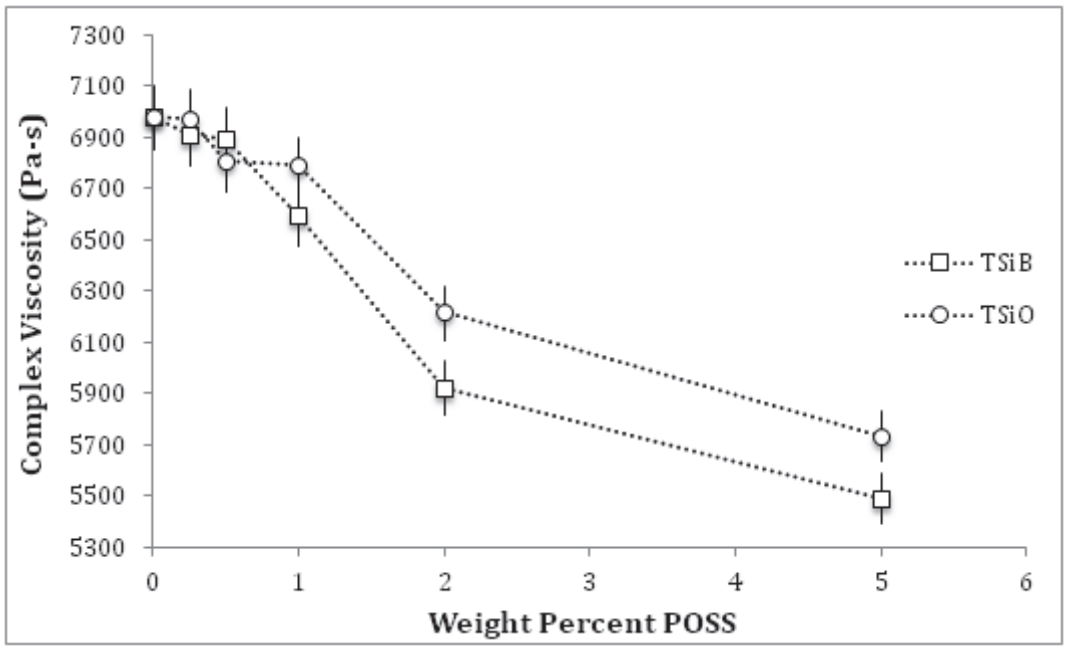

Figure 10. Complex viscosity of the open-cage POSS blends as a function of increasing POSS concentration.

These combined studies indicate that multiple mechanisms are involved in the viscosity modification behavior of the HDPE/POSS melt blends. The OiO, TSiO and TSiB POSS molecules behave as liquid plasticizers and lubricants in both the extruder torque and rheological studies. It is assumed that the mechanism of viscosity reduction is similar to that of other low molecular weight plasticizers.[65-67] This gives further evidence to the condensation of TSiB POSS into a non-recoverable liquid at the HDPE processing temperature. OM and OiB POSS, on the other hand, appear to remain largely in the solid state during processing and rheological testing, and are presumed to enhance flow by increasing free volume and decreasing chain entanglement.[31,44,50] At low loading levels, it is assumed that the POSS molecules are well dispersed and able to provide flow enhancement, while at higher loading levels the POSS molecules aggregate and increase melt viscosity. The greater flow enhancement observed for POSS molecules with longer chain alkyl substituents is attributed to greater compatibility with the HDPE matrix. The trisilanol POSS molecules reduce viscosity to a greater extent than the closed-cage OiO POSS, potentially due to effects on miscibility caused by trisilanol cage condensation.

Figures 11 and 12 show plots of storage modulus (*G'*) as a function of frequency for the 0.5 and 5 wt. % blends, respectively. Plots of loss modulus (*G"*) as a function of frequency display similar behavior (Figures 13 and 14). Error for these measurements ranged from 4.2-6.4%. At low concentration, storage modulus is reduced for all POSS blends compared to that of the neat HDPE. The solid OiB and OM POSS provide the greatest levels of modulus reduction, while the liquid POSS molecules provide only a minor reduction compared to the neat HDPE. The modulus reduction is attributed to increased free volume and reduced chain entanglement resulting from finely dispersed

OiB and OM POSS molecules, as was the case in the complex viscosity reduction at low POSS loadings (Figure 9).

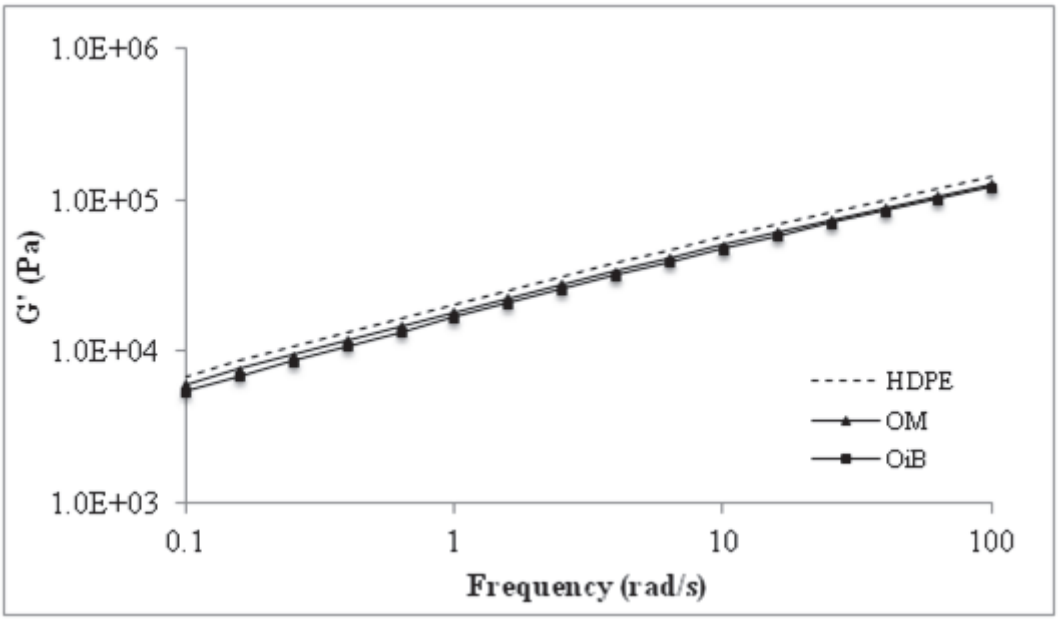

Figure 11. Storage modulus as a function of frequency for the 0.5 wt. % solid POSS/HDPE blends.

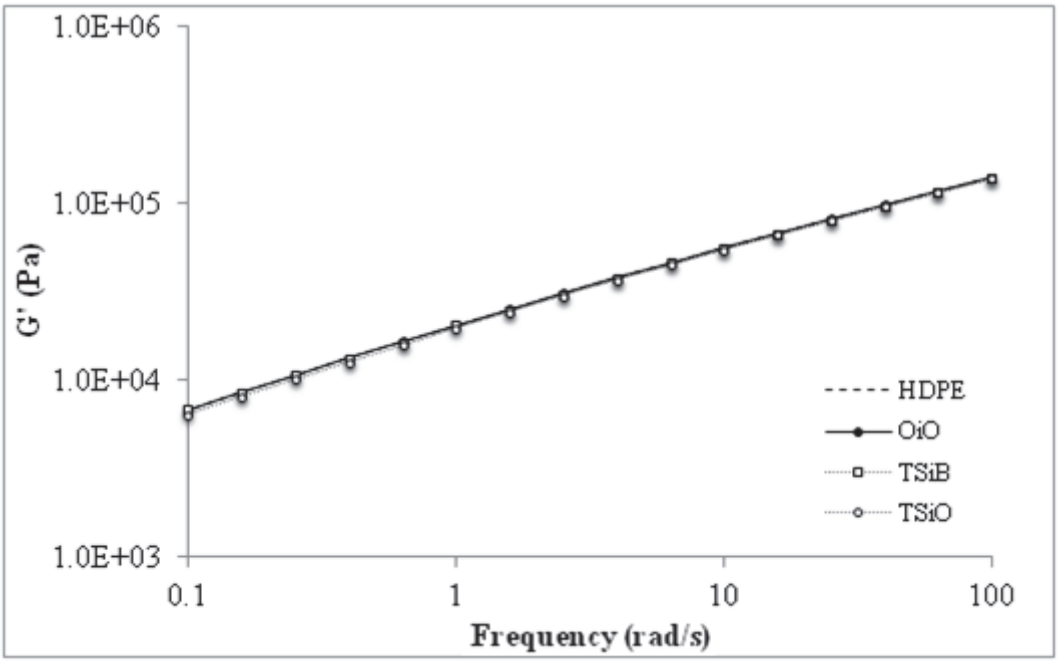

Figure 12. Storage modulus as a function of frequency for the 0.5 wt. % liquid POSS/HDPE blends.

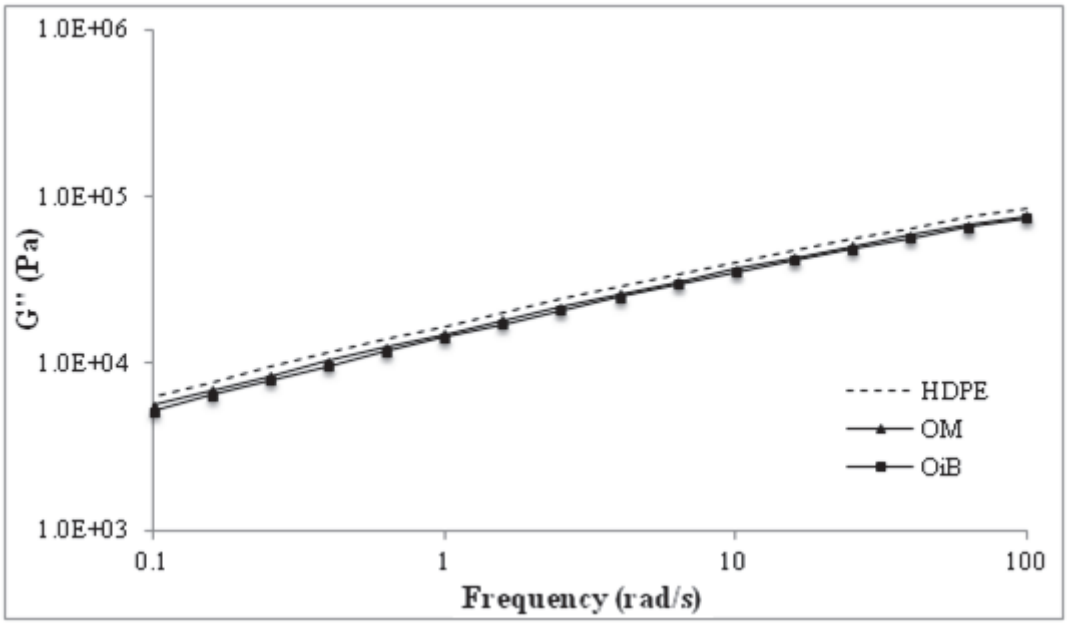

Figure 13. Loss modulus as a function of frequency for the 0.5 wt. % solid POSS/HDPE blends.

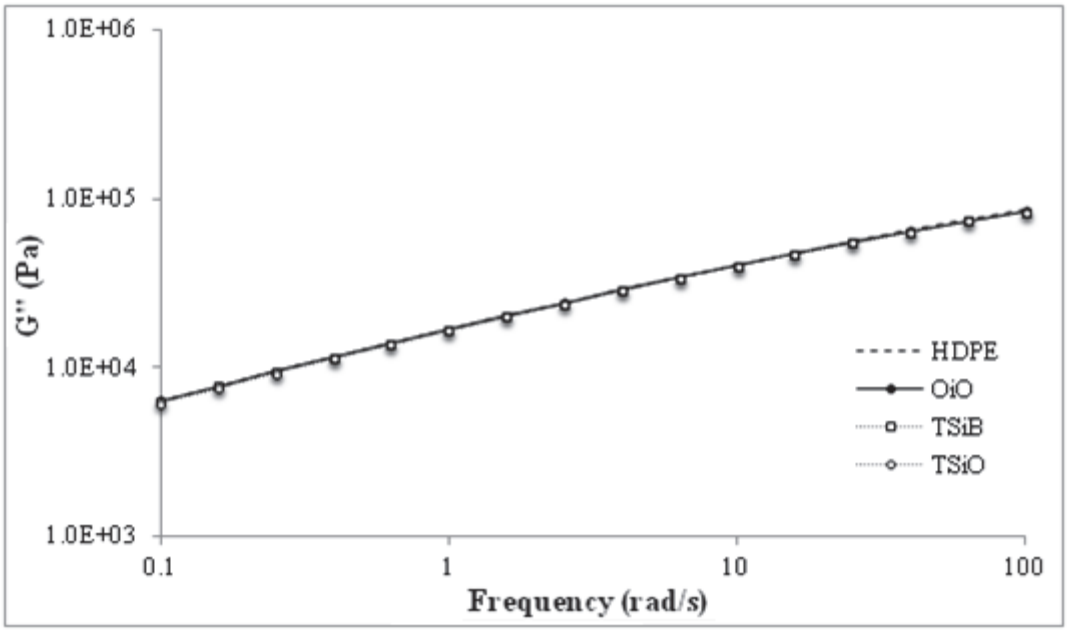

Figure 14. Loss modulus as a function of freqnency for the 0.5 wt. % liquid POSS/HDPE blends.

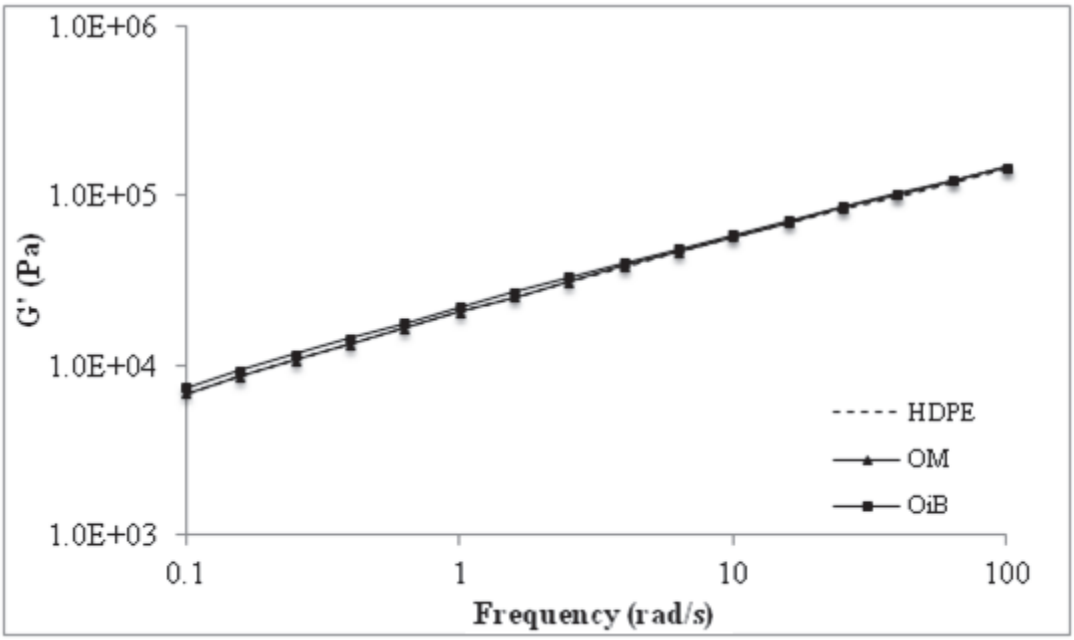

Figure 15. Storage modulus as a function of frequency for the 5 wt. % solid POSS/HDPE blends.

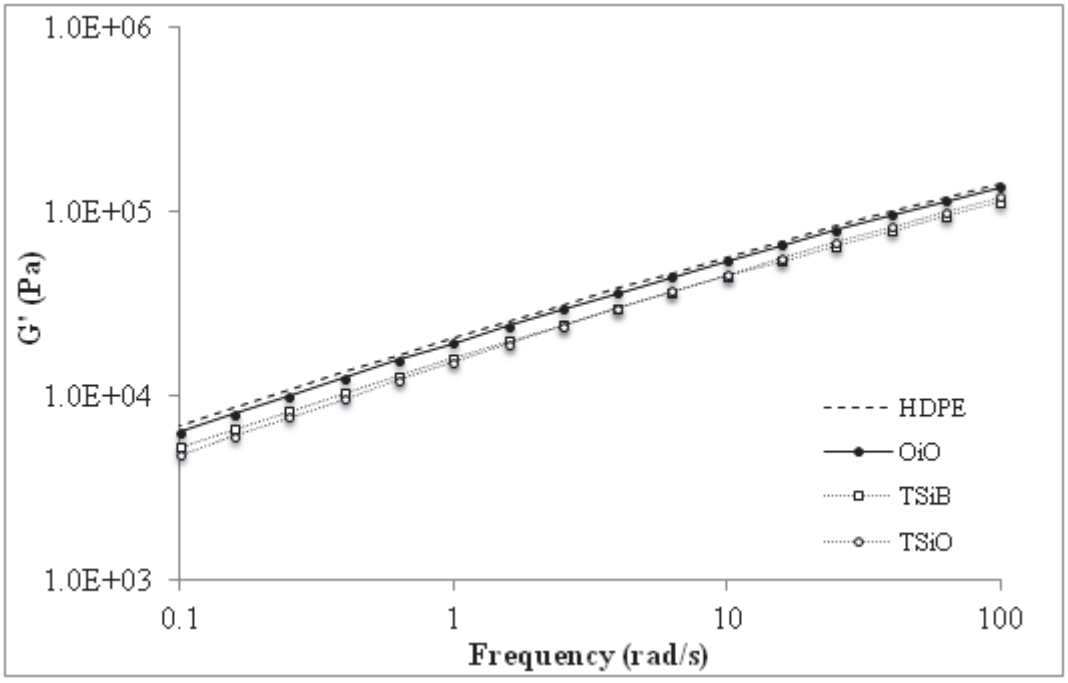

Figure 16. Storage modulus as a function of frequency for the 5 wt. % liquid POSS/HDPE blends.

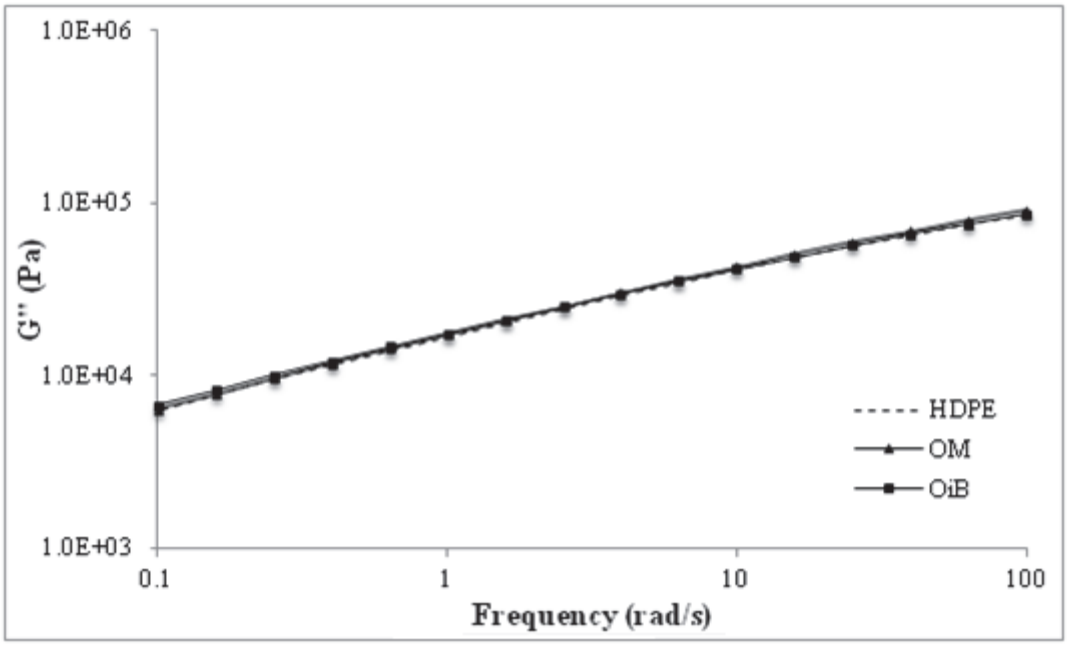

Figure 17. Loss modulus as a function of frequency for the 5 wt. % solid POSS/HDPE blends.

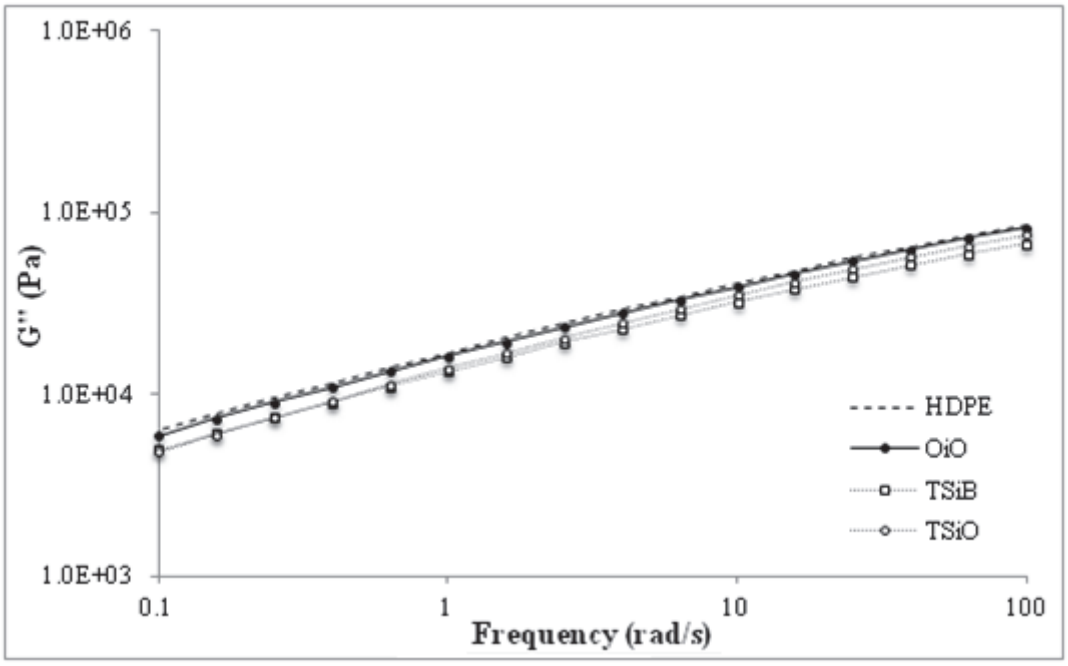

Figure 18. Loss modulus as a function of frequency for the 5 wt. % liquid POSS/HDPE blends.

At higher concentration, the solid OiB and OM POSS are shown to slightly increase storage modulus (Figure 15), while the liquid POSS molecules reduce the modulus (Figure 16). Again, loss modulus figures display similar behavior (Figure 17 and 18). The increase in modulus for solid POSS types is attributed to POSS aggregate formation and the resulting hindrance of chain movement. Zhao et al. reported similar storage modulus behavior for melt blends of polypropylene and crystalline octavinyl POSS.[50] The decreased storage modulus observed upon addition of liquid POSS molecules is attributed to plasticization.

Tensile Analysis

Figure 19 shows tensile modulus of the POSS blends as a function of increasing POSS concentration.

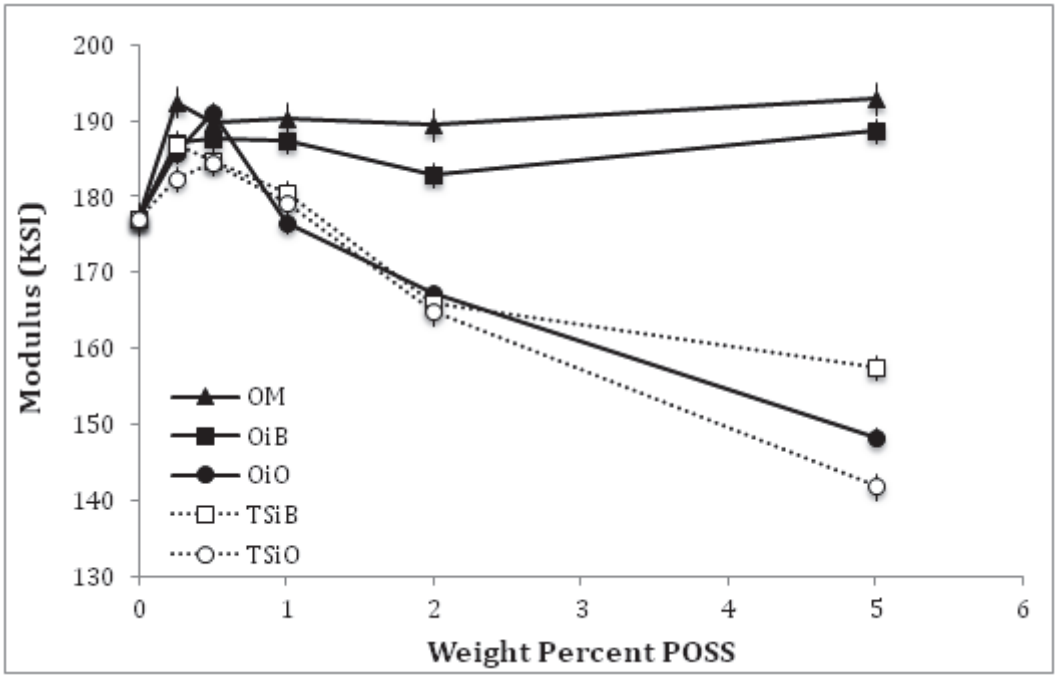

Figure 19. Tensile modulus as a function of increasing POSS concentration.

Neat HDPE is represented at 0 wt. % POSS. All POSS blends show an increase in tensile modulus in comparison to the neat HDPE at low concentration (<2%). As concentration

is increased, the OM and OiB blends retain their reinforcement performance, while the liquid OiO, TSiB and TSiO POSS blends show reduced tensile modulus compared to the neat HDPE. Similar behavior is observed for peak tensile stress of the POSS blends as a function of increasing POSS concentration (Figure 20).

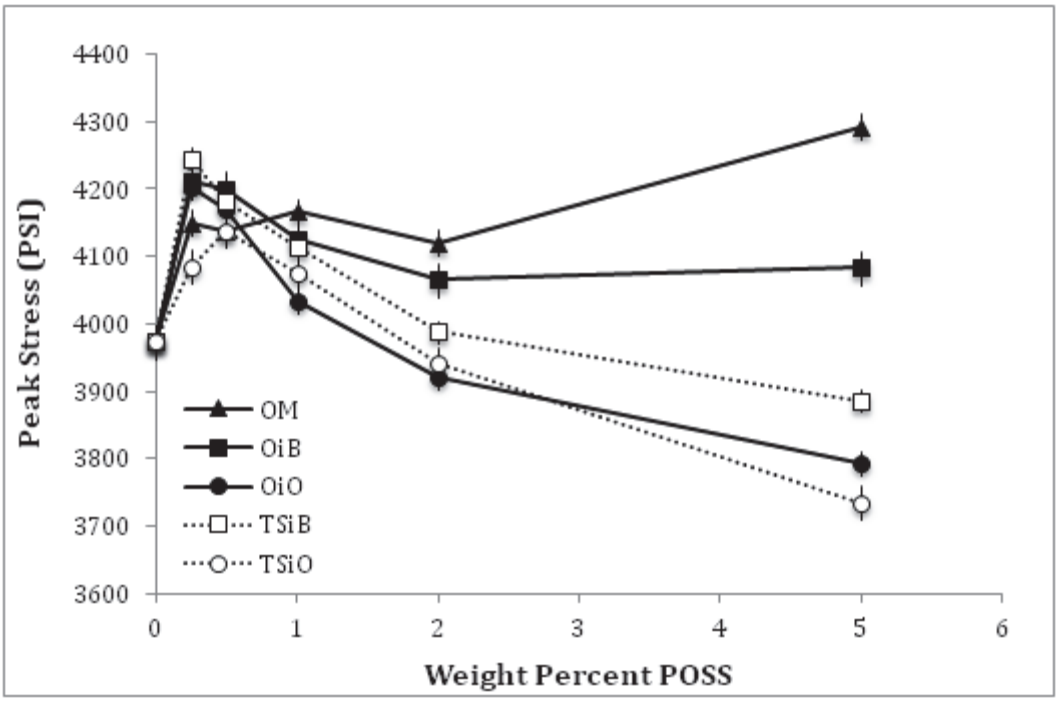

Figure 20. Peak tensile stress as a function of increasing POSS concentration.

This behavior is consistent with the mechanisms described above. Low-concentration tensile reinforcement can be attributed to good dispersion of small domains of POSS with excellent transmission of stresses from the matrix to the rigid POSS core.[65,68] As concentration is increased, the liquid POSS molecules show decreasing performance compared to the neat HDPE due to plasticization.[69] Figure 21 shows tensile strain at yield for the POSS blends as a function of increasing POSS concentration. Similar behavior is noted for tensile strain at break (Figure 22). Tensile strain is a function of the deformation capability of the matrix material, as well as the adhesion between phases

and, therefore, is a good indication of physical interaction between the POSS and HDPE matrix.

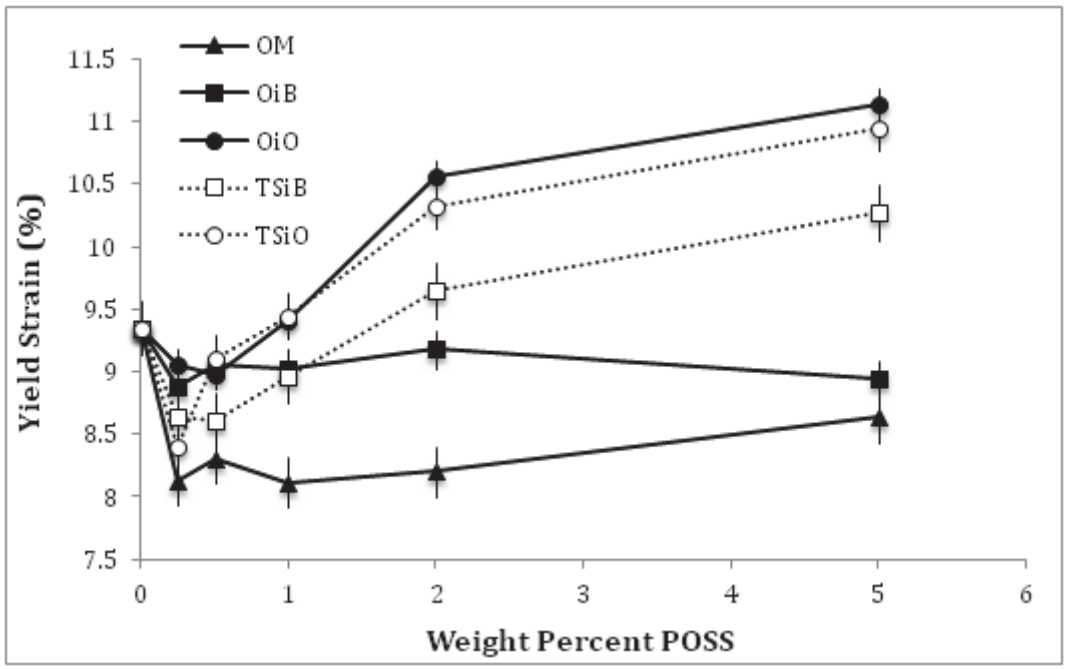

Figure 21. Tensile strain at yield as a function of increasing POSS concentration.

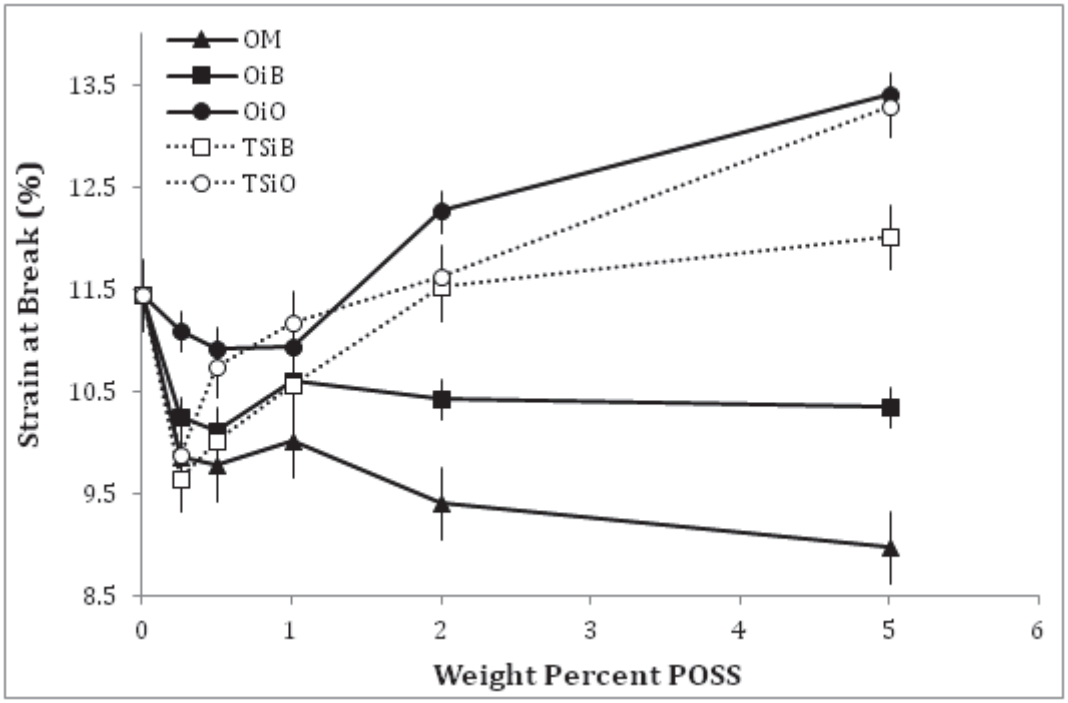

Figure 22. Tensile strain at break as a function of increasing POSS concentration.

At low concentrations, there is a decrease in tensile strain at yield for all blends, due, predominantly, to the largely non-deformable nature of the hard POSS core.[68] OM POSS shows the most dramatic decrease, indicative of inferior interaction with the HDPE matrix. At concentrations greater than 2%, OM and OiB solid POSS blends retain their reduced strain at yield, while liquid OiO, TSiB and TSiO POSS blends show increased strain at yield compared to the neat HDPE due to plasticization. The strain at yield of the OiB blends remains relatively unchanged until the highest POSS concentration, which, when coupled with modulus data, provides evidence for superior interaction between the HDPE and the longer chain OiB POSS as compared to that of HDPE and OM POSS. These results indicate that the physical state of the POSS has a greater effect on tensile reinforcement than either cage structure or alkyl chain length of the organic corona substituents.

Izod Analysis

Figure 23 shows notched Izod impact performance as a function of increasing POSS concentration. All samples show reduced impact strength compared to the neat HDPE at all concentrations analyzed. The solid OM and OiB POSS samples show continuous reduction in impact performance with increasing POSS concentration. The liquid POSS samples show an opposite trend, with the greatest decrease in performance compared to the neat HDPE occurring at 0.25 wt. %, the lowest concentration analyzed. As concentration is increased, impact strength is slowly recovered and at 5 wt. % POSS loading performance is similar to the neat HDPE. For the HDPE/POSS blends, the continuous decrease in impact performance with increasing concentration for the solid OM and OiB POSS molecules is attributed to POSS residing in the amorphous fraction of

the HDPE matrix acting as stress concentrators, thereby reducing impact performance. Similar behavior was reported by Zhao et al. for polycarbonate/TSP POSS blends, where a 20% decrease in impact strength was observed at three wt. % POSS loading.[50]

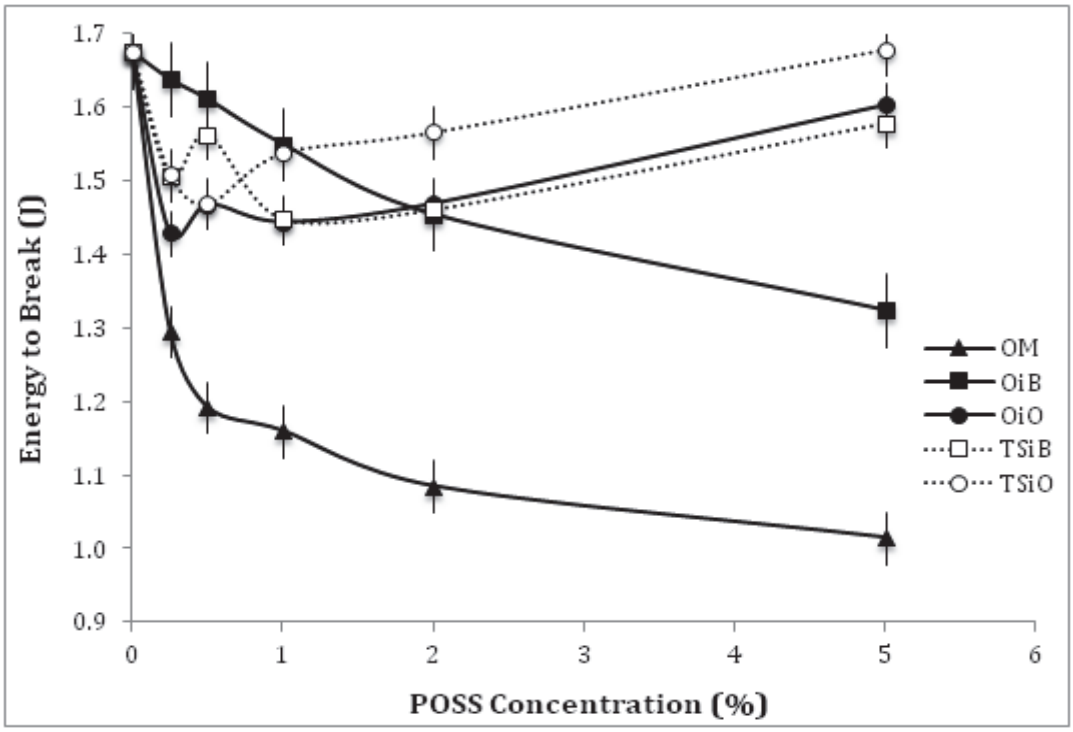

Figure 23. Izod impact strength as a function of increasing POSS concentration.

Further increase in POSS concentration leads to the formation of larger POSS aggregates with decreased interaction with the HDPE chains, leading to a further decrease in impact performance.[70,71] For the liquid POSS molecules, initial decreases in impact performance are attributed to dispersion of the hard POSS cores through the amorphous domains of the HDPE matrix acting as stress concentrators.[50] As concentration is increased, plasticization effects due to the liquid nature of POSS molecules supersede the stress-concentrator effects, leading to increased chain mobility and increased ductility in the blends.[69]

Conclusions

HDPE/POSS blends were successfully prepared via melt-blending and their bulk properties analyzed. Incorporation of POSS is shown to have limited effect on HDPE degradation under nitrogen, though thermooxidative performance is shown to increase at low POSS concentration due to the formation of a silica-like char layer restricting oxygen diffusion into the blend. Levels of thermooxidative enhancement are shown to be dependent on POSS miscibility and dispersion level. DSC analysis shows that while incorporation of POSS results in no significant effects on blend peak melting or peak crystallization temperatures, bulk crystallinity is shown to decrease slightly with increasing POSS loading. This behavior is further verified by WAXD analysis. POSS substituent chain length and cage structure appear to play dominant roles in blend crystallinity, with trisilanol POSS molecules resulting in larger reductions than their closed-cage analogues. Among POSS molecules with similar cage structure, increased chain length results in better miscibility and ultimately decreased effect on bulk crystallinity.

Though TSiO POSS is assumed to not undergo significant degradation during processing, TSiB POSS is shown to have the potential to condense into and remain a liquid under the HDPE processing conditions. During processing, the liquid POSS molecules behave as liquid plasticizers and lubricants, resulting in decreased melt viscosity and increased processing efficiency. The solid POSS molecules, which appear to remain largely in the solid state during processing, are presumed to enhance flow by increasing free volume and decreasing chain entanglement in the melt. Additionally, rheological analysis reveals that solid POSS molecules cause a significant decrease in

complex viscosity and increase in storage modulus at low concentration, which is attributed to the finely dispersed POSS aggregates serving to decrease chain entanglement and increase free volume. At higher concentration, storage modulus is shown to increase due to chain hindrance caused by the formation of larger POSS aggregates. Complex viscosity and storage modulus are shown to continually decrease with increasing liquid POSS concentration due to plasticization.

POSS physical state appears to dominate mechanical performance. Tensile performance is shown to increase at low concentration for all POSS types, which is attributed to a good dispersion of small phases of POSS with excellent transmission of stresses from the matrix to the rigid POSS core. At higher concentrations, solid POSS molecules are shown to retain their enhanced performance, while liquid POSS samples show decreasing performance due to plasticization effects. Impact analysis shows decreasing performance with increasing solid POSS content, attributed to the formation of progressively larger POSS aggregates which serve as stress concentrations. Liquid POSS molecules shows initial decreases in impact performance attributed to a fine dispersion of the hard POSS cores acting as stress concentrators in the HDPE matrix, though as concentration is increased plasticization effects lead to increased chain mobility and increased ductility/impact performance vs. their low-concentration counterparts.

The behaviors demonstrated by the individual POSS blends are shown to depend not only on the R-group functionally of the POSS structure, but also on the physical state and cage structure of the molecule. Physical state is shown to dominate processing behavior as well as blend mechanical and rheological performance. On the other hand,

POSS substituent chain length and solubility/miscibility play the dominant role in blend bulk crystallinity and thermal performance. Among POSS molecules of similar physical state, miscibility appears to be governed by alkyl chain length, with longer chains showing better interaction with the HDPE matrix. Additionally, trisilanol POSS blends display slightly different behavior than their closed-cage analogues, attributed primarily to cage condensation and the resulting effects on POSS molecular structure and miscibility.

Acknowledgements

This work was supported by a fellowship from the National Science Foundation GK-12 program "Connections in the Classroom: Molecules to Muscles", Award # 0947944 through the University of Southern Mississippi.

This work was supported in part by the Office of Naval Research, Award No. N00014-07-1057.

REFERENCES

1. Hall, L. M.; Jayaraman, A.; Schweizer, K. S. Curr. Opin. Solid State Mater. Sci. **2010**, 14, 38-48.

2. Jancar, J.; Douglas, J.; Starr, F. W.; Kumar, S.; Cassagnau, P.; Lesser, A.; Sternstein, S. S.; Buehler, M. Polymer **2010**, 51, 3321-3343.

3. Vaia, R. A.; Giannelis, E. P. MRS Bull. **2001**, 26, 394-401.

4. Usuki, A.; Kojima, Y.; Kawasumi, M.; Okada, A.; Fukushima, Y.; Kurauchi, T.; Kamigaito, O. J. Mater. Res. **1993**, 8, 1179-1184.

5. Ajayan, P.; Zhou, O. Carbon Nanotubes **2001**, 80, 391-425.

6. Rodriguez, N. J. Mater. Res. **1993**, 8, 3233-3250.

7. Wu, Y.; Cui, Y.; Huynh, L.; Barrelet, C. J.; Bell, D. C.; Lieber, C. M. Nano Letters **2004**, 4, 433-436.

8. Haddon, R. Science **1993**, 261, 1545.

9. LeBaron, P. C.; Wang, Z.; Pinnavaia, T. J. Appl. Clay Sci. **1999**, 15, 11-29.

10. Balazs, A. C.; Emrick, T.; Russell, T. P. Science **2006**, 314, 1107.

11. Schmidt, G.; Malwitz, M. M. Curr. Opin. Colloid Interface Sci. **2003**, 8, 103-108.

12. Hussain, F.; Hojjati, M.; Okamoto, M.; Gorga, R. E. J. Compos. Mater. **2006**, 40, 1511-1575.

13. Chrissafis, K.; Paraskevopoulos, K.; Tsiaoussis, I.; Bikiaris, D. J. Appl. Polym. Sci. **2009**, 114, 1606-1618.

14. Jordan, J.; Jacob, K. I.; Tannenbaum, R.; Sharaf, M. A.; Jasiuk, I. Mater. Sci. Eng., A **2005**, 393, 1-11.

15. Lau, K.; Gu, C.; Hui, D. Composites, Part B **2006**, 37, 425-436.

16. Manias, E.; Touny, A.; Wu, L.; Strawhecker, K.; Lu, B.; Chung, T. Chem. Mater. **2001**, 13, 3516-3523.

17. Lichtenhan, J. D. Comments Inorg. Chem. **1995**, 17, 115-130.

18. Baumann, T. F.; Jones, T. V.; Wilson, T.; Saab, A. P.; Maxwell, R. S. J. Polym. Sci., Part A: Polym. Chem. **2009**, 47, 2589-2596.

19. Huang, J. M.; Huang, H. J.; Wang, Y. X.; Chen, W. Y.; Chang, F. C. J. Polym. Sci., Part B: Polym. Phys. **2009**, 47, 1927-1934.

20. Lach, R.; Michler, G. H.; Grellmann, W. Macromol. Mater. Eng. **2010**, 295, 484-491.

21. Liang, K.; Toghiani, H.; Pittman, C. U. J. Inorg. Organomet. Polym. Mater. **2011**, 1-15.

22. Madbouly, S. A.; Otaigbe, J. U. Progress in polymer science **2009**, 34, 1283-1332.

23. Paul, D. R.; Mark, J. E. Prog. Polym Sci. **2010**, 35, 893-901.

24. Fina, A.; Monticelli, O.; Camino, G. J. Mater. Chem. **2010**, 20, 9297-9305.

25. Gnanasekaran, D.; Madhavan, K.; Reddy, B. J. Sci. Ind. Res. **2009**, 68, 437-464.

26. Zheng, L. Diss. Abstr. Int., B **2002,** 63, 4708-4806.

27. Qin, Y. W.; Dong, J. Y. Chin. Sci. Bull. **2009**, 54, 38-45.

28. Zhang, H.; Shin, Y.; Yoon, K.; Lee, D. Eur. Polym. J. **2009**, 45, 40-46.

29. Zhou, Z.; Cui, L.; Zhang, Y.; Yin, N. Eur. Polym. J. **2008**, 44, 3057-3066.

30. Xu, H.; Yang, B.; Wang, J.; Guang, S.; Li, C. J. Polym. Sci., Part A: Polym. Chem. **2007**, 45, 5308-5317.

31. Kopesky, E. T.; Haddad, T. S.; McKinley, G. H.; Cohen, R. E. Polymer **2005**, 46, 4743-4752.

32. Zhang, W.; Fu, B. X.; Seo, Y.; Schrag, E.; Hsiao, B.; Mather, P. T.; Yang, N. L.; Xu, D.; Ade, H.; Rafailovich, M. Macromolecules **2002**, 35, 8029-8038.

33. Kopesky, E. T.; Haddad, T. S.; Cohen, R. E.; McKinley, G. H. Macromolecules **2004**, 37, 8992-9004.

34. Lee, A.; Xiao, J.; Feher, F. J. Macromolecules **2005**, 38, 438-444.

35. Wu, J.; Haddad, T. S.; Kim, G. M.; Mather, P. T. Macromolecules **2007**, 40, 544-554.

36. Romo-Uribe, A.; Mather, P.; Haddad, T.; Lichtenhan, J. J. Polym. Sci., Part B: Polym. Phys. **1998**, 36, 1857-1872.

37. Baldi, F.; Bignotti, F.; Fina, A.; Tabuani, D.; Ricco, T. J. Appl. Polym. Sci. **2007**, 105, 935-943.

38. Chen, J. H.; Yao, B. X.; Su, W. B.; Yang, Y. B. Polymer **2007**, 48, 1756-1769.

39. Fina, A.; Tabuani, D.; Carniato, F.; Frache, A.; Boccaleri, E.; Camino, G. Thermochim. Acta **2006**, 440, 36-42.

40. Fu, B. X.; Gelfer, M. Y.; Hsiao, B. S.; Phillips, S.; Viers, B.; Blanski, R.; Ruth, P. Polymer **2003**, 44, 1499-1506.

41. Fu, B. X.; Yang, L.; Somani, R. H.; Zong, S. X.; Hsiao, B. S.; Phillips, S.; Blanski, R.; Ruth, P. J Polym. Sci., Part B: Polym. Phys. **2001**, 39, 2727-2739.

42. Joshi, M.; Butola, B. Polymer **2004**, 45, 4953-4968.

43. Joshi, M.; Butola, B. J. Appl. Polym. Sci. **2007**, 105, 978-985.

44. Joshi, M.; Butola, B.; Simon, G.; Kukaleva, N. Macromolecules **2006**, 39, 1839-1849.

45. Lim, S. K.; Hong, E. P.; Choi, H. J.; Chin, I. J. J. Ind. Eng. Chem. (Washington, D. C.) **2010**, 16, 189-192.

46. Misra, R.; Fu, B. X.; Morgan, S. E. J. Polym. Sci., Part B: Polym. Phys. **2007**, 45, 2441-2455.

47. Pracella, M.; Chionna, D.; Fina, A.; Tabuani, D.; Frache, A.; Camino, G. Macromol. Symp. **2006**, 234, 59-67.

48. Scapini, P.; Figueroa, C. A.; Amorim, C. L. G.; Machado, G.; Mauler, R. S.; Crespo, J. S.; Oliveira, R. V. B. Polym. Int. **2010**, 59, 175-180.

49. Wheeler, P. A.; Misra, R.; Cook, R. D.; Morgan, S. E. J. Appl. Polym. Sci. **2008**, 108, 2503-2508.

50. Zhou, Z.; Zhang, Y.; Yin, N. J. Polym. Sci., Part B: Polym. Phys. **2008**, 46, 526-533.

51. Zhou, Z.; Zhang, Y.; Zeng, Z. J. Appl. Polym. Sci. **2008**, 110, 3745-3751.

52. Mantz, R.; Jones, P.; Chaffee, K.; Lichtenhan, J.; Gilman, J.; Ismail, I.; Burmeister, M. Chem. Mater. **1996**, 8, 1250-1259.

53. Fina, A.; Tabuani, D.; Frache, A.; Boccaleri, E.; Camino, G. Fire Retard. Polym., [Eur. Meet. Fire Retard. Prot. Mater.], 9th, **2005**, 202-220.

54. Feher, F. J.; Newman, D. A.; Walzer, J. F. J. Am. Chem. Soc. **1989**, 111, 1741-1748.

55. Zeng, J.; Bennett, C.; Jarrett, W. L.; Iyer, S.; Kumar, S.; Mathias, L. J.; Schiraldi, D. A. Compos. Interfaces **2005**, 8, 673-685.

56. Voronkov, M.; Lavrent'yev, V. Inorg. Ring Sys.**1982**, 199-236.

57. Atkins, P.; de Paula, J. Chemical equilibrium. In *Physical chemistry*; Oxford University Press: New York, 1998; 7th Ed., Chapter 6, pp 140-142.

58. Zeng, J.; Kumar, S.; Iyer, S.; Schiraldi, D. A.; Gonzalez, R. High Perform. Polym. **2005**, 17, 403-424.

59. Russell, K.; Hunter, B.; Heyding, R. Polymer **1997**, 38, 1409-1414.

60. Zheng, L.; Waddon, A. J.; Farris, R. J.; Coughlin, E. B. Macromolecules **2002**, 35, 2375-2379.

61. Peacock, A. J.Characterization and testing. In *Handbook of polyethylene: structures, properties, and applications*; CRC: New York, 2000; Chapter 6, pp 301.

62. Chavarria, F.; Paul, D. Polymer **2004**, 45, 8501-8515.

63. Aharoni, S.; Sharma, R.; Szobota, J.; Vernick, D. J. Appl. Polym. Sci. **1983**, 28, 2177-2186.

64. Zhou, Z.; Cui, L.; Zhang, Y.; Yin, N. J. Appl. Polym. Sci., Part B: Polym. Phys. **2008**, 46, 1762-1772.

65. Jones, P. J.; Cook, R. D.; McWright, C. N.; Nalty, R. J.; Choudhary, V.; Morgan, S. E. J. Appl. Polym. Sci. **2011**, 121, 2945-2956.

66. Zweifel, H.; Maier, R. D.; Schiller, M. PVC stabilizers. In *Plastics additives handbook*; Hanser Verlag, Germany, 2009: Chapter 3, pp 497.

67. Murphy, J. Modifying processing characteristics: plasticizers. In *Additives for plastics handbook*; Oxford University Press, New York, 2001: Chapter 14, pp 172-175.

68. Sanchez-Soto, M.; Schiraldi, D. A.; Illescas, S. Eur. Polym. J. **2009**, 45, 341-352.

69. Soong, S. Y.; Cohen, R. E.; Boyce, M. C. Polymer **2007**, 48, 1410-1418.

70. Zhao, Y.; Schiraldi, D. A. Polymer **2005**, 46, 11640-11647.

71. Moody, L. E. Proceedings from the 37th annual SAMPE Fall Technical Conference,Seattle, WA, Oct. 3rd, **2005**.

CHAPTER IV

SURFACE PROPERTIES OF HIGH DENSITY POLYETHYLENE (HDPE)/POLYHEDRAL OLIGOMERIC SILSESQUIOXANE (POSS) BLENDS

Abstract

Hybrid organic/inorganic blends based on polyhedral oligomeric silsesquioxane (POSS) nanostructured chemicals and high density polyethylene (HDPE) were prepared via melt blending. Five POSS molecules were identified as suitable for evaluation due to their predicted compatibility with the HDPE matrix, as well as their thermal stability under the necessary HDPE processing conditions. POSS derivatives chosen were octamethyl (OM), octaisobutyl (OiB), octaisooctyl (OiO), trisilanol isobutyl (TSiB) and trisilanol isooctyl (TSiO). Surface characterization revealed that blend behavior is dependent not only on POSS R-group functionality, but also on POSS physical state and cage structure. Variable-angle ATR-FTIR indicated enhanced surface segregation for trisilanol POSS derivatives over their closed-cage analogues, as well as decreased surface crystallinity for all POSS blends compared to the neat HDPE. Surface and bulk imaging (AFM) revealed significant differences in blend morphology and roughness for the solid and liquid POSS derivatives; among POSS types of similar physical state, miscibility appeared to be governed by R-group alkly chain length. Nanoindentation and pin-on-disk tribology also suggest decreased surface crystallinity due to the incorporation of POSS, as well as significant difference in behavior between POSS molecules of different physical state.

Introduction

Performance of polymer composites has been shown to be highly dependent on homogeneity of dispersed filler material, as well as level of interaction between the filler surfaces and organic matrix.[1-3] Due to the highly-polar nature of conventional inorganic nanofillers, homogeneous filler dispersion is especially challenging in the formulation of high performance polymer nanocomposites.[4,5] In most cases, surface modification is necessary to enhance filler miscibility, though the introduction of time consuming and complicated reaction schemes may limit the commercial applicability of the resulting materials.[6-8] Fortunately, an exciting class of nanomaterial exists which has the potential to be tailored for miscibility in a wide range of polymer matrices not by chemical surface modification, but through modification of the molecular structure of the filler itself. Polyhedral oligomeric silsesquioxane (POSS) molecules are hybrid organic-inorganic nanostructures consisting of an inorganic Si-O-Si cage surrounded by a corona of organic substituents, described by the molecular formula $(RSiO)_{1.5}$.[9] The inorganic cage may be a fully condensed "closed" or "open" structure (Figure 3). The organic groups (R) are attached to the cage at the corner silicon atoms, and can be modified to tailor the performance and solubility characteristics of the POSS molecule. In essence, this gives researchers the ability to tune the solubility of POSS for good theoretical miscibility into a wide variety of organic matrices.

In our lab as well as others, POSS has been shown to produce a wide range of interesting surface and bulk property enhancements when dispersed in melt-blended polyolefin matrices.[10-24] Bulk properties are reported to be heavily influenced by concentration and dispersion level of the POSS molecules, where homogeneous

distribution of POSS nanocrystals has been shown to result in enhanced bulk degree of crystallinity and thermal stabiity.[10-14] In the melt state, incorporation of small amounts of POSS has been reported to enhance processability through viscosity reduction, attributed to increased free volume in the polymer melt due to well dispersed POSS cages reducing chain entanglement.[18,24] Tensile property enhancements have been reported for low-concentration POSS blends, attributed to good transfer of stresses from the olefin matrices to the stiff POSS cores.[15,19] Compared to conventional nanofillers, enhanced thermal, rheological and mechanical performance of POSS blends comes at relatively low filler concentration, attributed to the extremely small size (1-3 nm) and therefore high surface-area interaction between the POSS and polymer matrix.[25-27]

Though melt-blending is an attractive and relatively low-cost process, there are limited reports focusing on the surface characteristics of melt-processed POSS/polymer blends.[20,28,29] Other surface studies have primarily focused on either fluorinated POSS derivatives, or systems in which POSS is chemically bonded to the polymer matrix. Miyamoto et al. and Paul et al. reported enhanced dewetting of thin films of polystyrene and poly(tert-butyl acrylate), respectively, attributed to surface blooming of chemically incorporated POSS cages.[30,31] In the poly(tert-butyl acrylate) study, it was reported that increasing annealing temperature from 75°C to 95°C resulted in enhanced POSS phase separation and surface segregation, as verified by AFM and X-ray photoelectron spectroscopy.[31] Mammeri et al. chemically reacted dimethylsiloxy isobutyl POSS with both cyclohexylmethacrylate and tetra-ethoxylatedbisphenol A, and using goniometry reported a 30° water contact angle increase for the POSS blends, attributed to the highly-hydrophobic POSS cages residing on the sample surfaces.[32] Tujeta et al. and Iacono et al.

have reported highly hydrophobic and oleophobic surfaces for blends of fluorinated POSS with PMMA and perfluorocyclobutyl aryl ether polymers respectively, attributed to increased surface roughness and enhanced reentrant surface effects.[33,34] Koh et al. have also reported surface enrichment in fluorinated-POSS/PMMA nanocomposites, where XPS analysis revealed a 50% increase in POSS surface concentration for annealed samples (180°C for five days) compared to non-annealed samples, as well as a depth-dependent POSS concentration gradient (15 wt. % POSS concentration decrease over the first 8 nm of penetration).[35] Surface enrichment was attributed to the low surface free energy of the POSS molecules, and annealing led to increased surface segregation.

Results from our lab show preferential surface segregation of crystalline POSS in a variety of organic matrices.[20,28,29] AFM analysis revealed that incorporation of 10 wt. % OiB POSS into polypropylene via melt blending resulted in a 90% increase in RMS surface roughness , and an 80% decrease in nano-scale coefficient of friction (C.O.F.), while nanoindentation revealed a 100% increase in surface modulus. Increased surface roughness and modulus were attributed to migration of the robust POSS nanocrystals to the sample surface, affecting overall surface energy and mechanical performance. Variable-angle attenuated total reflectance Fourier transform infrared spectroscopy (ATR-FTIR) of the same nanocomposites revealed higher concentrations of POSS near the sample surface as compared to the bulk, attributed to decreased miscibility and competing enthalpic/entropic interactions between the highly-polar POSS molecules and the non-polymer matrices driving segregation.[20] Additional findings reported from our lab are decreased surface energy for Nylon-6 upon incorporation of 10 wt. % OiB and trisilanol phenyl (TSP) POSS (48% and 45%, respectively), as well as changes in

observed POSS miscibility (verified by TEM-EDAX) based on molecular structure.[28,29] At the present time, no reports have been found in the literature which relate POSS substituent chain length, cage structure, or physical state to observed surface behaviors of POSS/polymer blends. Additionally, no surface-specific studies have been found relative to incorporation of POSS into a highly-crystalline matrix. Degree of crystallinity has been shown to be a dominant factor in polyethylene surface properties.[36] Though depth profiling has shown the propensity of POSS to surface segregate in melt-blended matrices, there are no reports as to the effects of POSS on surface degree of crystallinity.

This study is an attempt to understand the effect of POSS physical state, cage structure and R-group functionality on miscibility and surface properties of HDPE/POSS blends prepared via melt processing. Five types of POSS were identified as suitable for evaluation due to their predicted compatibility with the HDPE matrix, as well as their thermal stability under the necessary HDPE processing conditions. Depth-dependent distribution of POSS, as well as depth-dependent surface crystallinity, of the HDPE/POSS blends will be monitored using variable-angle ATR-FTIR. Surface and bulk morphology of the blends will be imaged using atomic force microscopy (AFM). Effects of POSS on surface hardness/modulus will be examined using load-controlled nanoindentation analysis. Finally, macro-scale C.O.F. will be monitored through pin-on-disk tribology.

Experimental

Variable-Angle ATR-FTIR

ATR-FTIR spectra were collected using a Thermo Scientific Nicolet 6700 spectrometer (Waltham, MA) equipped with a MCT-A detector and a Pike Technologies

Multiple Reflection Horizontal ATRMax II variable angle stage (Madison, WI.). To obtain semi-quantitative depth profiles, the surface of each melt-pressed sample was analyzed using KRS-5 and germanium (Ge) internal reflection elements (56 x 10 x 4 mm with a face cut angle of 45°). Depth of penetration, D_p, of the evanescent IR beam was estimated using the equation:

$$D_p = \frac{\lambda}{2\pi n_1 \sqrt{\sin^2\theta - \left(\frac{n_2}{n_1}\right)^2}} \tag{11}$$

where λ is the wavelength of IR radiation measured normal to the surface, θ is the effective angle of incidence measured normal to the surface, n_1 is the refractive index of KRS-5 (2.37) or Ge (4.00), and n_2 is the refractive index of the neat HDPE (1.53). All spectra were corrected for optical effects using Thermo Scientific Ominc 8.0 and Grams 7.02 software suites.

To determine depth-dependent POSS concentration, absolute peak areas for the 1115cm^{-1} (Si-O stretching), 1472 cm^{-1} and 1462 cm^{-1} (CH_2 bending) absorption bands were calculated by integration using the method suggested by Mirabella et al.[37] Ratios of these bands were used to determine relative concentration of POSS at each angle of incidence. To determine depth-dependent degree of crystallinity, absorption bands at 722 cm^{-1} (HDPE amorphous fraction), 730 cm^{-1} and 719 cm^{-1} (HDPE crystalline fraction) were peak fitted using a mixed Gaussian-Lorentzian routine at each angle of incidence. Relative concentration of crystalline and amorphous phases was extracted in the form of absolute integrals using the method suggested by Gregoriou et al.[38]

Atomic Force Microscopy (AFM)

Morphological studies were conducted on an AFM 5500 scanning probe microscope from Agilent Technologies (Santa Clara, CA). Probes were purchased from Veeco Probes (Santa Barbara, CA). A silicon probe with a 125 μm long silicon cantilever, nominal force constant of 40 N/m, and resonance frequency of 275 KHz was used for tapping mode surface topography studies. 2 μm x 2 μm scan size areas were evaluated with an image resolution of 512 x 512 pixels at a scan rate of 1 Hz. Multiple areas were imaged, and figures show representative morphology.

Nanoindentation

Specimen surface hardness and modulus were determined using a Hysitron Triboindenter (Minneapolis, MN) with a calibrated, pyramidal Berkovich probe. For each sample, a series of 10 indentations were performed at room temperature utilizing a 2 x 5 grid pattern. To determine optimum indentation parameters for HDPE, preliminary data were collected via two series of 10 indentations; one test ranging in force from 100 μN to 1000 μN (shallow depth), and the other from 1000 μN to 10,000 μN (deeper depth). The loads selected for constant force testing were determined by examining the data and locating the force values with the highest degree of grouping (500 μN and 4000 μN, respectively). Samples were then analyzed by loading at a constant rate over a 30 s time period, holding for 10 s, and unloading at a rate identical to that of the loading period. The total test time was approximately 70 s. Ten repeats were completed for each sample, with the resulting values reported along with their associated standard deviations.

Pin-on-Disk Tribology

Macroscale C.O.F. measurements were performed using a Micro Photonics pin-on-disk tribometer (Philadelphia,PA), according to ASTM G99. Each sample (approximately 30 mm X 50 mm) was tested inside a controlled environment chamber at a relative humidity of 10% and at a temperature of 22°C. Testing was conducted at low humidity to reduce the effects of moisture as a lubricant on the surface. Samples were affixed to a rotating steel disk (radius of path 3 mm) against a steel ball (3 mm diameter, Small Parts Inc., Miami Lakes, FL) at 20 rpm for 10 min. Surface friction measurements were conducted at a load of 5 N. For reproducibility, three measurements were taken for each sample and the average is reported.

Results and Discussion

Variable Angle ATR-FTIR

Figure 24 shows grazing angle (0.45 μm depth) ATR-FTIR spectra for the neat HDPE, neat OiB POSS, and 1 and 5 wt. % OiB/HDPE blends. The neat OiB POSS displays a characteristic absorbance shoulder at 1115cm^{-1}, attributed to Si-O stretching vibrations. The neat HDPE displays characteristic absorptions at 1472 cm^{-1} and 1462 cm^{-1}, attributed to CH_2 bending. The absorbance at 1115cm^{-1} due to POSS is absent in the neat HDPE spectrum, but appears in both of the POSS blend spectra verifying the presence of POSS in these systems. Figure 25 shows variable-angle ATR-FTIR spectra for the 1 wt. % OiB/HDPE blend at different penetration depths. Data for the other POSS blends display similar trends (Figures 26-29). In all cases, the intensity of the absorbance peak due to POSS decreases with increasing penetration depth into the blend, indicating preferential surface segregation of the POSS molecules.

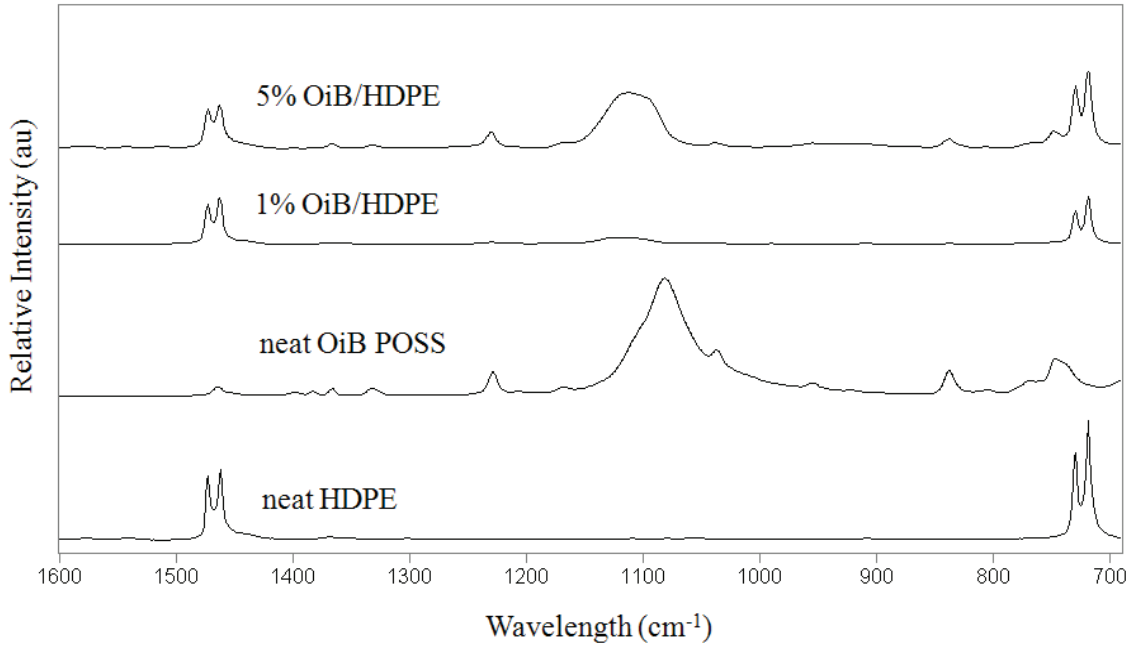

Figure 24. Grazing-angle ATR-FTIR spectra for the neat HDPE, neat OiB POSS, 1 and 5 wt. % OiB/HDPE blends.

Previous studies in our laboratory showed similar surface segregation of OiB POSS in a polypropylene matrix.[20] Figure 30 shows differential relative POSS concentration as a function of penetration depth for the 1 wt. % POSS/HDPE blends. The highest level of relative POSS concentration for each blend is observed near the surface. The surface relative POSS concentration for each blend was normalized to 0%, while the differential shows the percent decrease in POSS concentration as a function of penetration depth. For each blend, the relative POSS concentration decreases rapidly with increasing depth and each approach constant values between 0.53 to 0.59 μm depth. The trisilanol POSS molecules show a greater differential in surface and bulk concentration, indicating a higher degree of surface segregation. This is attributed to the lower miscibility of the trisilanol molecules with the HDPE matrix.

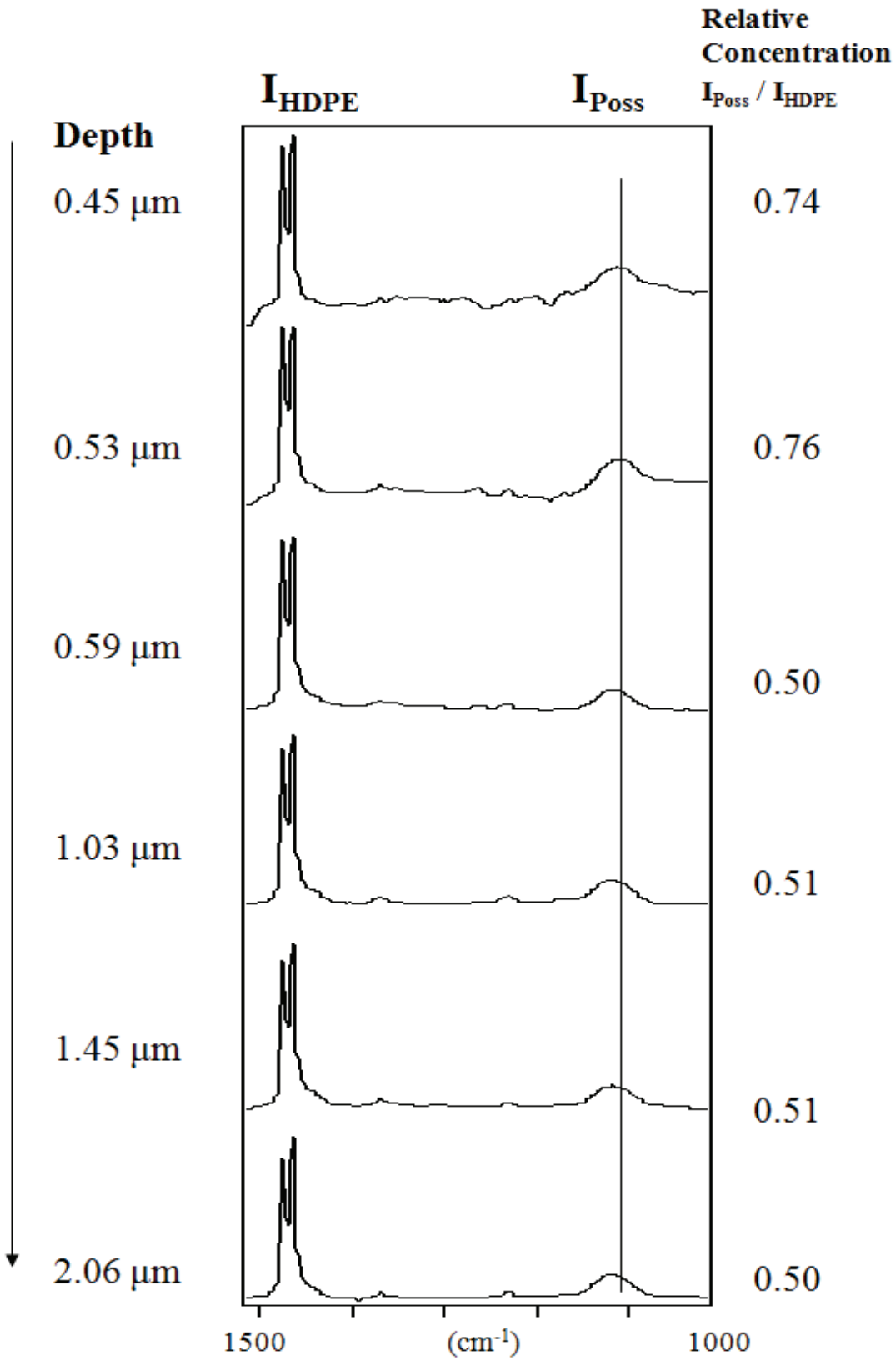

Figure 25. Variable-angle ATR-FTIR spectra for the 1 wt. % OiB/HDPE blend.

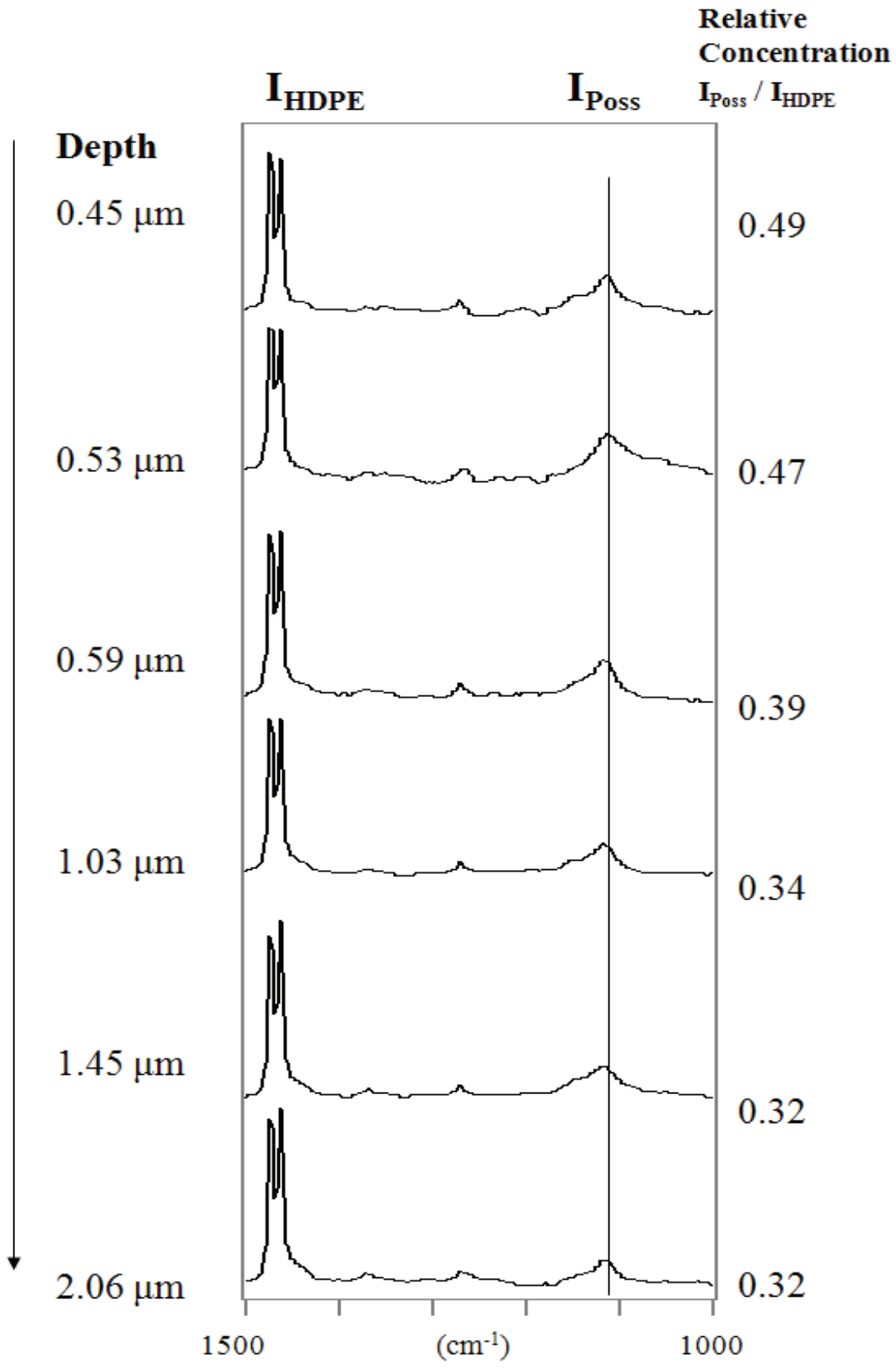

Figure 26. Variable-angle ATR-FTIR spectra for the 1 wt. % OM/HDPE blend.

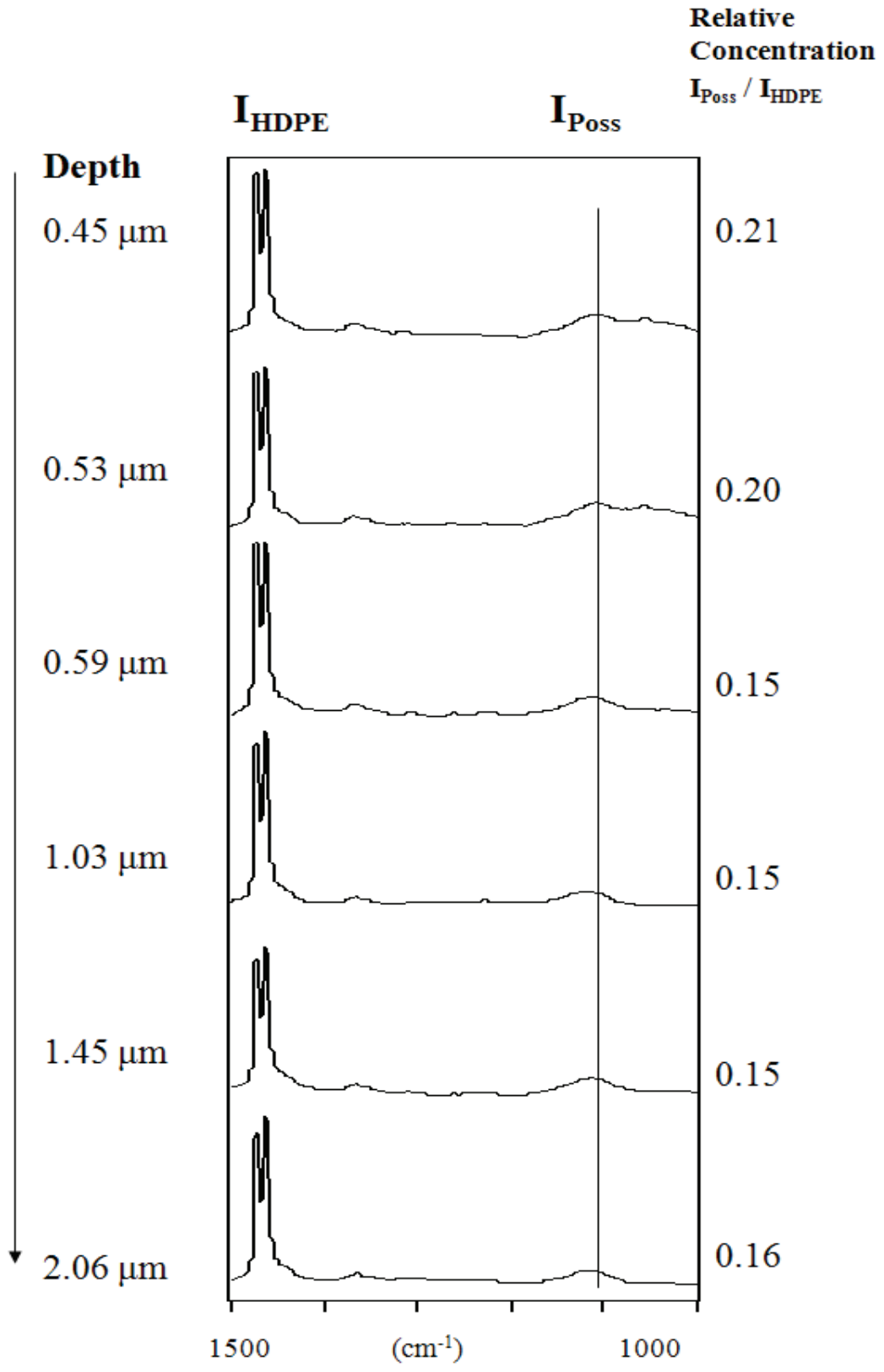

Figure 27. Variable-angle ATR-FTIR spectra for the 1 wt. % OiO/HDPE blend.

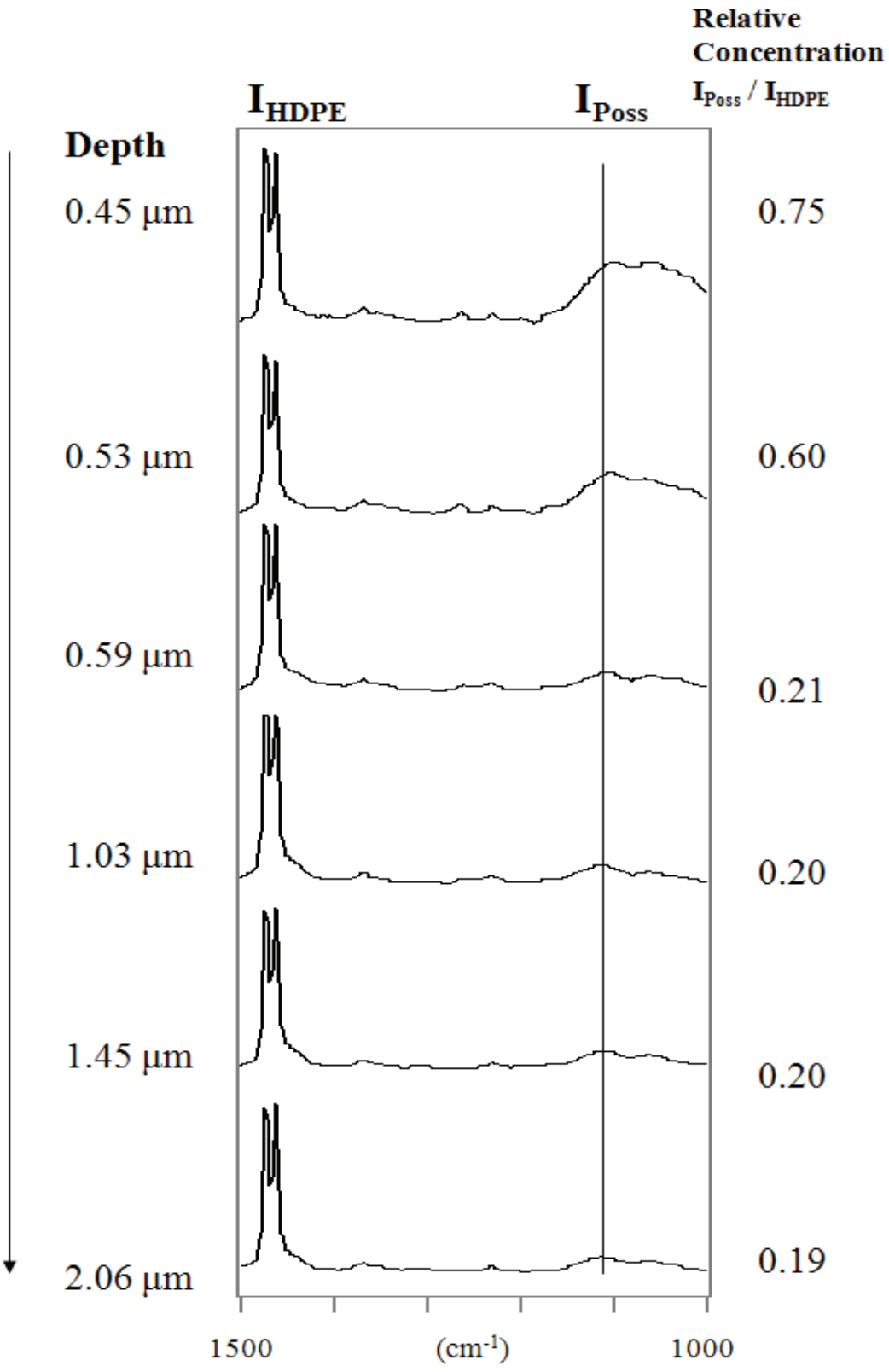

Figure 28. Variable-angle ATR-FTIR spectra for the 1 wt. % TSiB/HDPE blend.

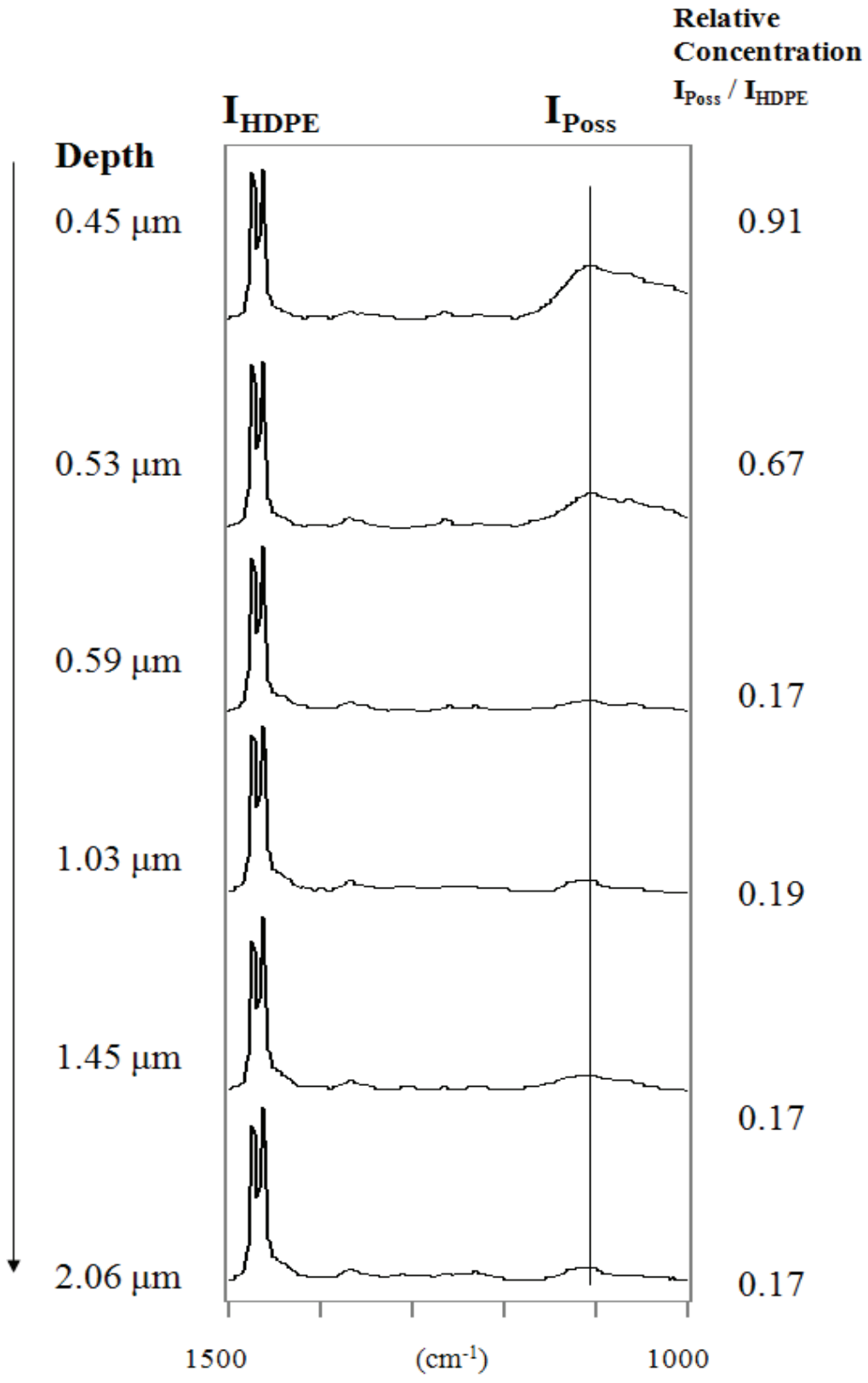

Figure 29. Variable-angle ATR-FTIR spectra for the 1 wt. % TSiO/HDPE blend.

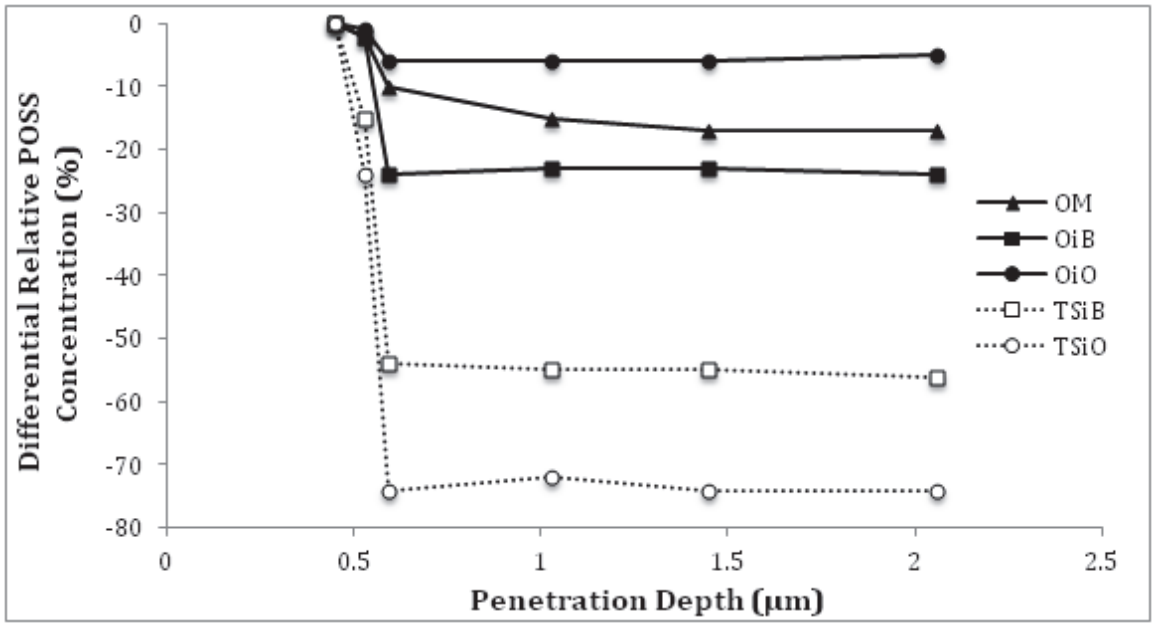

Figure 30. Differential relative POSS concentration as a function of penetration depth for the 1 wt. % POSS/HDPE blends.

Additionally, Feher et al. reported condensation of the trisilanol POSS cage at temperatures above 200°C, slightly below that used for processing our HDPE/POSS blends.[39] Low molecular weight condensation species are expected to have higher mobility and a greater propensity to move to the surface.

Figure 31 shows degree of crystallinity as a function of penetration depth for the neat HDPE and 1 wt. % POSS/HDPE blends. For all samples crystallinity is highest near the surface. The crystallinity approaches a constant level of 66-70% at depths of 1 μm and greater, which is similar to bulk crystallinity values obtained by DSC and WAXD (Chapter III). Chen et al. reported similar surface behavior for compression molded polypropylene samples, where a 25% decrease in surface crystallinity was observed via variable-angle ATR-FTIR over the first 2 μm of penetration.[40] This behavior can be attributed to rapid polymer crystallization at the interface in the formation of the lowest-energy surface, below which crystallization is reduced due to decreased chain mobility

towards the bulk.[41,42] This effect can be further catalyzed if the polymer melt is allowed to cool against a high energy surface, as is the case with our samples (SiO_2).[43,44]

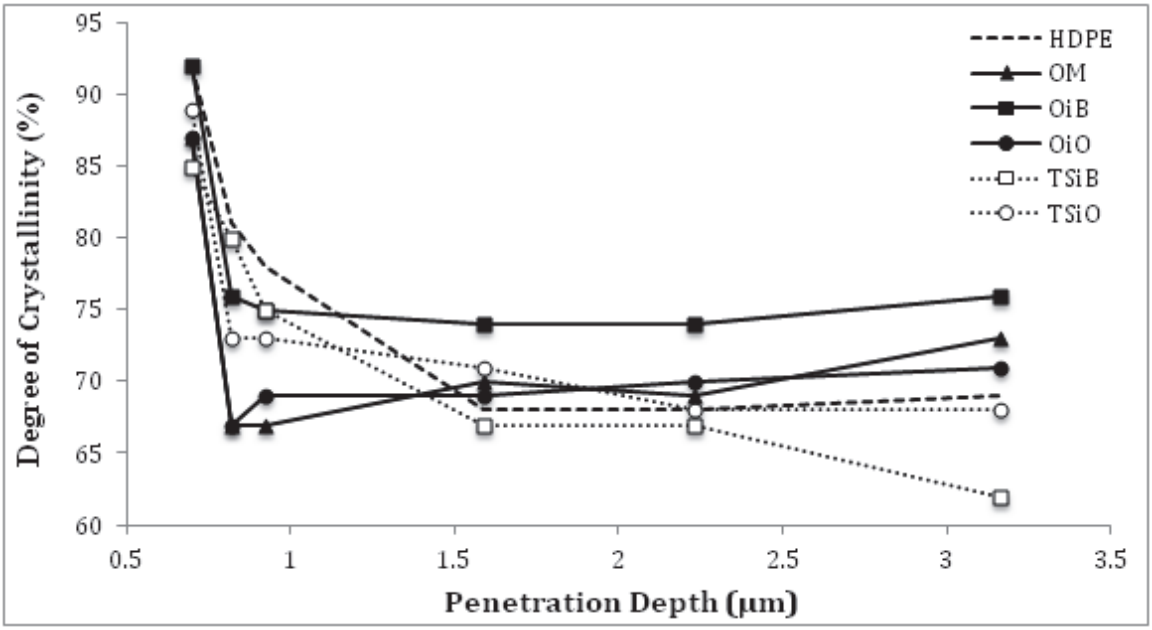

Figure 31. Degree of crystallinity as a function of penetration depth for the neat HDPE and 1 wt. % POSS/HDPE blends.

The HDPE/POSS blends show a generally rapid decrease in crystallinity as a function of depth from the surface, while the neat HDPE shows a more gradual decrease. This is attributed to the propensity of POSS to segregate to the high energy interface (SiO_2 in this case) during film formation, as is verified in Figure 30. In general, the POSS blends display a greater reduced degree of crystallinity than the neat HDPE for depths of less than 1 μm. In this surface region, the higher relative concentration of POSS molecules (Figure 30) can lead to decreased HDPE chain mobility, resulting in the observed decreased crystallinity. At depths of 1.5 μm and greater, the POSS appears to have little effect on the overall crystallinity of the HDPE, though variable-angle IR verifies the presence of POSS at all analyzed depths (2 μm max). This may be due in part

to the reduced relative concentration of POSS at these depths, leading to decreased impact on chain mobility during crystal formation.

Atomic Force Microscopy

Figure 32 shows AFM height (left) and phase (right) images of the neat HDPE, and the 5 wt. % OM and OiB/HDPE (solid POSS) blends. Figure 33 shows AFM surface height (left) and phase (right) images of the 5 wt. % OiO, TSiB and TSiO/HDPE (liquid POSS) blends. The neat HDPE shows morphology characteristic of a crystalline polyolefin, with areas of highly-ordered lamellae and no apparent contamination effects due to compression molding.[36] In all cases, the addition of POSS results in different surface morphology than that of the neat HDPE, as well as increased surface roughness (Table 8). We previously reported increased surface roughness on incorporation of POSS in polypropylene, Nylon-6 and polystyrene matrices, attributed to surface segregation of the POSS molecules.[20,28,29] AFM phase imaging provides information about differences in stiffness and modulus across the sample surface. For the solid POSS molecules, the crystalline lamellae are less visible, surface crystallinity appears to be disrupted and high stiffness spheroidal features are observed. The spheroidal features are attributed to POSS aggregates, which have been observed in previous studies of polypropylene and Nylon-6 POSS nanocomposites (verified by TEM-EDAX).[20,29] The aggregates in the OM POSS sample are approximately 92 nm in diameter. Those in the OiB POSS sample are approximately 32 nm in diameter and appear to be more evenly dispersed across the surface. For the liquid POSS samples (Figure 33), crystalline lamellar features are clearly visible. Larger, less regular lamellae are observed for the OiO and TSiO samples.

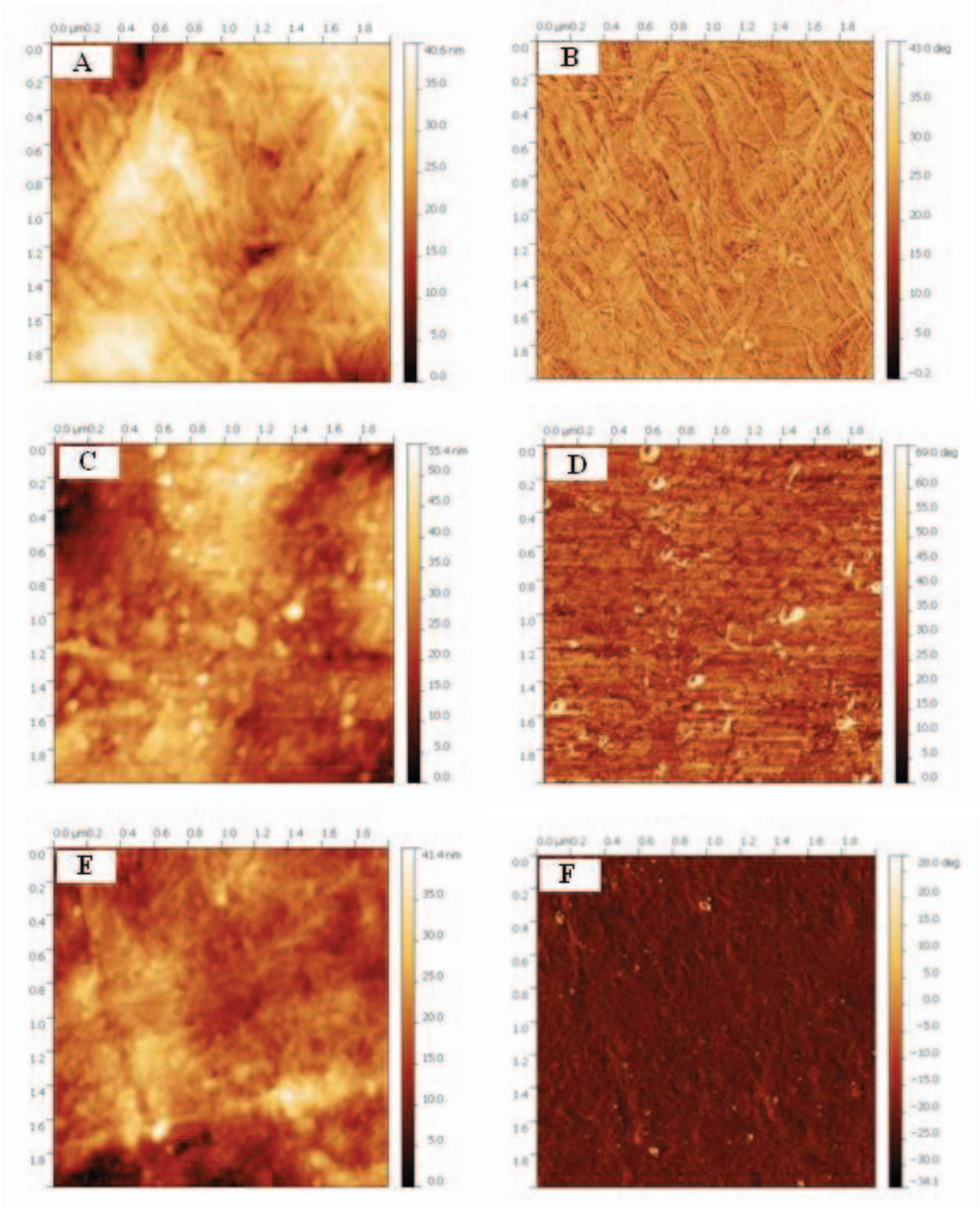

Figure 32. AFM surface images of neat HDPE and the 5 wt. % solid POSS blends: A) neat HDPE height, B) neat HDPE phase, C) OM height, D) OM phase, E) OiB height, F) OiB phase.

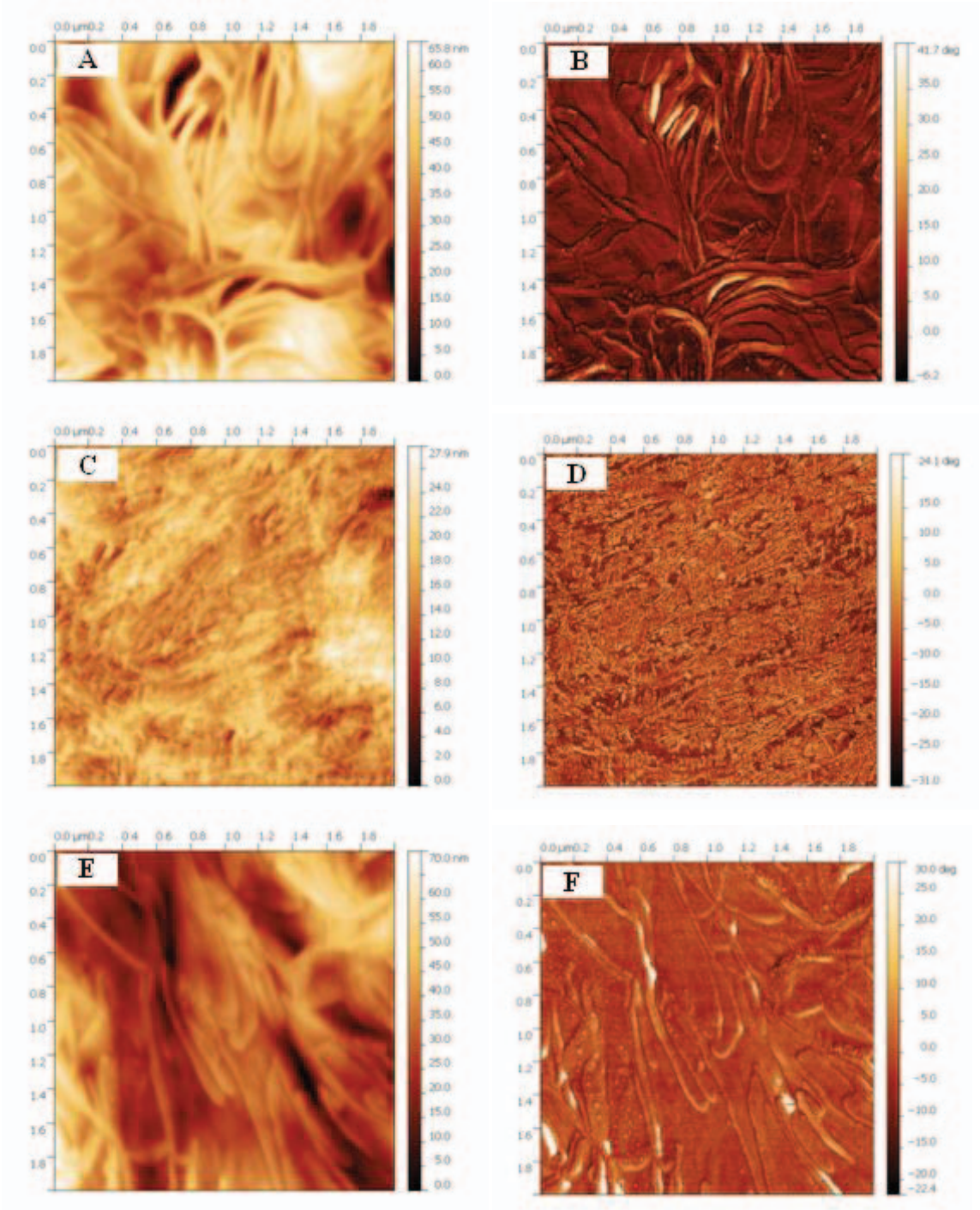

Figure 33. AFM surface images of the 5 wt. % liquid POSS blends: A) OiO height, B) OiO phase, C) TSiB height, D) TSiB phase, E) TSiO height, F) TSiO phase.

Small spheroidal features are observed, particularly in the TSiB sample. The OiO and TSiO samples are liquids at room temperature, while the TSiB sample is a solid at room temperature but expected to condense and liquefy at processing temperatures (Chapter

III). It is possible that the TSiB is not completely condensed during reaction and may contain solid particles. It is also possible that solid products result from the condensation reaction.

Table 8 shows AFM surface RMS roughness for the neat HDPE and the 1 and 5 wt. % POSS/HDPE blends.

Table 8

AFM surface RMS roughness for the neat HDPE and HDPE/POSS blends

Material	RMS 0 wt. % (nm)	1 wt. % (nm)	5 wt. % (nm)
HDPE	3.0	-	-
OM	-	7.2	10.2
OiB	-	4.2	7.2
OiO	-	4.1	4.1
TSiB	-	6.5	11.2
TSiO	-	5.6	9.1

For all samples incorporation of POSS results in an increase in surface roughness with increasing POSS concentration, as has been observed for other POSS nanocomposites.[20,28,29] For the solid POSS molecules, OM POSS blends display larger overall surface roughness than OiB POSS blends. This can be attributed to better miscibility of the OiB POSS with the HDPE, resulting in formation of smaller and more homogeneously dispersed POSS aggregates on the sample surface. For the liquid POSS molecules, OiO POSS displays smaller effects on surface roughness than the TSiB and TSiO POSS. This is attributed to superior miscibility of OiO with HDPE due to its

longer chain alkyl groups, and to the greater propensity of the trisilanol molecules to segregate to the surface than their closed-cage analogues. Of the trisilanol POSS molecules, TSiO blends display a smaller increase in surface roughness than the TSiB blends, attributed to superior miscibility with HDPE.

Samples were microtomed, and the surfaces created were imaged by AFM to gain greater understanding of the bulk morphology (Figures 34 and 35). As observed in the surface images, bulk analysis shows that all POSS blends display different morphology than the neat HDPE. For the solid POSS molecules, OM and OiB blends display a dispersion of POSS aggregates, with OM POSS aggregates (68 nm in diameter) appearing much larger than OiB (22 nm in diameter). The aggregates appear smaller and more widely dispersed in the bulk than at the surface, providing further evidence of the propensity of POSS to move to the surface. For the blends containing liquid POSS molecules, the crystalline structure observed in the bulk is finer than the lamellae observed on the surface, and more similar to the morphology of the neat HDPE. The observed differences in surface and bulk morphology are attributed to the high degree of surface segregation of POSS for these systems, as indicated by the ATR-FTIR studies.

Nanoindentation

Figures 36 and 37 show the effect of increasing POSS concentration on nanoindentation modulus and hardness, respectively at a load of 4000 μN. At 1 wt. % POSS, all blends show a slight decrease in modulus and hardness compared to the neat HDPE. At 5 wt. % POSS, the liquid OiO, TSiO and TSiB blends show further decrease in hardness/modulus, while solid OM and OiB POSS blends show increased performance compared to their 1 wt. % counterparts.

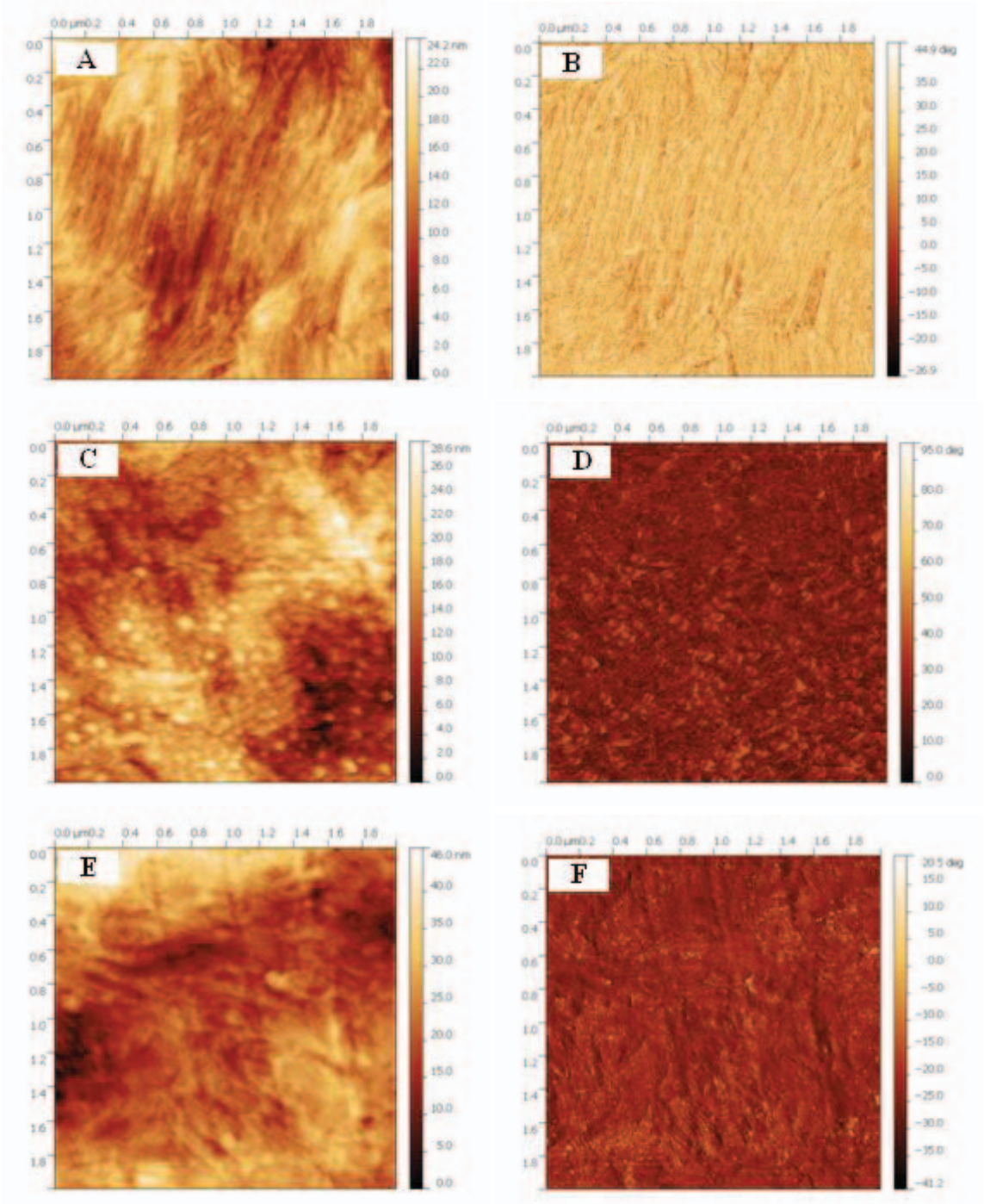

Figure 34. AFM bulk images of neat HDPE and the 5 wt. % solid POSS blends: A) neat HDPE height, B) neat HDPE phase, C) OM height, D) OM phase, E) OiB height, F) OiB phase.

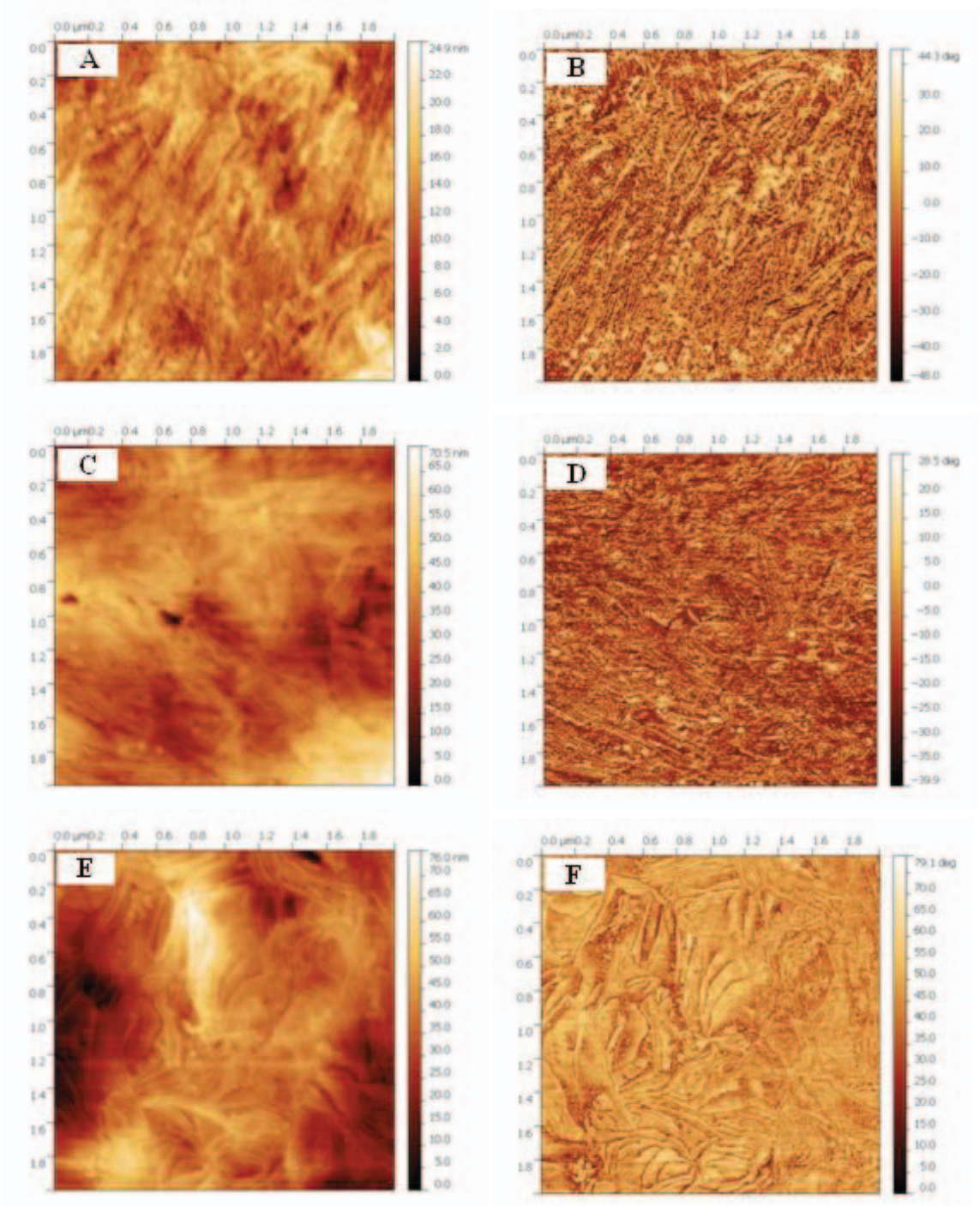

Figure 35. AFM bulk images of the 5 wt. % liquid POSS blends: A) OiO height, B) OiO phase, C) TSiB height, D) TSiB phase, E) TSiO height, F) TSiO phase.

Figures 38 and 39 show the effect of increasing POSS concentration on nanoindentation modulus and hardness (respectively) at a load of 500 μN. Testing at a lower load reveals performance closer to the sample surface. Though the values of modulus and hardness

are higher for all samples when measured closer to the surface, similar decreases are observed on incorporation of POSS in HDPE.

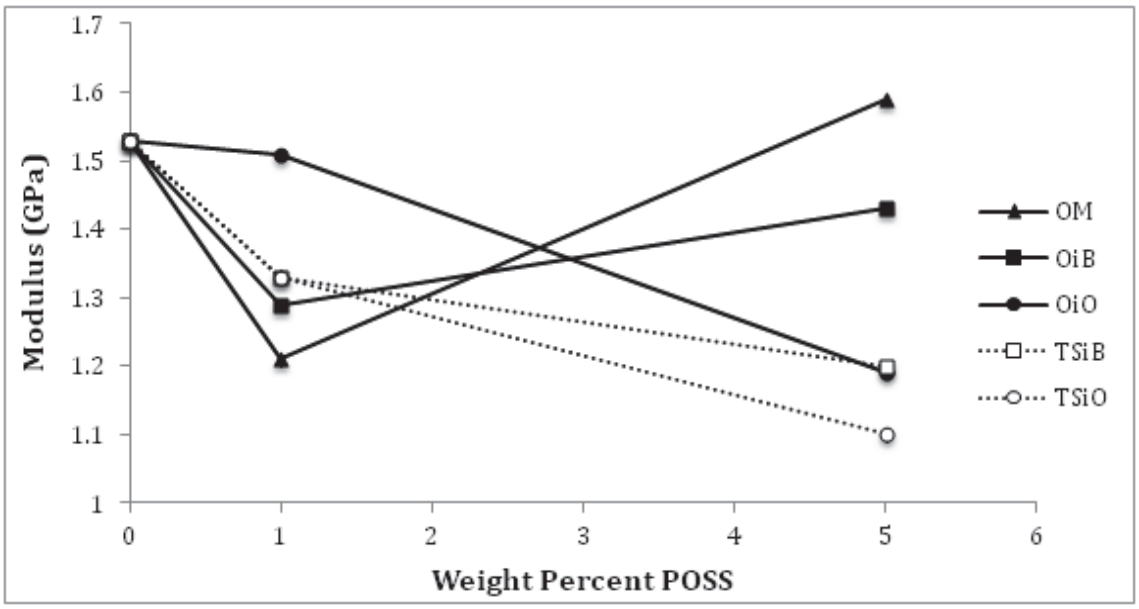

Figure 36. Nanoindentation modulus as a function of increasing POSS concentration at a load of 4000 μN.

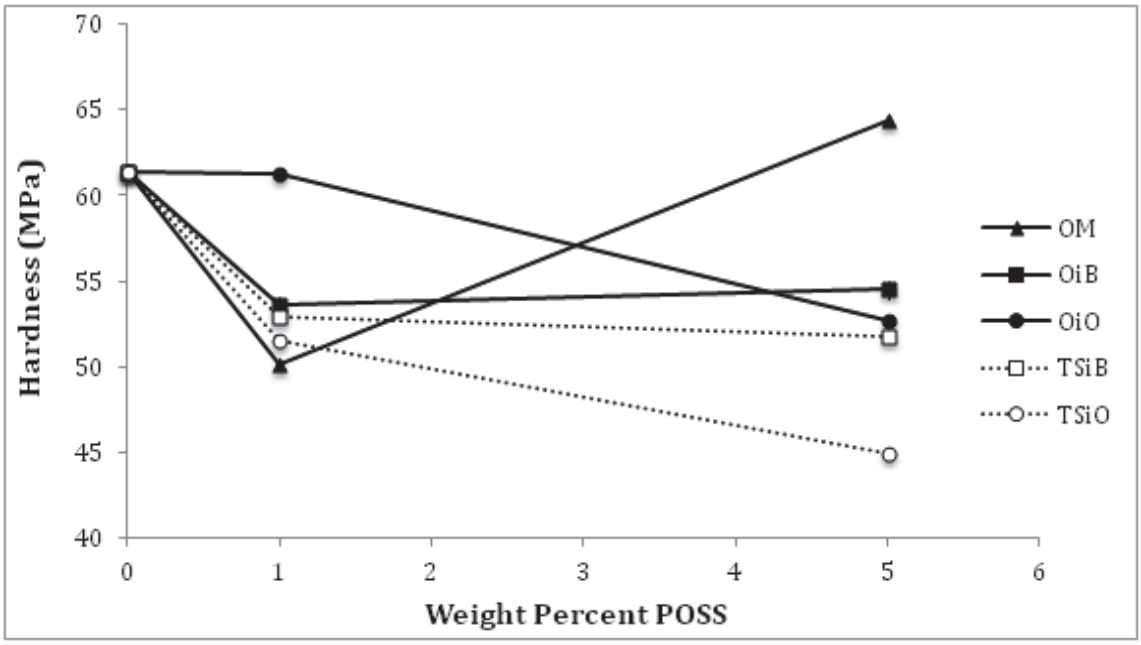

Figure 37. Nanoindentation hardness as a function of increasing POSS concentration at a load of 4000 μN.

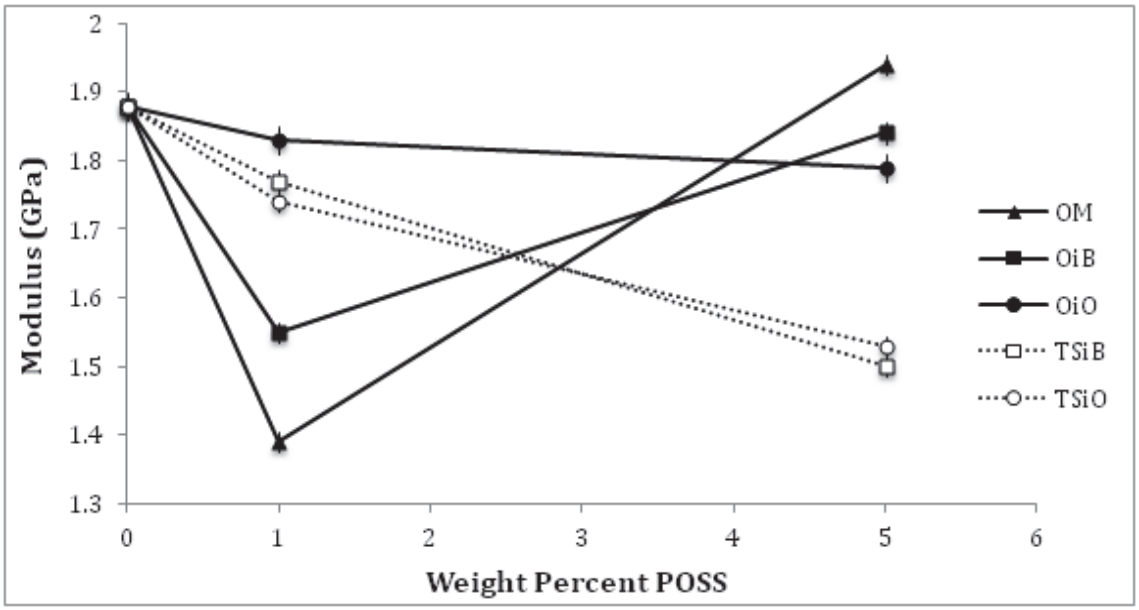

Figure 38. Nanoindentation modulus as a function of increasing POSS concentration at a load of 500 μN.

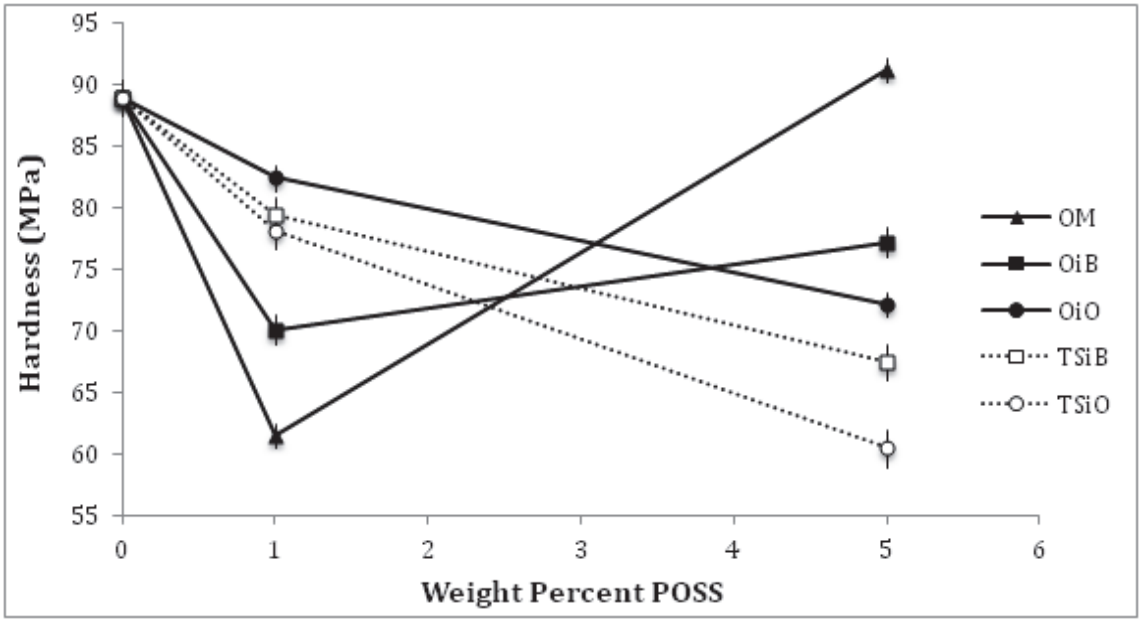

Figure 39. Nanoindentation hardness as a function of increasing POSS concentration at a load of 500 μN.

The reduced surface hardness and modulus for the blends is attributed to the reduced surface crystallinity observed for the POSS-containing blends in comparison to the neat HDPE. The findings contrast with our previous reports relative to

polypropylene/POSS and Nylon-6/POSS blends, where increased surface hardness and modulus were observed.[20,29] In those systems, the increase in hardness and modulus was attributed to full coverage of the surface with the POSS aggregates, verified by AFM. In the HDPE blends, on the other hand, widely dispersed POSS aggregates are observed in only the solid POSS systems. At high solid POSS concentrations, where greater POSS surface coverage is observed, the hardness and modulus values increase. Thus, it appears that good surface coverage is necessary for improved hardness and modulus, and, in the case of HDPE, the reduction in surface crystallinity has a greater negative effect on surface hardness and modulus than the improvements provided by incorporation of POSS. For the liquid POSS samples, the reductions in surface modulus are attributed to plasticization of the HDPE, as observed in bulk mechanical testing (Chapter III).

Pin-on-Disk Tribology

Figure 40 shows the effect of increasing POSS concentration on the macro-scale C.O.F. of HDPE. The solid OM and OiB POSS samples show a slight increase in C.O.F. compared to the neat HDPE at 1 wt. % POSS, with a further increase at 5 wt. %. The liquid OiO, TSiO and TSiB POSS samples show a decrease in C.O.F. compared to the neat HDPE at all concentrations. The decreased C.O.F. observed for the liquid POSS molecules is attributed to surface lubrication. The increased friction observed for the solid POSS molecules is attributed to decreased HDPE surface crystallinity and to the generation of wear particles on incorporation of POSS. Wang et al. reported similar behavior relative to PEEK melt blended with ZrO_2 nanoparticles, where phase separation of filler resulted in the formation of wear particles (verified by SEM-EDAX).[45]

In our previous reports of PP-POSS and Nylon 6-POSS nanocomposites, decreased C.O.F. was observed which was attributed to uniform coverage of the surfaces with POSS aggregates.[20,29]

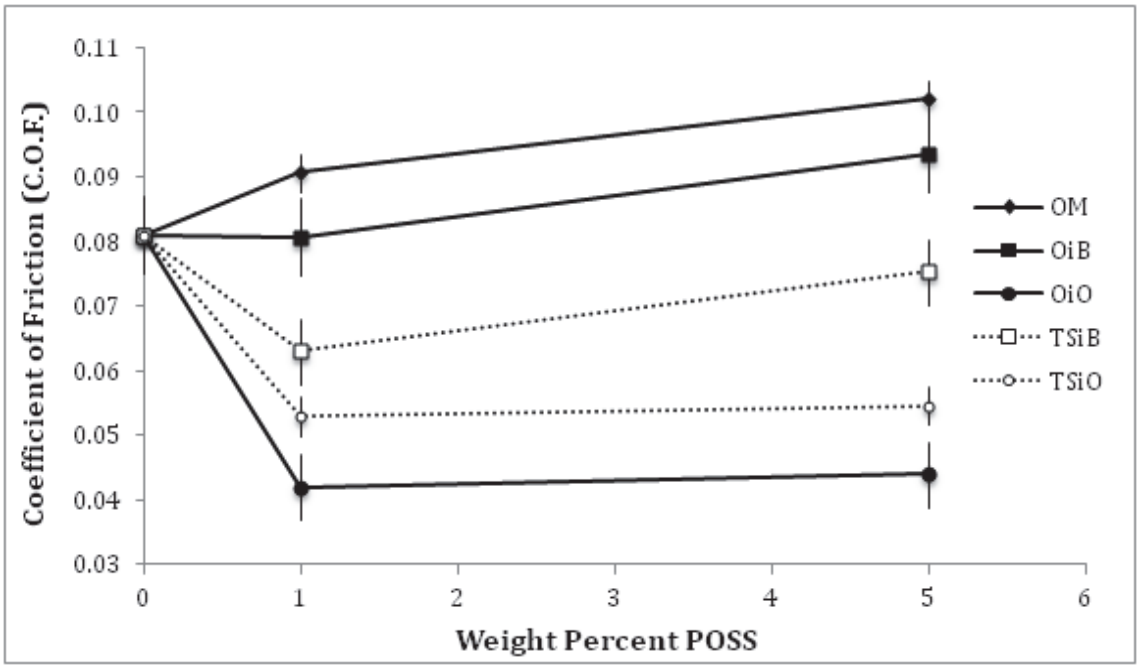

Figure 40. Pin-on-disk coefficient of friction (C.O.F.) as a function of increasing POSS concentration (5N, 10% relative humidity).

The mechanisms involved in our current study appear to be different, with the physical form of the POSS molecule playing the greatest role in determining surface properties of the HDPE blends. The liquid POSS molecules segregate to the surface and provide plasticization and lubrication, while the solid POSS molecules segregate to a smaller extent and disrupt surface crystallinity.

Conclusions

HDPE/POSS blends were successfully prepared via melt-processing and their surface and bulk properties analyzed. Variable-angle ATR-FTIR analysis of the blends revealed surface-segregating behavior for all POSS molecules, with trisilanol POSS

derivatives appearing to segregate to a much greater extent than their closed-cage analogues, though IR specrta revealed the presence of POSS at all depths analyzed (up to 2 μm). Increased concentration of POSS near the sample surfaces (<1 μm) resulted in a slight decrease in surface crystallinity, attributed to POSS affecting chain mobility. Reduced concentration of POSS towards the bulk (>1.5 μm) allowed the HDPE to crystallize under more regular conditions. AFM imaging revealed that the addition of POSS resulted in different surface morphology than that of the neat HDPE, as well as increased surface roughness. The solid POSS molecules resulted in decreased visibility of crystalline lamellae, as well as the formation of high stiffness spheroidal features. These affects were more predominant at the surface than in the bulk, attributed to POSS surface segregation. Size and dispersion of spheroidal features appear to be governed by POSS miscibility with the HDPE. The liquid POSS molecules resulted in larger, less regular lamellae, as well as the presence of small spheroidal features (particularly in the TSiB sample) which may be products formed due to cage condensation. The crystalline structure observed in the bulk was similar to that of neat HDPE, attributed to the high degree of surface segregation of POSS for these systems. TSiO blends displayed a smaller increase in surface roughness than TSiB, again attributed to superior miscibility. Nanoindentation revealed decreased surface hardness/modulus compared to the neat HDPE for all blends. For the solid POSS blends, this was attributed to a small degree of surface coverage of the stiff POSS cages, as well as reduced surface crystallinity. For the liquid molecules, this was attributed to plasticization. Increased C.O.F. for the solid POSS blends was also attributed to reduced surface crystallinity, as well as the potential of wear particle formation due to POSS phase separation. This is more apparent for the

OM blends than the OiB, attributed to decreased miscibility. For the liquid POSS blends, decreased surface C.O.F. is attributed to lubrication.

Acknowledgements

This work was supported by a fellowship from the National Science Foundation GK-12 program "Connections in the Classroom: Molecules to Muscles", Award # 0947944 through the University of Southern Mississippi.

This work was supported in part by the Office of Naval Research, Award No. N00014-07-1057.

REFERENCES

1. Balazs, A. C.; Emrick, T.; Russell, T. P. Science **2006**, 314, 1107.

2. Chrissafis, K.; Paraskevopoulos, K.; Tsiaoussis, I.; Bikiaris, D. J. Appl. Polym. Sci. **2009**, 114, 1606-1618.

3. Coleman, J. N.; Khan, U.; Blau, W. J.; Gun'ko, Y. K. Carbon **2006**, 44, 1624-1652.

4. Gacitua, W.; Ballerini, A.; Zhang, J. Maderas. Cienc. Tecnol. (Washington, D. C.) **2005**, 7, 159-178.

5. Hussain, F.; Hojjati, M.; Okamoto, M.; Gorga, R. E. J. Compos. Mater. **2006**, 40, 1511-1575.

6. Lau, K.; Gu, C.; Hui, D. Composites, Part B **2006**, 37, 425-436.

7. LeBaron, P. C.; Wang, Z.; Pinnavaia, T. J. Appl. Clay Sci. **1999**, 15, 11-29.

8. Manias, E.; Touny, A.; Wu, L.; Strawhecker, K.; Lu, B.; Chung, T. Chem. Mater. **2001**, 13, 3516-3523.

9. Lichtenhan, J. D. Comments on Inorg. Chem. **1995**, 17, 115-130.

10. Chen, J. H.; Yao, B. X.; Su, W. B.; Yang, Y. B. Polymer **2007**, 48, 1756-1769.

11. Fu, B. X.; Yang, L.; Somani, R. H.; Zong, S. X.; Hsiao, B. S.; Phillips, S.; Blanski, R.; Ruth, P. J. Polym. Sci., Part B: Polym. Phys. **2001**, 39, 2727-2739.

12. Joshi, M.; Butola, B. Polymer **2004**, 45, 4953-4968.

13. Joshi, M.; Butola, B. J. Appl. Polym. Sci. **2007**, 105, 978-985.

14. Pracella, M.; Chionna, D.; Fina, A.; Tabuani, D.; Frache, A.; Camino, G. Macromol. Symp. **2006**, 234, 59-67.

15. Baldi, F.; Bignotti, F.; Fina, A.; Tabuani, D.; Ricco, T. J. Appl. Polym. Sci. **2007**, 105, 935-943.

16. Fina, A.; Tabuani, D.; Frache, A.; Camino, G. Polymer **2005**, 46, 7855-7866.

17. Fu, B. X.; Gelfer, M. Y.; Hsiao, B. S.; Phillips, S.; Viers, B.; Blanski, R.; Ruth, P. Polymer **2003**, 44, 1499-1506.

18. Joshi, M.; Butola, B.; Simon, G.; Kukaleva, N. Macromolecules **2006**, 39, 1839-1849.

19. Lim, S. K.; Hong, E. P.; Choi, H. J.; Chin, I. J. J. Ind. Eng. Chem. (Washington, D. C.) **2010**, 16, 189-192.

20. Misra, R.; Fu, B. X.; Morgan, S. E. J. Polym. Sci., Part B: Polym. Phys. **2007**, 45, 2441-2455.

21. Scapini, P.; Figueroa, C. A.; Amorim, C. L. G.; Machado, G.; Mauler, R. S.; Crespo, J. S.; Oliveira, R. V. B. Polym. Int. **2010**, 59, 175-180.

22. Wheeler, P. A.; Misra, R.; Cook, R. D.; Morgan, S. E. J. Appl. Polym. Sci. **2008**, 108, 2503-2508.

23. Zhou, Z.; Zhang, Y.; Yin, N. J. Polym. Sci., Part B: Polym. Phys. **2008**, 46, 526-533.

24. Zhou, Z.; Zhang, Y.; Zeng, Z. J. Appl. Polym. Sci. **2008**, 110, 3745-3751.

25. Fina, A.; Monticelli, O.; Camino, G. J. Mater. Chem. **2010**, 20, 9297-9305.

26. Gnanasekaran, D.; Madhavan, K.; Reddy, B. J. Sci. Ind. Res. **2009**, 68, 437-464.

27. Li, G.; Wang, L.; Ni, H.; Pittman, C. U. J. of Inorg. Org. Polym. **2001**, 11, 123-154.

28. Misra, R.; Alidedeoglu, A. H.; Jarrett, W. L.; Morgan, S. E. Polymer **2009**, 50, 2906-2918.

29. Misra, R.; Fu, B. X.; Plagge, A.; Morgan, S. E. J. Polym. Sci., Part B: Polym. Phys. **2009**, 47, 1088-1102.

30. Miyamoto, K.; Hosaka, N.; Kobayashi, M.; Otsuka, H.; Yamada, N.; Torikai, N.; Takahara, A. Polym. J. **2007**, 39, 1247-1252.

31. Paul, R.; Karabiyik, U.; Swift, M. C.; Esker, A. R. Langmuir **2008**, 24, 5079-5090.

32. Mammeri, F.; Bonhomme, C.; Ribot, F.; Babonneau, F.; Direa, S. Chem. Mater. **2009**, 21, 4163-4171.

33. Tuteja, A.; Choi, W.; Ma, M.; Mabry, J. M.; Mazzella, S. A.; Rutledge, G. C.; McKinley, G. H.; Cohen, R. E. Science **2007**, 318, 1618.

34. Iacono, S. T.; Budy, S. M.; Smith, D. W.; Mabry, J. M. J. Mater. Chem. **2010**, 20, 2979-2984.

35. Koh, K.; Sugiyama, S.; Morinaga, T.; Ohno, K.; Tsujii, Y.; Fukuda, T.; Yamahiro, M.; Iijima, T.; Oikawa, H.; Watanabe, K. Macromolecules **2005**, 38, 1264-1270.

36. Peacock, A. J. Use and fabrication of polyethylene products. In *Handbook of polyethylene: structures, properties, and applications*; CRC Press: New York, 2000, Chapter 9, pp 502-204.

37. Mirabella Jr, F. Spectroscopy **1990**, 5, 20-30.

38. Tzavalas, S.; Gregoriou, V. G. Appl. Spec. **2005**, 59, 1148-1154.

39. Feher, F. J.; Newman, D. A.; Walzer, J. F. J. Am. Chem. Soc. **1989**, 111, 1741-1748.

40. Chen, G.; Fina, L. J. J. Appl. Polym. Sci. **1993**, 48, 1229-1240.

41. Zerbi, G.; Gallino, G.; Del Fanti, N.; Baini, L. Polymer **1989**, 30, 2324-2327.

42. Tshmel, A.; Vettegren, V.; Zolotarev, V. J. Macro. Sci., Part B: Phys. **1982**, 21, 243-264.

43. Fitchmun, D.; Newman, S. J. Polym. Sci., Part B: Polym. Phys. **1970**, 8, 1545-1564.

44. Papageorgiou, G. Z.; Achilias, D. S.; Bikiaris, D. N.; Karayannidis, G. P. Thermochim. Acta **2005**, 427, 117-128.

45. Wang, Q.; Xue, Q.; Liu, H.; Shen, W.; Xu, J. Wear **1996**, 198, 216-219.

CHAPTER V

DETERMINATION AND UTILITY OF THEORETICAL SOLUBILITY PARAMETERS FOR POLYHEDRAL OLIGOMERIC SILSESQUIOXANE NANOCHEMICALS VIA GROUP CONTRIBUTION AND MOLECULAR DYNAMICS SIMULATION METHODS

Abstract

Theoretical solubility parameters based on both group contribution theory and molecular dynamics simulations were calculated for five polyhedral oligomeric silsesquioxane (POSS) molecules of different cage structure, physical state and R-group functionality. POSS derivatives chosen were octamethyl (OM), octaisobutyl (OiB), octaisooctyl (OiO), trisilanol isobutyl (TSiB) and trisilanol isooctyl (TSiO). Solubility parameters calculated by the different methods showed similar results and trends, though molecular dynamics simulations may more effectively represent solubility at the elevated temperatures encountered during blend processing. POSS molecules with longer R-group alkyl chain length were predicted to have superior miscibility and interaction when melt blended with a high density polyethylene (HDPE) matrix due to closer proximity of calculated solubility parameters to that of neat HDPE. Surface and bulk characterization of HDPE/POSS blends revealed that theoretical solubility parameters are only applicable for predicting miscibility among POSS derivatives of similar physical state and cage structure. Additionally, the effect of trisilanol cage condensation on solubility parameter reliability was addressed.

Introduction

Polyhedral oligomeric silsesquioxane (POSS) molecules are hybrid organic-inorganic nanostructures consisting of an inorganic Si-O-Si cage surrounded by a corona of organic substituents described by the general chemical structure $RSiO_{1.5}$.[1] The inorganic cage may be a fully condensed "closed" or "open" structure (Figure 3). The organic groups (R) are attached to the cage at the corner silicon atoms, and can be modified to tailor the performance and solubility characteristics of the POSS molecule. In our lab as well as others, POSS has been shown to produce a wide range of remarkable surface and bulk property enhancements when dispersed in melt-blended olefin matrices.[2-23] Bulk properties are reported to be heavily influenced by concentration and dispersion level of the POSS, where homogeneous distribution of POSS nanocrystals has been shown to result in enhanced degree of crystallinity and thermal stabiity.[2-8] In the melt state, incorporation of small amounts of POSS has been reported to enhance processability through viscosity reduction, attributed to increased free volume in the polymer melt due to well dispersed POSS cages reducing chain entanglement.[9,10] Tensile property enhancements have been reported for low-concentration POSS blends, attributed to good transfer of stresses from the olefin matrices to the stiff POSS cores.[11,12] Additionally, incorporation of POSS has been shown to provide surface enhancements, examples from our lab including surface modification through the apparent propensity of POSS to segregate towards the air surface in melt-blended systems.[20] Once the solubility limit for POSS has been reached in a particular matrix, POSS has been shown to form large aggregates, resulting in decreased crystallization rate and physical performance.[4,9,11]

The solubility limit and behavior for POSS in a particular matrix has been shown to be highly dependent on POSS molecular structure.[8,11,17]

To attain desirable composite traits such as mechanical, surface, thermomechanical and optical property enhancements, predictable solubility between a filler and matrix material is crucial.[24,25] Homogeneous dispersion of the filler, commonly verified by a combination of AFM microscopy and TEM-EDAX analysis, is largely related to the proximity of solubility parameters of the composite components, which can be determined experimentally for some systems and theoretically for most systems.[26] During processing, the cohesive energy densities and resulting solubility parameters of the composite components govern the Gibbs free energy of mixing (ΔG_m) of the system.[27] Equation 12 defines Gibbs free energy of mixing as:

$$\Delta G_m = \Delta H_m - T\Delta S_m \tag{12}$$

where ΔH_m is the enthalpy of mixing, ΔS_m is the entropy of mixing, and T is the absolute temperature of the system[25]. If ΔG_m is negative, the two substances will be soluble and homogenous mixing should occur.[28] In terms of solubility parameter utilization in the creation of composites, Hildebrand elaborated on Equation 12 to define Equation 13 as:

$$\Delta H_m = V\left(\delta_1 - \delta_2\right)^2 \Phi_1 \Phi_2 \tag{13}$$

where ΔH_m is the enthalpy of mixing per unit volume, V is the total volume of the composite, Φ is the volume fraction of components 1 and 2, and δ is the solubility parameter of components 1 and 2.[29,30] This equation estimates that two substances with equal solubility parameters should be soluble due to the resulting negative entropy value. This is in agreement with the general rule that chemical and structural similarity favors

solubility, or "like dissolves like". It is assumed that as the difference between δ_1 and δ_2 decreases, the likelihood of solubility increases.[24]

Based on the above equations, it can be postulated that for optimum dispersion of POSS into a host material, POSS types with similar solubility parameters to the matrix should be selected. Unfortunately due to their chemical nature and degradation behavior, most POSS molecules do not evaporate and therefore their cohesive energy densities and resulting solubility parameters cannot be determined experimentally.[31] Luckily, indirect determinations of the individual solubility parameters can be performed using group contribution theory.[25,26] Two popular methods by which to calculate solubility parameter are the group contribution methods developed by Hoy and van Krevelen.[32,33] Both methods employ the formula:

$$\delta = \left(\frac{\rho \sum G_i}{M_o} \right) \tag{14}$$

where δ is the theoretical solubility parameter, ρ is the material density, G_i is a molar attraction constant representing one of the various structural groups present in the molecule, and M_o is the molecular weight of the material.[25] Previous work in our lab has utilized the Hoy method to calculate theoretical solubility parameters for octaisobutyl (OiB) and trisilanol phenyl (TSP) POSS, with the goal of determining which would be more soluble in the creation of melt-blended polystyrene and Nylon-6 nanocomposites.[20,24] For both matrices, the TSP POSS showed closer theoretical solubility, and enhanced POSS disperion over the OiB POSS was demonstrated via AFM and TEM elemental mapping. In similar studies, Lim et al. used the van Krevelen method to calculate solubility parameters for octamethl (OM), OiB and octaphenyl (OP) POSS for melt blending with polyethylene and PET matrices, and found correlation

between tensile performance and predicted solubility parameter proximity to the matrix.[12,34] A fundamental difference between the results from our lab and those reported by Lim et al. is the lack of inclusion of the POSS cage structure in solubility parameter estimations in the latter studies, where the authors attributed the majority of POSS/matrix interactions with the organic corona surrounding the POSS cage.

As an alternative to group contribution methods, molecular dynamics simulations are gaining popularity as a means by which to predict the cohesive energy density of various materials, and as such have potential to be used in the calculation of a theoretical solubility parameter.[35-38] In this technique, the total intermolecular energy (or cohesive energy density) of a simulated material system is calculated for a specific temperature and pressure profile. The resulting predicted values have been shown to compare favorably with experimentally determined cohesive energy densities for various materials, establishing the accuracy of the technique.[39,40] An advantage that molecular dynamics simulations have over theoretical group contribution methods is that values for cohesive energy densities are calculated directly from the chemical structure of the material in question and are not limited by the need for tabulated group molar attractive constants. For group contribution method calculations, cohesive energy density is estimated relative to a limited table of group molar attractive constants in which some chemical groups are not represented.[26] Another advantage of using molecular dynamics simulations is that cohesive energy densities can be calculated over a wide range of temperatures and pressures. Unlike group contribution methods, which assume that solubility parameter estimations are performed at room temperature, molecular dynamics simulations can model solubility parameters at the elevated temperatures and pressures

encountered during blend processing. Performing the simulations at elevated temperatures has the added benefit that the solubility parameters can be more accurately predicted for species of POSS that are crystalline at room temperature as group additive techniques are not intended for use with crystalline materials.

Though limited documented attempts were found in the literature relative to assigning a solubility parameter to individual POSS molecules via molecular dynamics simulations, studies have been completed which attempt to model how the solubility parameters of polymers change once co-polymerized with varying amounts/types of POSS. Bharadwaj et al. used molecular dynamics simulations to determine the effect of introducing pendant POSS moieties substituted with cyclopentyl and cyclohexyl rings on the solubility parameter of polynorbornenes.[35] They determined experimentally that cyclopentyl POSS had more efficient interactions with the host matrix, as well as a closer simulated theoretical solubility parameter. Bizet et al. used molecular dynamics simulations to investigate the effects of introducing increasing concentrations of monofunctional POSS as pendant groups on a poly methyl(methyl methacrylate) (PMMA) backbone.[36] They reported that as POSS concentration increased, solubility parameter changed dramatically due to reduced intermolecular interactions in the PMMA blends. Similarly, Zhang et al. modeled PMMA composites containing increasing concentrations of OiB POSS, and via simulation determined that increasing POSS content lead to increasing disparity of solubility parameter between the POSS composites and the neat matrix material due to aggregation of the POSS molecules.[38]

As is shown, both group contribution methods and molecular dynamics simulations have the potential to be utilized in the estimation of solubility parameters for

the different types of POSS. This could lead to larger utilization of POSS as an industrial filler material, but with a more accurate prediction of which POSS types have the potential to be soluble in which organic matrices. It is the goal this research to theoretically determine solubility parameters for a series of POSS molecules with different cage structures and functionalities by both group contribution and molecular dynamics theory, and to determine if there is a correlation between the theoretical parameters themselves, as well as the surface and bulk properties of melt-blended HDPE/POSS systems.

Experimental

Molecular Dynamics Simulations

All simulation work was conducted using the Accelerys Materials Studio Suite v.5.0 (San Diego, CA). The COMPASS27 force field was used for all simulations. Each simulation job was launched to a distributed computing cluster with 100 processors. Depending on calculation intensity, each job was run on up to eight processors. The overall simulation strategy was to first create a set of atomic coordinates for a large number of POSS molecules (~40) and to create a computational space around these coordinates. This space is referred to as an amorphous cell. The amorphous cell has periodic boundary conditions which allow these 40 POSS molecules to represent bulk behavior. The initial amorphous cell was created with a very low density and then compressed by gradually reducing the volume of the cell during a molecular dynamic simulation. This has the effect of increasing the density while also reducing the likelihood that an unnatural conformation may be “frozen into” the cell. A slow compression while also slowly reducing the temperature to 25°C allows each POSS

molecule to adopt a low-energy, realistic conformation and position within the amorphous cell. After compression, a 100,000 step molecular dynamic simulation was run at 25°C and 1 atmosphere to assess the stability of the amorphous cell. The amorphous cell was determined to be realistic if the density remained stable near the value reported in literature.[41]

Amorphous cells were annealed at a temperature of 240°C to understand solubility behavior at temperatures similar to those encountered during processing. Elevated temperature simulations are also advantageous as this raises the temperature of each molecule above the melting point of crystalline POSS species. As with room temperature simulations, the density of each elevated temperature amorphous cell was compared to the measured density of each POSS species at elevated temperature. The density of each POSS species was determined with a 2 mL pycnometer heated to 240°C in silicone oil. POSS was not visually observed to be soluble in silicone oil, although a small degree of solubility at this temperature is anticipated. Regardless, these values were found to be a good guide for comparison with the simulated elevated temperature amorphous cells. Good agreement was found between measured and simulated densities at 240°C. Elevated temperature cells were determined to be acceptable if they were found to have a stable density and internal energy during a 100,000 step molecular dynamics simulation at 240°C and 1 atm.

Once a realistic amorphous cell was obtained, a molecular dynamics simulation was performed to allow a large number (2,000) of likely atomic positions and intermolecular distances to be determined. The cohesive energy density was then

calculated as the sum of intermolecular forces in each amorphous cell. These 2,000 values were then averaged to give the cohesive energy density.

The simulation steps can be summarized as follows:

1. The series of POSS molecules were drawn using the Visualizer module and then energy minimized to a maximum derivative of less that 0.001 with the Discover Minimization module using the Steepest Descent, Conjugate Gradient and Newton minimization algorithms.
2. The Amorphous Cell module was then used to create cells of each molecule. Each cell was energy minimized to a maximum derivative of less than 0.001. Enough POSS molecules were added to yield a cell containing 5,000 atoms. Cell density was set to half the desired final density. Any cells with catenation or excessively high internal energy were rejected (approximately 50% rejection rate). Ten different amorphous cells of each molecule were created.
3. An "annealing" script was written with alternating constant volume/constant pressure segments. This script was run on each amorphous cell using the Discover Dynamics module. This script slowly compressed the low-density cell to an acceptable density to give realistic molecular configurations. Each molecule required a different script. The initial temperature was typically 700 K which was ramped down over a series of 5-7 alternating NVT (canonical ensemble) and NPT (isothermal-isobaric ensemble) runs. The pressure of the initial NPT run was generally set to around 2.5 GPa which was gradually reduced to 0.0001 GPa (1 atm). The final 0.0001 GPa NPT was allowed to run for 100,000 steps while the cell volume and energy were monitored to ensure they were stable. Stable

volume and energy was taken to indicate that the cell had equilibrated and was a realistic model of bulk POSS.

4. A 1,000,000 step constant volume and temperature molecular dynamic simulation was carried out on each of the 10 cells for each POSS species. Every 5,000th step was saved. These 200 "snapshots" of each of the 10 amorphous cells gave 2,000 potential configurations of each POSS species.
5. The Forcite module was used to calculate the cohesive energy density of each of the 2,000 potential configurations of each POSS species. The solubility parameter was then calculated as the square root of the cohesive energy density.

Results and Discussion

Solubility Parameters via Group Contribution Methods

Table 9 shows the theoretical solubility parameters calculated via the van Krevelen and Hoy methods for HDPE and the POSS molecules. The values obtained by the two methods are not equal, and this is due to the different algorithmic methods by which the parameters are estimated. Though these methods use different means to arrive at a final parameter, the values that are estimated are usually within 10% of each other, as is the case in this study, leading to the common practice of calculating solubility via both methods and taking the average.[25] Experimentally, polyethylene has been shown to have a solubility parameter ranging from 7.7 to 8.4 $cal^{1/2}/cm^{-3/2}$, with HDPE residing towards the upper end of these values.[42] As is shown, theoretical solubility parameters calculated are different for the different POSS molecules. Materials with closer solubility parameters to HDPE are expected to exhibit greater compatibility and better dispersion characteristics.[25,26]

Table 9

Group contribution theoretical solubility parameters including POSS cage ($cal^{1/2}/cm^{-3/2}$)

Material	Hoy	van Krevelen	Average
HDPE	8.36	8.49	8.43
OM	11.54	12.20	11.87 (Δ=3.44)
OiB	9.13	9.90	9.52 (Δ=1.09)
OiO	8.60	9.19	8.90 (Δ=0.47)
TSiB	9.59	10.52	10.06 (Δ=1.63)
TSiO	8.52	9.38	8.95 (Δ=0.52)

From Table 9, it can be seen that as the functional R-groups attached to the POSS molecules are increased in length, the difference in calculated solubility parameter with that of HDPE becomes smaller, regardless of cage structure. This is expected, as the POSS molecules with longer alkyl chains are more similar to the structure of HDPE and are thus expected to have greater solubility.

Table 10 shows the theoretical solubility parameters of the different POSS molecules as well, but in this case the cage structure of the POSS molecules was not included in the calculations. These calculations were conducted due to the theory that the organic corona of the POSS molecule is primarily what interacts with the polymer matrix, while the cage has limited interaction or effect. What can be seen is that though the values are different from those in Table 9, the same trend exists in that samples with longer alkyl chains show closer theoretical solubility with the HDPE matrix.

Table 10

Group contribution theoretical solubility parameters excluding POSS cage ($cal^{1/2}/cm^{-3/2}$)

Material	Hoy	van Krevelen	Average
HDPE	8.36	8.49	8.43
OM	18.15	20.37	19.26 (Δ=10.83)
OiB	10.84	12.17	11.51 (Δ=3.08)
OiO	9.58	10.37	9.98 (Δ=1.55)
TSiB	9.71	13.57	11.64 (Δ=3.21)
TSiO	8.69	10.63	9.66 (Δ=1.23)

Solubility Parameters via Molecular Dynamics Simulations

Figure 41 shows the computed theoretical solubility parameters for the five POSS molecules, as well as the experimentally-determined parameters for HDPE.[42]

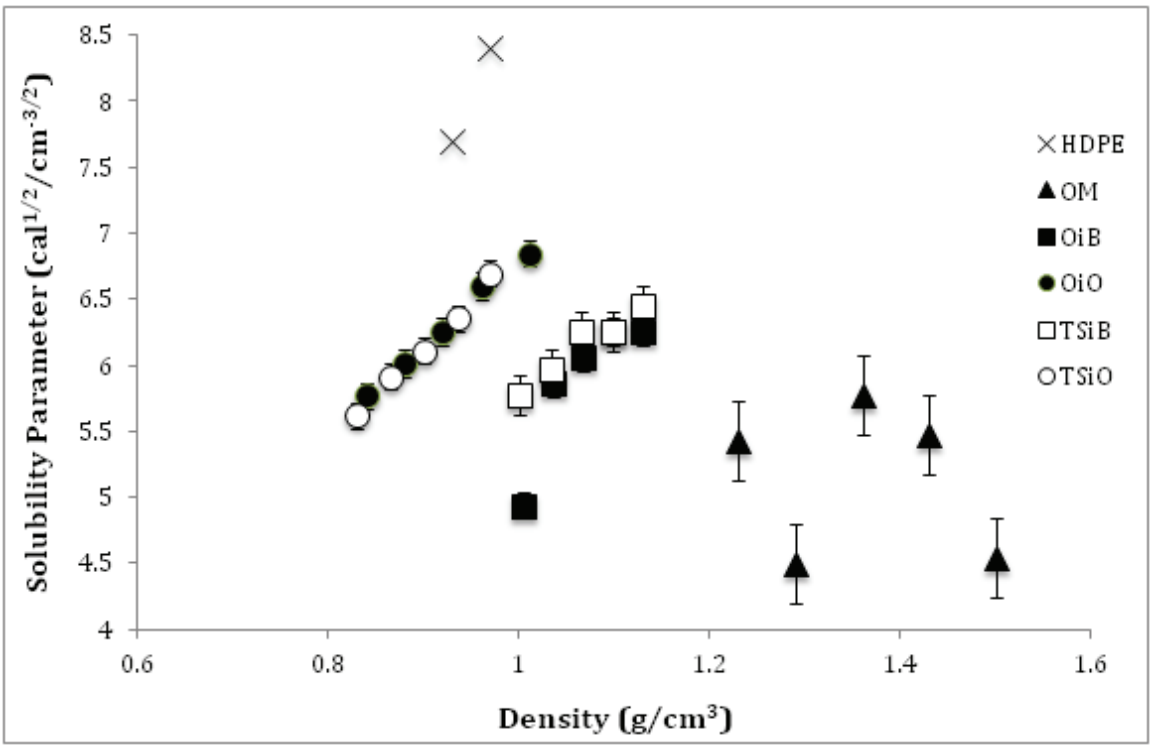

Figure 41. POSS solubility parameters calculated via molecular dynamics simulations.

Due to differences in final density of the annealed cells for each POSS molecule, it is impossible to assign an exact solubility parameter to each individual POSS derivative, though general trends are present. In agreement with the values calculated via the Hoy and van Krevelen methods, the OiO and TSiO POSS types show very similar values, and reside closest in proximity to the neat HDPE. OiB and TSiB POSS show similar trends with the group contribution calculations as well, with the data points lying nearly on top of each other. OM POSS, which is predicted to be least compatible via group contribution methods, is also predicted to be least compatible via molecule dynamics simulations. It is important to note the difference in temperatures between the molecular dynamics simulations and the group contribution calculations. The value of the solubility parameter is temperature dependent and this is likely reflected in the difference in the solubility parameter values obtained by the two different methods.[25,26] Increasing the temperature decreases the cohesive energy density and consequently also the solubility parameter.[43] The difference between the two methods is fairly consistent.

Bulk and Surface Characterization

Bulk characterization of the HDPE/POSS blends (Chapter III) revealed mixed trends relative to the incorporation of the different POSS molecules. The behaviors demonstrated by the individual POSS blends were shown to depend not only on the substituent alkyl chain length of the POSS structure, but also on the physical state and cage structure of the POSS molecule. Physical state was shown to dominate processing behavior as well as mechanical and rheological performance, while POSS substituent chain length and solubility/miscibility were shown to play the dominant role in bulk degree of crystallinity and thermal performance. Solubility parameters estimated by

molecular dynamics simulation and group contribution theory do not take component physical state into account, though among POSS molecules of similar physical state, miscibility was shown to be governed by alkyl chain length. For this reason, theoretical solubility parameters estimated for POSS molecules appear to only be comparable if among POSS types of similar physical state. Additionally, trisilanol POSS blends displayed slightly different behavior than their closed-cage analogues, limiting the applicability of solubility parameter estimations based only on organic substituent functionality. This is attributed primarily to the cage condensation reactions possible for trisilanol POSS molecules, and the resulting effects on POSS molecular structure. Trisilanol cage condensation has been reported to result in formation of degradation products with molecular weights both above and below that of the original starting material.[44] Since both group contribution and molecular dynamics simulations rely exclusively on knowing the exact molecular structure of the component in question, the potential of heat-induced cage condensation can make estimating a solubility parameter for trisilanol POSS molecules processed above 200°C (the reported temperature of cage condensation) difficult if not impossible.[44]

Surface properties of the HDPE/POSS blends (Chapter IV) were also shown to rely not only on POSS substituent chain length, but also on cage structure and physical state. Variable-angle ATR-FTIR analysis revealed a higher propensity for surface segregation for the trisilanol POSS molecules over their closed cage analogues, attributed to changes in molecular structure and miscibility due to cage condensation.[44] Within the solid POSS molecules, AFM and WAXD analysis revealed that increasing POSS substituent chain length resulted in enhanced miscibility and decreased phase separation

in the HDPE matrix, in agreement with solubility parameter estimations. Among the liquid POSS molecules, AFM analysis revealed smaller effects of surface roughness for the OiO compared to the TSiO blends, again showing the influence of the POSS cage structure and/or potential cage condensation effects on miscibility. Between the TSiB and TSiO molecules (similar cage structure and physical state) TSiO showed superior miscibility in the HDPE, in agreement with solubility parameter estimations.

Conclusions

HDPE/POSS blends were successfully prepared via melt extrusion and their surface and bulk properties analyzed. Theoretical solubility parameters were estimated via group contribution theory and molecular dynamics simulations to determine if a correlation could be found between POSS solubility and blend performance. Solubility parameters of POSS molecules obtained by molecular dynamics simulations compared reasonably with solubility parameters obtained by the more traditional group contribution technique. In relation to POSS molecules, it was shown that calculated solubility parameters are only applicable among POSS derivatives with similar cage structures and within the same physical state. Among POSS molecules of similar cage structure and physical state, solubility parameter calculations appeared to accurately represent POSS miscibility. Among POSS molecules of similar physical state but different cage structure, solubility parameter calculations did not appear to predict miscibility, revealing the importance of including the POSS cage structure in solubility parameter calculations/simulations. For our HDPE/POSS blends, trisilanol cage condensation was shown to be a major factor affecting POSS surface segregation, surface roughness and

bulk crystallinity, revealing the importance of knowing exact molecular structure for accurate solubility parameter calculations.

Though calculation of solubility parameters using the group contribution methods of Hoy and van Krevelen is appealing due to the relative ease of calculation, simulation via molecular dynamics is an attractive technique in that solubility parameters are able to be calculated at the temperatures and pressures commonly encountered during polymer processing. Additionally, molecular dynamic simulation may give a more accurate prediction of solubility parameter than group contribution methods due to that fact that these techniques are limited to temperatures at which some species of POSS are still in the crystalline state, therefore not effectively modeling miscibility during processing.

Acknowledgements

This work was supported primarily by a fellowship from the National Science Foundation GK-12 program “Connections in the Classroom: Molecules to Muscles”, Award # 0947944 through the University of Southern Mississippi.

This work was supported in part by the Office of Naval Research, Award # N00014-07-1057.

REFERENCES

1. Lichtenhan, J. D. Comments on Inorg. Chem. **1995**, 17, 115-130.

2. Chen, J. H.; Yao, B. X.; Su, W. B.; Yang, Y. B. Polymer **2007**, 48, 1756-1769.

3. Chen, J. H.; Chiou, Y. D. J. Polym. Sci., Part B: Polym. Phys. **2006**, 44, 2122-2134.

4. Fina, A.; Tabuani, D.; Camino, G. Eur. Polym. J. **2010**, 46, 14-23.

5. Fu, B. X.; Yang, L.; Somani, R. H.; Zong, S. X.; Hsiao, B. S.; Phillips, S.; Blanski, R.; Ruth, P. J. Polym. Sci., Part B: Polym. Phys. **2001**, 39, 2727-2739.

6. Joshi, M.; Butola, B. Polymer **2004**, 45, 4953-4968.

7. Joshi, M.; Butola, B. J. Appl. Polym. Sci. **2007**, 105, 978-985.

8. Pracella, M.; Chionna, D.; Fina, A.; Tabuani, D.; Frache, A.; Camino, G. Macromol. Symp. **2006**, 234, 59-67.

9. Joshi, M.; Butola, B.; Simon, G.; Kukaleva, N. Macromolecules **2006**, 39, 1839-1849.

10. Zhou, Z.; Zhang, Y.; Zeng, Z. J. Appl. Polym. Sci. **2008**, 110, 3745-3751.

11. Baldi, F.; Bignotti, F.; Fina, A.; Tabuani, D.; Ricco, T. J. Appl. Polym. Sci. **2007**, 105, 935-943.

12. Lim, S. K.; Hong, E. P.; Choi, H. J.; Chin, I. J. J. Ind. Eng. Chem. (Washington, D. C.) **2010**, 16, 189-192.

13. Bolln, C.; Tsuchida, A.; Frey, H.; Malhaupt, R. Chem. Mater. **1997**, 9, 1475-1479.

14. Carniato, F.; Fina, A.; Tabuani, D.; Boccaleri, E. Nanotechnology **2008**, 19, 475701.

15. Fina, A.; Tabuani, D.; Carniato, F.; Frache, A.; Boccaleri, E.; Camino, G. Thermochim. Acta **2006**, 440, 36-42.

16. Fina, A.; Abbenhuis, H. C. L.; Tabuani, D.; Camino, G. Polym. Degrad. Stab. **2006**, 91, 2275-2281.

17. Fina, A.; Tabuani, D.; Frache, A.; Camino, G. Polymer **2005**, 46, 7855-7866.

18. Fu, B. X.; Gelfer, M. Y.; Hsiao, B. S.; Phillips, S.; Viers, B.; Blanski, R.; Ruth, P. Polymer **2003**, 44, 1499-1506.

19. Hato, M. J.; Ray, S. S.; Luyt, A. S. Macromol. Mater. Eng. **2008**, 293, 752-762.

20. Misra, R.; Fu, B. X.; Morgan, S. E. J. Polym. Sci., Part B: Polym. Phys. **2007**, 45, 2441-2455.

21. Takala, M.; Karttunen, M.; Salovaara, P.; Kortet, S.; Kannus, K.; Kalliohaka, T. IEEE Trans. Dielectr. Electr. Insul. **2008**, 15, 40-51.

22. Tang, Y.; Lewin, M. Polym. Avd. Technol. **2009**, 20, 1-15.

23. Wheeler, P. A.; Misra, R.; Cook, R. D.; Morgan, S. E. J. Appl. Polym. Sci. **2008**, 108, 2503-2508.

24. Misra, R.; Fu, B. X.; Plagge, A.; Morgan, S. E. J. Polym. Sci., Part B: Polym. Phys. **2009**, 47, 1088-1102.

25. van Krevelen, D. W. Cohesive properties and solubility. In *Properties of polymers*; Elsevier: New York, 2009, Chapter 7, pp 201-221.

26. Barton, A. Calculated cohesion parameters. In *CRC handbook of solubility parameters and other cohesion parameters*; CRC: New York, 1991, Chapter 6, pp 183-190.

27. Tadmor, Z.; Gogos, C. G. Mixing. In *Principles of polymer processing*; Wiley: New York, 2006, Chapter 7, pp 322-357.

28. Flory, P. J. Determination of molecular weight. In *Principles of polymer chemistry*; Cornell University Press: New York, **1953**, Chapter 7, pp 507-509.

29. Hildebrand, J. H. J Am. Chem. Soc. **1916**, 38, 1452-1473.

30. Hildebrand, J. H. J Am. Chem. Soc. **1919**, 41, 1067-1080.

31. Romo-Uribe, A.; Mather, P.; Haddad, T.; Lichtenhan, J. J. Polym. Sci., Part B: Polym. Phys. **1998**, 36, 1857-1872.

32. Van Krevelen, D.; Hoftyzer, P. J. Appl. Polym. Sci. **1967**, 11, 2189-2200.

33. Hoy, K. J. Paint Technol. **1970**, 42, 76.

34. Lim, S.-K.; Hong, E.-P.; Choi, H. J.; Chin, I.-J. J. Ind. Eng. Chem. (Amsterdam, Neth.) **2010**, 16, 189-192.

35. Bharadwaj, R.; Berry, R.; Farmer, B. Polymer **2000**, 41, 7209-7221.

36. Bizet, S.; Galy, J.; Gerard, J. F. Polymer **2006**, 47, 8219-8227.

37. Patel, R. R.; Mohanraj, R.; Pittman Jr, C. U. J. Polym. Sci., Part B: Polym. Phys. **2006**, 44, 234-248.

38. Zhang, Q. G.; Liu, Q. L.; Wu, J. Y.; Chen, Y.; Zhu, A. M. J. Membr. Sci. **2009**, 342, 105-112.

39. Eichinger, B.; Rigby, D. R.; Muir, M. H. Comput. Polym. Sci. **1995**, 5, 147-164.

40. Pavel, D.; Shanks, R. Polymer **2003**, 44, 6713-6724.

41. Hybrid Plastics, POSS User's Guide. http://hybridplastics.com/docs/user-v2.06.pdf (accessed October 22, 2011)

42. Peacock, A. J. Properties of polyethylene. In *Handbook of polyethylene: structures, properties, and applications*; CRC Press: New York, **2000**, Chapter 5, pp 123-128.

43. Bicerano, J. Cohesive energy and solubility parameter. In *Prediction of polymer properties*; CRC Press, New York, **2002**, Chapter 5, pp 137-144.

44. Feher, F. J.; Newman, D. A.; Walzer, J. F. J. Am. Chem. Soc. **1989**, 111, 1741-1748.

CHAPTER VI

RECOMMENDED FUTURE WORK

In this research, we have demonstrated the successful processing of HDPE/POSS blends utilizing POSS derivatives of varying cage structure, R-group functionality and physical state. Both qualitative and quantitative characterization of bulk and surface properties reveal behavior dependent on these variables to different degrees. Though it is shown that TSiB POSS is likely to condense into and remain a liquid at the temperatures encountered during HDPE/POSS blend processing, it would be beneficial to determine concrete condensation onset, peak and end temperatures for the various trisilanol POSS derivatives. Additionally, extraction and characterization (Si-NMR) of condensed trisilanol POSS products from melt-blended blends could lead to a better understanding of condensation product structures after processing. Rheological characterization reveals strong blend storage/loss modulus dependence on POSS physical state and loading level; solid state DMA would be beneficial for refinement of mechanistic understanding of this phenomena. Thermooxidative degradation enhancement is shown to be dependent on POSS loading level in our blends; TEM-EDAX would be useful to characterize regularity of dispersed POSS phase in the systems, further refining the mechanism of thermal protection.

In our studies we have demonstrated a depth-dependent concentration gradient of POSS in the HDPE matrix, where preferential surface segregation was illustrated for all systems; transmission ATR-FTIR, as well as XPS, could be used to quantify behavioral differences between the individual POSS derivatives. A depth-dependent crystallinity gradient was also observed for the blends; controlled-depth nanoindentation analysis

would give interesting insight as to differences in mechanical properties relative to calculated degree of crystallinity. Though AFM imaging reveals distinct differences between the morphology of blends containing solid and liquid POSS molecules, the appearance of small spheroidal features in the TSiB and TSiO samples are of particular interest. TEM-EDAX analysis of these spheroidal features would be useful to determine if they are solid products formed due to trisilanol cage condensation, imaging artifacts, or another type of entity.

Solubility parameters calculated via group contribution theory and molecular dynamics simulations are shown to have applicability in predicting miscibility among POSS types of similar physical state and cage structure. It would be interesting to computationally model how solubility parameter changes relative to simulation temperature for individual POSS molecules. Additionally, modeling and calculating a solubility parameter for characterized trisilanol condensation products could lead to a better mechanistic understanding as to the higher degree of trisilanol POSS surface segregation observed in our systems.